

2019-04-01

Understanding Soil Liquefaction of the 2016 Kumamoto Earthquake

Donald Jared Anderson
Brigham Young University

Follow this and additional works at: <https://scholarsarchive.byu.edu/etd>

BYU ScholarsArchive Citation

Anderson, Donald Jared, "Understanding Soil Liquefaction of the 2016 Kumamoto Earthquake" (2019). *All Theses and Dissertations*. 7135.
<https://scholarsarchive.byu.edu/etd/7135>

This Thesis is brought to you for free and open access by BYU ScholarsArchive. It has been accepted for inclusion in All Theses and Dissertations by an authorized administrator of BYU ScholarsArchive. For more information, please contact scholarsarchive@byu.edu, ellen_amatangelo@byu.edu.

Understanding Soil Liquefaction of the
2016 Kumamoto Earthquake

Donald Jared Anderson

A thesis submitted to the faculty of
Brigham Young University
in partial fulfillment of the requirements for the degree of
Master of Science

Kevin Franke, Chair
Kyle Rollins
Gus Williams

Department of Civil and Environmental Engineering
Brigham Young University

Copyright © 2019 Donald Jared Anderson

All Rights Reserved

ABSTRACT

Understanding Soil Liquefaction of the 2016 Kumamoto Japan Earthquake

Donald Jared Anderson
Department of Civil and Environmental Engineering, BYU
Master of Science

The Kumamoto earthquake of April 2016 produced two foreshocks of moment magnitude 6.0 and 6.2 and a mainshock of 7.0, which should have been followed by widespread and intense soil liquefaction. A Geotechnical Extreme Events Reconnaissance team (GEER) led by Professor Rob Kayen of UC Berkley was dispatched to the Kumamoto Plain –which is in Kumamoto Prefecture, the southern main island of Japan –immediately following the earthquake. The Japanese and U.S. engineers in the GEER team observed mostly minor and sporadic liquefaction, which was unexpected as the local site geology, known soil stratigraphy, and intensity of the seismic loading made the Kumamoto Plain ripe for soil liquefaction. The paucity and limited scale of liquefaction shows a clear gap in our understanding of liquefaction in areas with volcanic soils. This study is a direct response to the GEER team’s preliminary findings regarding the lack of significant liquefaction.

An extensive literature review was conducted on the Kumamoto Plain and its volcanic soil. The liquefaction of the 2016 Kumamoto Earthquake was also researched, and several sites were selected for further analysis. Four sites were analyzed with SPT, CPT, and laboratory testing during the spring of 2017. A slope stability analysis and undisturbed testing were performed for specific sites. The results of the analysis show a general over-prediction of SPT and CPT methods when determining liquefaction hazard. The Youd et al. (2001) NCEES method was the most consistent and accurate in determining liquefaction. The soils in the area including sands and gravels had high levels of fines, plasticity, and organic matter due to the weathering of volcanic ash and pyroclastic material. The volcanically derived coarse-grained soils may also have exhibited some crushability, which gave lower resistance readings. Filled river channels had the worst liquefaction with natural levees and the Kumamoto flood plains having only minor liquefaction. Publicly available boring logs rarely showed laboratory test data of bore holes which led to a general inaccurate soil classification. Boring logs were also not updated with laboratory classifications and data. Undisturbed cyclic triaxial testing of soils at one site showed that volcanic soils had relatively high resistance to soil liquefaction, though drying of samples may have compromised the results. Embankment cracking at one test location was calculated a lateral spread and a seismic slope failure along the pyroclastic flow deposit.

Keywords: liquefaction, 2016 Kumamoto Earthquake, volcanic soils, allophanic soils

ACKNOWLEDGEMENTS

I would first like to thank the National Science Foundation under Grant No. CMMI-1727594, CMMI-1454431, and CMMI-1743159 for funding this collaborative research project. It was the perfect project for me, given my interest in earthquake engineering and Japan. I was able to collaborate with many Japanese which also enriched my learning experience.

I would like to thank my colleague in the lab, Jenny, for answering the many questions I asked her. I would like to thank my Japanese counterpart, Masa, for helping me out with some Japanese questions I had for him. I am grateful for Kevin Franke, Kyle Rollins, and Gus Williams for their feedback and support during this endeavor. I would also like to thank my family for supporting me during my master's degree and always maintaining an optimistic attitude. In the Anderson family, there is no such thing as individual success or failure.

TABLE OF CONTENTS

LIST OF TABLES	vii
LIST OF FIGURES	viii
1 Introduction	1
2 Liquefaction	3
2.1 Susceptibility	3
2.1.1 Groundwater Depth	4
2.1.2 Geological.....	4
2.1.3 Historical	4
2.1.4 Compositional.....	5
2.1.5 Initial State Criteria	8
2.2 Initiation	10
2.2.1 Methods for Predicting Liquefaction Initiation.....	13
2.3 Liquefaction Effects	16
2.3.1 Liquefaction Hazards.....	18
3 Geology and Geotechnics.....	21
3.1.1 Kyushu Island.....	21
3.1.2 The Kumamoto Plain.....	26
3.2 Regional Tectonic Setting	31
4 Volcanic Soils of the Kumamoto Plain	36
4.1 Primary Materials of the Kumamoto Plain	36
4.1.1 Soil Crushability	37
4.2 Secondary Materials of the Kumamoto Plain	38
4.2.1 Allophane and Imogolite	39
4.2.2 Halloysite.....	41
4.2.3 Organic Contents of Allophanic Soils.....	43

4.2.4	Allophanic Soil Sensitivity to Laboratory Testing Procedures	43
5	The 2016 Earthquake Sequence	46
5.1.1	Foreshocks	46
5.1.2	Mainshock	47
5.2	General Damage After the Event	50
5.3	Liquefaction Damage Summary.....	51
5.3.1	Zone 1: Man-made Island and Coastline of West Kumamoto	54
5.3.2	Zone 2: Ancient River Channels in Kumamoto City	55
5.3.3	Zone 3: Rivers to the South of Kumamoto.....	56
6	Liquefaction Susceptibility and Initiation of Select Sites	60
6.1	Methods of Testing.....	61
6.2	Site 1: Small Neighborhood on Natural Levee with no Liquefaction.....	64
6.2.1	Geomorphology.....	67
6.2.2	SPT Susceptibility and Initiation Analysis	68
6.2.3	CPT Liquefaction Susceptibility and Initiation	68
6.3	Site 2-1: Downtown Kumamoto with Severe Liquefaction.....	70
6.3.1	Geomorphology.....	74
6.3.2	SPT Susceptibility and Initiation Analysis	74
6.3.3	CPT Susceptibility and Initiation Analysis	75
6.4	Cyclic Triaxial Testing of Samples at Site 2-1	77
6.5	Site 2-2: Downtown Kumamoto with no Liquefaction.....	79
6.5.1	Geomorphology.....	82
6.5.2	SPT Susceptibility and Initiation Analysis	82
6.5.3	CPT Susceptibility and Initiation Analysis	83
6.6	Site 4: Levee Located Near the Epicenter with Minor Liquefaction	85

6.6.1	Geomorphology.....	88
6.6.2	SPT Analysis.....	90
6.6.3	CPT Analysis.....	90
6.7	Slope Stability Analysis of Site 4.....	92
7	Discussion of Results.....	98
7.1	SPT-based Analysis with Boulanger and Idriss (2014).....	98
7.2	CPT-based Analysis Methods Comparison.....	98
7.3	Soil Crushability and Soil Plasticity.....	101
7.4	Regional Geology.....	102
7.5	Misreading of Japanese Logs.....	104
8	Conclusion.....	106
	References.....	108

LIST OF TABLES

Table 3-1: Geological time adapted from Geology for Engineers and Environmental Scientists (Alan, 2006)	24
Table 5-1: Acceleration recordings for various stations	48
Table 6-1: Site 2-1 SPT analysis using Boulanger and Idriss method (2016)	75
Table 6-2: Site 2-2 SPT analysis using Boulanger and Idriss method (2016)	82
Table 7-1: Sample Japanese classification and US classification.....	105
Table B-1. Kunijiban sandy low blow count profiles throughout the Kumamoto Plain	136

LIST OF FIGURES

Figure 1-1. Scope of Kumamoto Earthquake liquefaction research highlighted in red. Image from Google Maps	2
Figure 2-1: Liquefaction susceptibility criteria for fine-grained soils (Boulanger & Idriss, 2006).....	6
Figure 2-2: Liquefaction susceptibility criteria for fine-grained soils (Bray et al., 2004).....	7
Figure 2-3: Initial State Criteria. Drawn after Kramer (1996).....	10
Figure 2-4: Effects of density, A being most dense, C being loosest, on liquefaction. Drawn after Kramer (1996).....	10
Figure 2-5: Types of liquefaction failure. a) No liquefaction, b) flow liquefaction, and c) cyclic mobility (Kramer 1996).....	11
Figure 2-6: Flow liquefaction surface (dashed line) and SSL (Kramer 1996)	12
Figure 2-7: Cyclic loading test of loose sand (Seed and Idriss, 1982)	17
Figure 2-8: Example of ground oscillation, modeled after Youd (1984)	18
Figure 2-9: Sand boils on side of house in Kumamoto, showing volcanic material that was plastic and pumiceous in origin (Kayen 2017).....	18
Figure 3-1: Kyushu Island, Japan with geological Median Line. Image from Google Maps.....	22
Figure 3-2: Map of Kyushu, Japan: Sedimentary and metamorphic rocks older than Neogene Period. Yellow box shows the boundaries of the study area (Hashimoto 1991)	24
Figure 3-3: Map of Kyushu, Japan: Granites and rhyolites. Yellow box shows the boundaries of the study area (Hashimoto 1991).....	25
Figure 3-4: Map of Kyushu, Japan: Sedimentary and metamorphic rocks of Neogene Period. Yellow box shows the boundaries of the study area (Hashimoto 1991).....	25
Figure 3-5. Map of Kyushu, Japan: Quaternary Period sediments and volcanic rocks. Yellow box shows the boundaries of the study area (Hashimoto 1991).....	26
Figure 3-6: Image of the Kumamoto Plain river system, with key rivers labeled, shown in teal (GSI, 2018).....	27
Figure 3-7: Western Japan sea level fluctuations during the last 15,000 years (Ota et al., 1982).....	28
Figure 3-8: Ariake Bay sediments with Kumamoto Plain highlighted. Yellow box shows the boundaries of the study area (Otsubo et al., 1995).....	29
Figure 3-9: Aso-4 pyroclastic flow distribution. Yellow box shows the boundaries of the study area (GSJ, 2018)	30
Figure 3-10: Faults near the Kumamoto Plain (GSJ, 2018).....	32

Figure 3-11: Map of Japanese earthquakes and plate movement from 2003 to 2015 (Kato et al., 2016).....	33
Figure 3-12: Interactive geological map (GeoNavi) showing the Kumamoto Plain, Mt. Aso, and Median Zone (Naito, 2014)	34
Figure 3-13: Legend of Figure 3-12 geological map (Naito, 2014)	35
Figure 4.1: Formation of different volcanic secondary materials by rainfall (Parfitt et al., 1983).....	38
Figure 4-2: Allophane and imogolite (Henmi & Wada, 1976).....	39
Figure 4-3: Allophanic and non-allophanic clay distribution for direct deposits for Kyushu Island. Box shows the boundaries of the study area (Saigusa & Matsuyama, 1997; Takahashi & Shuji, 2002).....	40
Figure 4-4: Halloysite image with scale lines representing 0.5 μm (Nagasawa 1978).....	42
Figure 4-5: Increase in water content and Atterberg limits with increasing allophane content (Wesley 1973)	42
Figure 4-6: Effects of drying on allophanic soil grain size distribution. Y1 (left) is allophane dominant while R1 (right) is halloysite dominant soils. Altered from (Wesley 1973).....	44
Figure 4-7: Index properties differences based of test condition. First two samples (Y1 & Y2) are allophane dominant soils and the last two samples (R1 & R2) are halloysite dominant clays. Altered from (Wesley 1973)	44
Figure 4-8: Effects of soil drying on volcanic soil plasticity (Yamazaki & Takenaka, 1965)	45
Figure 5-1: Foreshock PGA with epicentral distance. Left: M 6.2. Right: M 6.0	47
Figure 5-2: Mainshock PGA with epicentral distance.....	48
Figure 5-3: Locations of seismic stations listed in Table 3-1.	49
Figure 5-4: Velocity and acceleration response spectrum of Mashiki (KMMH16)	49
Figure 5-5: Acceleration response spectrum of location directly east of Kumamoto City (KMM006)	50
Figure 5-6: Kumamoto City liquefaction hazards map (Kumamoto City, 2014).....	51
Figure 5-7. Harvested rice stalks being used to fertilize a field in Japan (Nippon, 2014).....	52
Figure 5-8. Field survey and aerial photograph interpretation of liquefaction damage in the Kumamoto Plain with zones of interest marked. Altered from (Mukunoki et al., 2016) ...	53
Figure 5-9: N-S liquefied river channel with liquefied sites (Wakamatsu et al., 2016)	56
Figure 5-10: MLIT damage survey for levees (MLIT, 2017).....	58
Figure 5-11: Lateral spread and levee cracking locations, altered from MLIT (2017)	59
Figure 6-1. Kumamoto Plain with test sites and faults located.....	60

Figure 6-2: Typical Atterberg limits for volcanic soils (Rao, 1996)	63
Figure 6-3: Atterberg limits summary chart	63
Figure 6-4: Site 1 SPT counts, soil layering, and laboratory test results	64
Figure 6-5. Site 1 CPT readings and SBT.....	65
Figure 6-6. Site 1 normalized CPT penetration resistance plotted against normalized friction ratio and I_c with depth.....	66
Figure 6-7: Map of liquefied locations with triangle representing boring location and geomorphological land classification map (Wakamatsu et al., 2016; GSI, 2018)	67
Figure 6-8: Before (1960s) with estimated modern day river course and after (2016) picture (GSI, 2018).....	68
Figure 6-9: Site 1 liquefaction analysis using Youd et al. (2001)	69
Figure 6-10. Site 1 surficial manifestation of liquefaction (Ishihara, 1985).....	70
Figure 6-11: Site 2-1 SPT counts, soil layering, and laboratory test results.....	71
Figure 6-12. Site 2-1 CPT results and SBT	72
Figure 6-13: Site 2-1 normalized CPT penetration resistance plotted against normalized friction ratio and I_c with depth.....	73
Figures 6-14: Geomorphological land classification map of site 2-1 with site 2-1 indicated by the triangle (GSI, 2018).....	74
Figure 6-15: Site 2-1 liquefaction analysis using Youd et al. (2001)	76
Figure 6-16. Site 2-1 surficial manifestation of liquefaction (Ishihara, 1985)	77
Figure 6-17: CSR vs. Number of cycles obtained experimentally on Kumamoto samples	78
Figure 6-18: Site 2-2 SPT counts, soil layering, and laboratory test results.....	79
Figure 6-19. Site 2-2 CPT results and soil behavior classification.....	80
Figure 6-20: Site 2-2 normalized CPT penetration resistance plotted against normalized friction ratio and I_c with depth.....	81
Figure 6-21. Site 2-2 surficial manifestation of liquefaction (Ishihara, 1985)	83
Figure 6-22: Site 2-2 liquefaction analysis using Youd et al. (2001)	84
Figure 6-23: Site 4 SPT counts, soil layering, and laboratory test results	85
Figure 6-24. Site 4 CPT results and soil behavior classification	86
Figure 6-25: Site 4 normalized CPT penetration resistance plotted against normalized friction ratio and I_c with depth.....	87
Figure 6-26. Hypothesized lateral spread at site 4 and observed fissures and ejecta (Kayen et al., 2017).....	88

Figures 6-27: Geomorphological map of site 4 (GSI, 2018)	89
Figure 6-28: Present day picture of area 2016 (left) and 1970 (right) (GSI, 2018).....	89
Figure 6-29. Site 4 surficial manifestation of liquefaction (Ishihara, 1985).....	90
Figure 6-30: Site 4 liquefaction analysis using Youd et al. (2001)	91
Figure 6-31: 2.612 factor of safety with rotational failure mechanic with static loading.....	94
Figure 6-32: 0.422 factor of safety with rotational failure mechanic with seismic loading	95
Figure 6-33: 2.323 factor of safety with block failure mechanic with static loading	96
Figure 6-34: 0.325 factor of safety with block failure mechanic with seismic loading.....	97
Figure 7-1: LPI for all sites with different methods	99
Figure 7-2: LSN for all sites with different methods	100
Figure 7-3: Predicted settlement for all sites with different methods.....	100
Figure 7-4: Predicted lateral spread for all sites with different methods	101
Figure 7-5: Kumamoto Plain geomorphological map with liquefaction sites. Circled sites are locations of former river channels (altered from Mukunoki et al., 2016).....	103
Figure A-1. Table explained the JMA Seismic Intensity Scale (JMA, 2019)	122
Figure A-2. Kumamoto City (KMM006) and Uto City (KMM008).....	123
Figure A-3. Upper 30 m average shear wave velocity from J-shis map.....	123
Figure A-4. Site Amplification Factor from J-shis map	124
Figure A-5. Observed soil liquefaction from GEER team (Kayen et al., 2017).....	124
Figure A-6: Japanese soil classification chart (translated to English)	125
Figure A-7: Observed soil liquefaction in Kumamoto City (Bhattacharya et al., 2018)	126
Figure B-1. Boring log for site 1.....	128
Figure B-2. Boring log for site 2-1	129
Figure B-3. Boring log for site 2-2	130
Figure B-4. Boring log for site 4.....	131
Figure B-5. Soil testing data for site 1	132
Figure B-6. Soil testing data for site 2-1	133
Figure B-7. Soil testing data for site 2-2.....	134
Figure B-8. Soil testing data for site 4	135

1 INTRODUCTION

The Kumamoto earthquake of April 2016 produced two foreshocks of moment magnitude 6.0 and 6.2 and a mainshock of 7.0, which should have been followed by widespread and intense soil liquefaction. A Geotechnical Extreme Events Reconnaissance team (GEER) led by Professor Rob Kayen of UC Berkeley was dispatched to the Kumamoto Plain –which is in Kumamoto Prefecture, the southern main island of Japan –immediately following the earthquake. The Japanese and U.S. engineers in the GEER team observed mostly minor and sporadic liquefaction, which was unexpected as the local site geology, known soil stratigraphy, and intensity of the seismic loading made the Kumamoto Plain ripe for soil liquefaction. The paucity and limited scale of liquefaction shows a clear gap in our understanding of liquefaction in areas with volcanic soils.

This study is a direct response to the GEER team’s preliminary findings regarding the lack of significant liquefaction. This study will attempt to explain the limited scale of liquefaction in the Kumamoto earthquake of 2016. The scope of my research is limited to only the Kumamoto Plain, on which Kumamoto City is located, and will exclude the Aso Caldera and areas farther away to the north and south (Figure 1-1). The Kumamoto Plain is mainly composed of volcanic sediments originating from the Aso Caldera and metamorphic and sedimentary rocks from the southernmost Median Zone mountain range. Conclusions from this report should not be applied

to other volcanic regions unless the regional differences are well understood, as volcanic soils can be unique to their regions.

I will first explain the theory behind soil liquefaction followed by a geological history of the Kumamoto plain, a discussion on volcanic soils, and a report of the liquefaction observed during the 2016 Kumamoto Earthquake. Next, I will present analysis and interpretation of test hole data that members of the GEER team and myself collected during a field expedition in the summer of 2017. I will also present the results of a cyclic triaxial testing performed at the University of Colorado, Boulder and a slope stability analysis at one of the test sites. I will conclude by discussing my results regarding the scarcity of soil liquefaction in the Kumamoto Plain and suggesting avenues of future research.



Figure 1-1. Scope of Kumamoto Earthquake liquefaction research highlighted in red. Image from Google Maps

2 LIQUEFACTION

Liquefaction is the temporary transformation of soil into a liquid state. If certain conditions are met, a soil subjected to a cyclic stress from an earthquake can build pore water pressure to the point where it is equal to the overburden pressure. At this point, a liquefied state is achieved until water can either escape or energy dissipate (Seed, 1982). Essentially, the soil transfers the overburden stress from the soil skeleton to the water. Water is incompressible and will be squeezed out, resulting in deformation and loss of soil strength to release built-up pressure, among other effects. In some rare instances, a soil may exhibit flow liquefaction, which is like a mudslide.

In this chapter, I will briefly explain the susceptibility of a soil to liquefaction, how liquefaction is initiated, and the effects of liquefaction on infrastructure and soils.

2.1 Susceptibility

Not all soil is susceptible to liquefaction. A soil first requires a minimum threshold of earthquake shaking to generate pore pressures. Then, several criteria must also be met for a soil to be considered susceptible to liquefaction, and many factors can completely remove the risk of liquefaction. A holistic view of a soil is needed because a soil's susceptibility to liquefaction is sensitive to each variable. The following criteria are key indicators of a soil's susceptibility to liquefaction.

2.1.1 Groundwater Depth

A soil must be saturated with water in order to liquefy. Liquefaction is a unique soil-water interaction. Typically, liquefaction occurs when the ground water table is only a few meters below the surface. If groundwater fluctuates, then the risk of liquefaction also fluctuates. Given that much of the Kumamoto Plain is covered with rice paddies, which are seasonally filled with water, the water table would have been near the surface. Publicly available boring logs confirm that ground water levels range from one to three meters below ground level in the Kumamoto Plain. Kumamoto is famous in Japan for having high ground water reserves and clean aquifers (Kumamoto City, 2015). There is also sufficient rainfall to regularly recharge the ground water, not to mention several large rivers in the area. The water levels were high enough for liquefaction to occur at any location across the Kumamoto Plain.

2.1.2 Geological

Young, freshly deposited soil is most susceptible to liquefaction. Late Pleistocene (10,000-130,000 years ago) and older sediments are more resilient to liquefaction while Holocene soils (10,000- present) are more vulnerable (Youd and Hoose, 1977). Loosely placed fill is the most susceptible. Time allows soil to cement, densify, and generate fines. Fluvial, colluvial, and aeolian deposits are also vulnerable and, in some instances, alluvial fan, alluvial plain, beach, terrace, playa, and estuarine deposits are vulnerable (Kramer, 1996). Younger and less compacted or weathered soils are also more susceptible to liquefaction (Youd and Hoose, 1977).

2.1.3 Historical

Seismic pre-shaking of a zone results in a decreasing risk of future liquefaction (El-Sekelly et al., 2017). Pre-shaking can refer to prior earthquakes or foreshocks. Each previous instance of

liquefaction allows a soil to build up a resistance to future liquefaction by way of densification; however, prior liquefaction will somewhat reset this process, though recovery speed from liquefaction is increased (Youd 1984; El-Sekelly et al., 2015). Pre-shaking reset was demonstrated during the 2011 Tohoku, Japan earthquake, in which many man-made and natural sites re-liquefied (Wakamatsu, 2012).

2.1.4 **Compositional**

Particle angularity and mineralogy that facilitate volume and density change increase susceptibility to liquefaction. Soils with rounded particles (commonly found in fluvial and alluvial environments) densify more easily than those with angular grains (Kramer, 1996). Rounded particles have lower maximum and minimum void ratios and can experience large volume and density changes. Angular soils tend to lock together and inhibit volume and density change and therefore are less susceptible to liquefaction unless the confining pressure is high (Vaid et al., 1985).

Fine grained material can impede particle rearrangement and reduce liquefaction susceptibility, though this relationship does have some exceptions, and soil plasticity is a better indicator for susceptibility to liquefaction. For example, non-plastic silts are fully capable of liquefying, indicating that particle size is less important than the plasticity of the soil (Ishihara, 1993; Bray & Sancio, 2006). Until recently, four Chinese criteria (Wang, 1979) were used to determine a fine-grained soil's susceptibility to liquefaction. The Chinese criteria are now discontinued in favor of the Boulanger and Idriss (2006) or the Bray et al. (2004) criteria. Soils with both high fines content and high plasticity are not susceptible to liquefaction. Figure 2-1 shows the limits of liquefaction susceptibility, as found by Boulanger and Idriss (2006). Bray et al. (2004) liquefaction susceptibility limits are shown in Figure 2-2. Boulanger and Idriss (2006)

set a plasticity index of seven and higher as not susceptible, with the four to seven range being possible, and less than four being susceptible. Bray et al. (2004) sets a plasticity index of 20 and above as not susceptible, 20 to 12 being possible, and less than 12 being increasingly susceptible. Bray et al. (2004) evaluates water content and liquid limit in conjunction with soil plasticity. Often times, both methods are used when evaluating liquefaction susceptibility of fine-grained soils. This paper will use the Boulanger and Idriss (2006) cutoff point of plasticity index of seven and higher as soil that is not susceptible to liquefaction for soils with significant fines content.

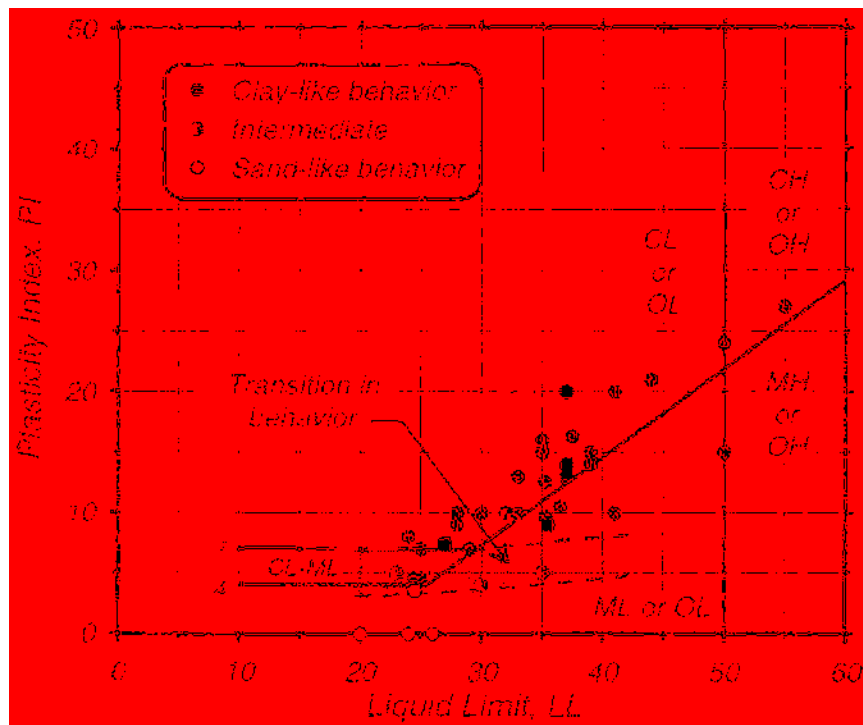


Figure 2-1: Liquefaction susceptibility criteria for fine-grained soils (Boulanger & Idriss, 2006)

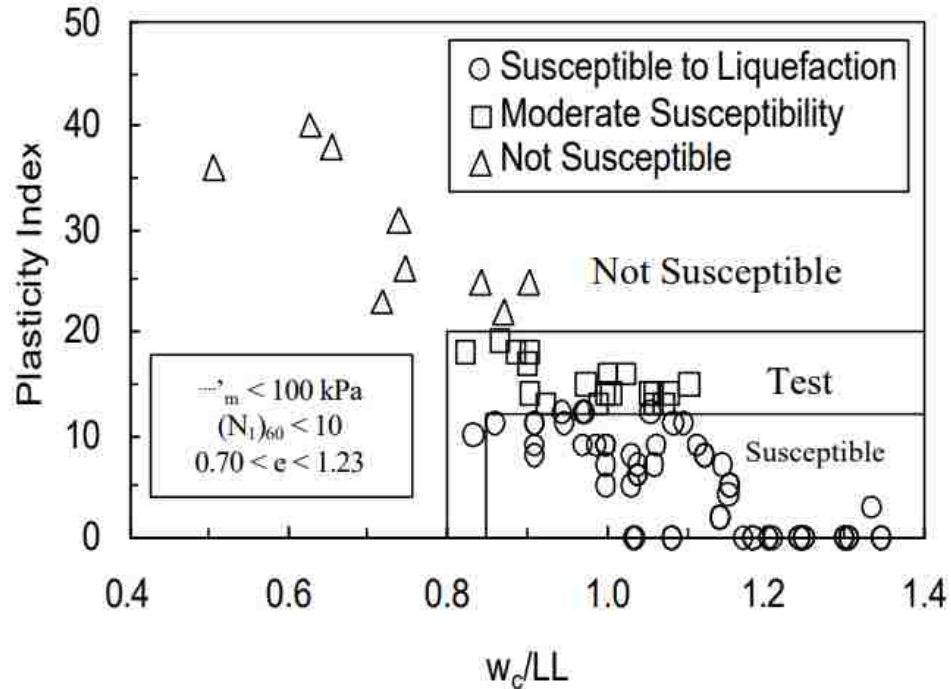


Figure 2-2: Liquefaction susceptibility criteria for fine-grained soils (Bray et al., 2004)

Materials with high relative density typically do not liquefy, since they dilate rather than contract with cyclic loading, which generate negative pore pressures (Cassagrande, 1936). Loose materials tend to generate positive pore pressures which lead to liquefaction. This concept is further explained in the initial state criteria section later in this chapter. Relative density is a poor predictor of the strength and behavior of crushable soils, such as pumice, and should be cautiously approached when considering susceptibility (Liu et al., 2015).

Soil classification is useful in providing an initial screening of suspect materials. Sands and silts can liquefy, while gravels and clays rarely liquefy. Sands experience high volume change, quickly generate pore water pressure, and usually have little to no plasticity. Silts are similar to sands when non-plastic and similar to clays when plastic (Boulanger and Idriss, 2006). Gravels dissipate pore pressures too quickly to exhibit liquefaction, unless the gravel is trapped between layers of impermeable materials such as clay. Sands with increasing gravel content also have

significantly increasing liquefaction resistance (Evans & Zhou, 1995). Clays, especially highly plastic clays, absorb and dampen much of the cyclic loading and tend to experience cyclic softening rather than liquefaction such as seen during the Adapazari, Turkey earthquake of 1999 (Boulanger and Idriss, 2006). Cohesion and inter-particle forces are significant with cyclic softening and so the effects of cyclic softening are much less significant than traditional liquefaction.

Well-graded soils are resistant to liquefaction, while poorly graded soils are more susceptible at lower relative densities. Well-graded soils have a wide distribution of particle sizes which fill voids, which at low relative densities hinder the generation of pore pressure (Vaid et al., 1990).

2.1.5 Initial State Criteria

Arthur Cassagrande (1936) found that soils tend to either dilate or contract to approach the same density, a point that he called the Critical Void Ratio (CVR). Soils strive to achieve equilibrium between loose and dense states. A loose material will naturally consolidate while a dense material will seek to expand and relieve stress. Cassagrande (1936) predicted that positive excess pore pressures are generated in loose soils and negative excess pore pressures in dense soils (Kramer, 1996). With this information, Cassagrande (1936) theorized the CVR line, which marked the difference between contractive and dilative behavior. The CVR line did not, however, hold true under undrained conditions as shown during the 1938 Fort Peck dam failure, where excess pore water pressures were generated and were unable to dissipate during the construction of the dam. While the concept of the CVR line was theoretically solid, there was something not accounted for in the theory.

Cassagrande's PhD student, Castro (1969), continued research on sands and corrected Cassagrande's CVR line. After the 1964 Alaska and Niigata, Japan earthquake liquefaction events, Castro went on to study the liquefaction of sand. Newer testing equipment allowed higher accuracy and improved methods of testing liquefaction phenomena. The corrected CVR line was developed from liquefied sand and had the line plotted below but parallel to the old CVR line and is known as the Steady State Line (SSL) (Castro 1969). The CVR and SSL lines are shown in Figure 2-3.

Non-susceptible materials under the SSL will generate negative pore pressures instead of positive pore pressures as shown in Figure 2-4 (Kramer, 1996). They will dilate and increase in strength. Susceptible materials above the SSL—such as a loose sandy— will generate positive pore pressures and will separate and liquefy. The soil will experience a sudden drop in strength. Medium dense sand will initially generate positive pore pressures which quickly become negative pore pressures through a process called phase transformation. Medium dense sand may experience partial liquefaction (Kramer, 1996). The initial density of a soil is critical in determining susceptibility to liquefaction.

The position of the SSL is unique to a soil and is dependent on its density, gradation, particle angularity, and other compositional criteria. While useful, finding the SSL of a soil requires specialized lab equipment and can be time consuming and expensive. In addition, in-situ soil conditions must be closely replicated for accurate results. Different testing procedures will yield slightly different values for the SSL (Vaid et al., 1990).

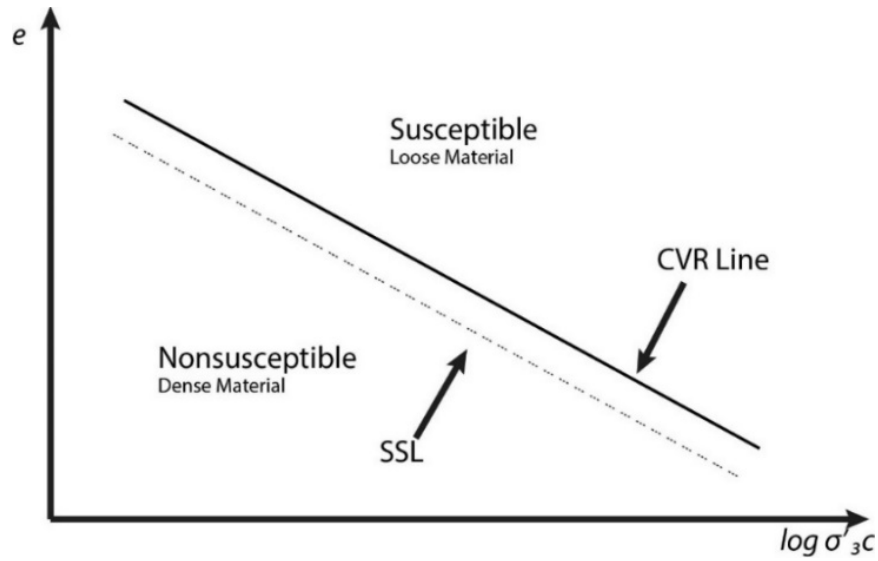


Figure 2-3: Initial State Criteria. Drawn after Kramer (1996)

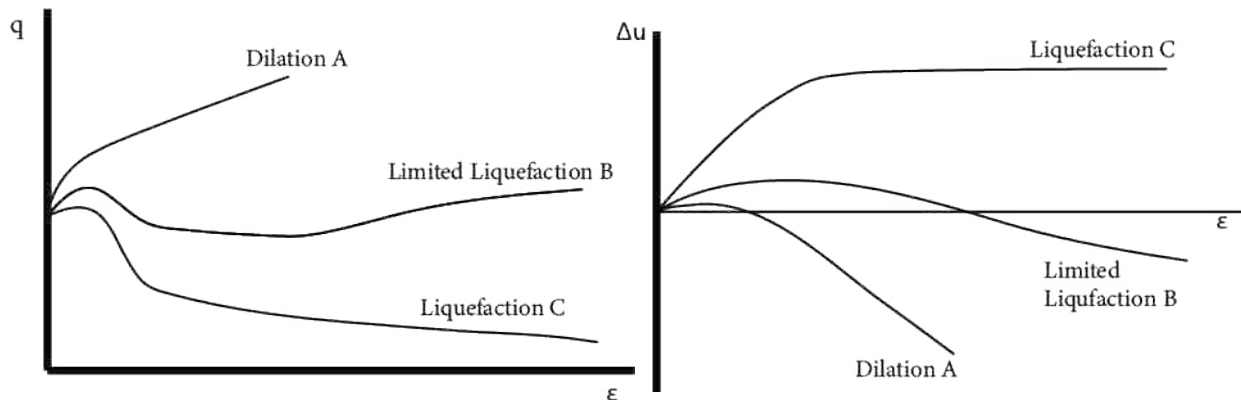


Figure 2-4: Effects of density, A being most dense, C being loosest, on liquefaction. Drawn after Kramer (1996)

2.2 Initiation

The initiation of liquefaction is considered after a soil is determined to be susceptible to liquefaction. A susceptible soil must be strained or stressed enough to induce liquefaction. If the cyclic stress on a soil is weak or short in duration, a susceptible soil may not reach a point of liquefaction. There are two types of liquefaction: flow liquefaction and cyclic mobility. If the

initial static stress is greater than the Steady State Point (SSP), the soil might flow liquefy as shown in Figure 2-5, panel b (Kramer, 1996). The soil will reach the SSP and will have less strength than the initial static stress. If the initial static stress is less than the SSP, the soil might be susceptible to cyclic mobility as shown in Figure 2-5, panel c. In cyclic mobility, the stress profile does not reach the SSL, but reaches a point of zero stress and oscillates between positive and negative stress states (Kramer, 1996).

Proximity to earthquake epicenters is essential when considering liquefaction initiation (Ambraseys, 1988). Liquefaction cannot occur without some sort of cyclic stress, which for this research is the earthquake ground motions. The ground motions alone are responsible in generating positive pore water pressure. At a certain distance, the ground motions are too minor to cause a significant enough rise in pore pressures. Of note, some subduction zone events can cause liquefaction in distant areas, such as the 2011 Tohoku, Japan earthquake, which caused liquefaction in sites in Tokyo, over 300 km away.

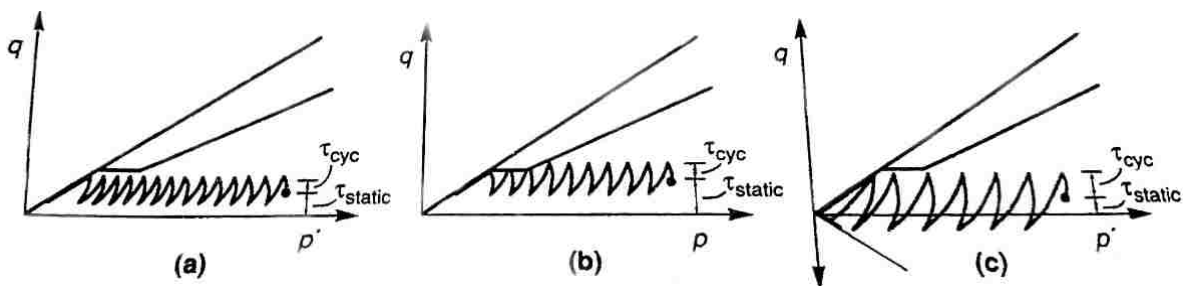


Figure 2-5: Types of liquefaction failure. a) No liquefaction, b) flow liquefaction, and c) cyclic mobility (Kramer 1996)

Soils will tend toward the SSP when undergoing large strains (Kramer, 1996); however, the stress paths of soils will vary as shown in Figure 2-6 (Kramer, 1996). Points below the SSL will dilate until they reach the SSP. Points above the SSL will have a contractive behavior. The peak of the contractive curves is called the flow liquefaction surface and is represented by the dashed line (Kramer 1996). When the flow liquefaction surface is reached, the soil rapidly loses strength and converges to the SSP passing a point of no return and flow liquefying.

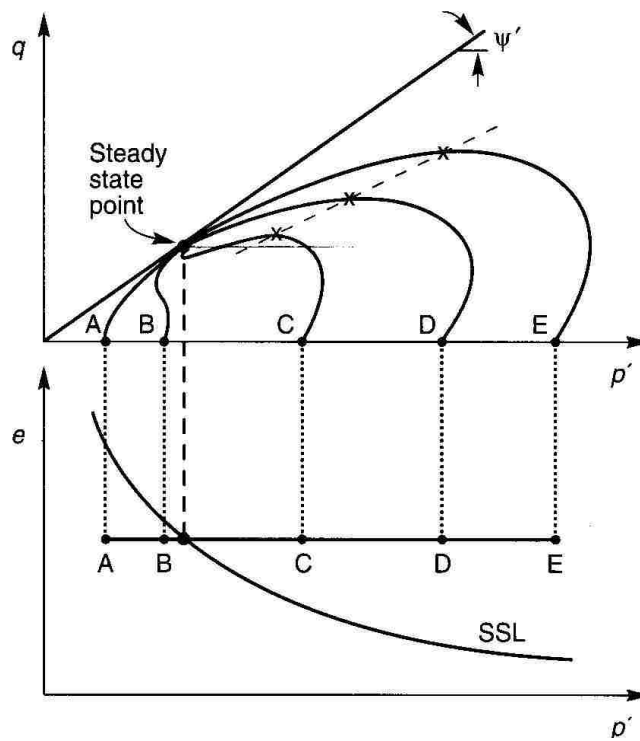


Figure 2-6: Flow liquefaction surface (dashed line) and SSL (Kramer 1996)

Cyclic mobility results from the generation of pore water pressure from cyclic loading. Given enough time and intensity, a soil may generate large enough pore pressures to where the effective stress of the soil becomes zero. The soil will oscillate around zero strength and accumulate large strains. However, a fine-grained soil will still maintain cohesive force, which will greatly hinder the initiation of liquefaction.

2.2.1 Methods for Predicting Liquefaction Initiation

There are multiple methods that use different soil properties to determine liquefaction initiation. Most methods use clean silica sands to determine correlations and should be used cautiously when dealing with natural deposits that differ significantly from silica sands. Example materials are calcareous and volcanic sands. However, most methods have been calibrated over time to include other sands and soil types and should have a reasonable degree of accuracy. The following section will describe the most common methods in both practice and research.

The cyclic stress approach is a popular method used in the United States and was pioneered by Harry Seed and others at the University of California Berkley (Seed, & Idriss, 1971). The cyclic stress approach estimates a cyclic stress ratio (CSR) with equation 2-1, which represents earthquake motions. A Cyclic Resistance Ratio (CRR) is estimated with equation 2-2, which corrects SPT blow counts and accounts for both earthquake proximity with a magnitude scaling factor (MSF) and overburden correction with K_σ . CRR equations are available for CPT and other methods as well (Idriss & Boulanger, 2012; Boulanger & Idriss, 2014; Robertson & Wride, 1998; Youd et al., 2001; Robertson, 2009). A factor of safety against liquefaction, given in equation 2-3, is defined as the ratio of CRR to CSR, with a value of one and above indicating no liquefaction. Pore pressures will still generate and lower the strength of the soil, but this will be less damaging than full liquefaction (Boulanger & Idriss, 2007). Typically, stress is used to compute the CSR because although there is a stronger correlation with cyclic strains, the difficulty in computing strains makes the stress approach more practical.

$$CSR = 0.65 \frac{\sigma_v}{\sigma'_v} \frac{a_{max}}{g} r_d \quad 2-1$$

$$CRR = \exp\left(\frac{(N_1)_{60cs}}{14.1} + \left(\frac{(N_1)_{60cs}}{126}\right)^2 - \left(\frac{(N_1)_{60cs}}{23.6}\right)^3 + \left(\frac{(N_1)_{60cs}}{25.4}\right)^4 - 2.8\right) \cdot MSF \cdot K_\sigma \quad 2-2$$

$$F.S. = \frac{\text{Cyclic Resistance Ratio}}{\text{Cyclic Stress Ratio}} = \frac{CRR}{CSR} \quad 2-3$$

The CSR value in equation 2-1 can also be acquired through ground response analysis which requires field testing and time history generation (Kramer, 1996). A ground response analysis applies soil conditions to a time history to determine average cyclic shear stress. Ground response analysis is difficult and complicated so a simplified method is commonly used (Seed and Idriss, 1971). The simplified method is shown in equation 2-1 and assumes shear stress to be 0.65 of the Peak Ground Acceleration (PGA). The simplified method compares well with the more complicated method. Publically available PGA models and predictions can be used to determine PGA such as those provided by the USGS.

One method to find the CRR is to test an undisturbed soil sample in the laboratory. The undisturbed soil sample is liquefied and the resistance to liquefaction is directly measured, corrected, and correlated to get a CRR. Laboratory testing to acquire CRR is slow, expensive, and difficult to do. Another method is described by Seed and Idriss (1971) and more recently Idriss and Boulanger (2012) and Boulanger and Idriss (2014). A CRR is found by normalizing SPT values, a simple, practical, and widely practiced method that has also been developed for CPT cone tip resistances. Fundamentally, all methods rely on soil relative density to calculate liquefaction initiation.

Shear wave testing is a less common method used to test for liquefaction initiation of soils but is a good companion test to a CPT analysis. The average shear wave velocity of the soil profile is determined using geophones and some form of wave generator. Shear wave testing is

the least conservative of the methods and requires a specialized operator for any degree of reliability (Kayen et al., 1992). The benefits of the shear wave test are: it is non-destructive to the soil, it can be quickly done, it is based on correlations independent of SPT/CPT, it directly measures a dynamic soil property, and it can be used for soils other than clean sands with good accuracy (Tokimatsu & Uchida, 1990). Therefore, this method of analysis may be beneficial in a volcanic setting such as Kumamoto. Unfortunately, this method does not allow for sample retrieval, which makes determining susceptibility criteria difficult. Shear wave testing indirectly relies on soil relative density to compute liquefaction initiation but should be compared to a CPT analysis for reliability (Kayen et al., 1992).

An energy dissipation approach that combines SPT correlations with earthquake energy and distance from source is also used to compute liquefaction initiation (Kramer, 1996). The energy dissipation approach is easier to apply than the simplified procedure, is more reliable, and applies energy felt by the water in the area into liquefaction potential (Law et al., 1990; Figueroa et al., 1994). The difficulty in comparing the dissipated energy with the seismic wave energy makes the approach unpractical for projects. The energy dissipation approach performs better than stress based methods when the earthquake acceleration is very low (Kokusho et al., 2015).

The effective stress-based response analysis approach is also currently being used and refined (Kramer, 1996). A constitutive model is applied to the soil to predict liquefaction based on the stress-strain response and pore pressure generation. The effective stress-based response analysis is a numerical approach that relates effective stress of the soil to liquefaction. The advantages when compared to other initiation approaches are that nonlinear ground response and dynamic response analysis become possible allowing for complex computer modeling and simulation (Kramer 1996). Because constitutive models for soil require significant calibration

and validation, there is considerable difficulty in acquiring the right parameters for the model (Kramer, 1996).

The final method that will be discussed is the probabilistic approach. The probabilistic approach attempts to account for the uncertainty in the earthquake ground motions and is used with the cyclic stress approach (Kramer, 1996). The probabilistic approach is a further refinement of the cyclic stress approach which allows for more realistic application of liquefaction analysis. The probabilistic approach is especially useful in low seismicity zones where computed maximum PGA may make foundation design impractical.

2.3 Liquefaction Effects

Soil liquefaction was first reported during the 1964 Niigata, Japan and Alaska earthquakes, and has been extensively studied since. Although earthquake engineering has significantly advanced with the advent of the seismograph, these earthquakes caused the soil, not steel and concrete, to fail. Not all earthquakes result in major liquefaction, but some liquefaction typically occurs in every sizeable earthquake. Minor liquefaction in earthquakes is not surprising. Some recent earthquakes with major liquefaction are the 2011 Tohoku, Japan and 2011 Christchurch, NZ earthquakes. Figure 2-7 provides an illustration of a soil that has liquefied (Seed & Idriss, 1982). There is a gradual increase in pore pressure followed by an abrupt change in shear strain and strength (Seed & Idriss, 1982).

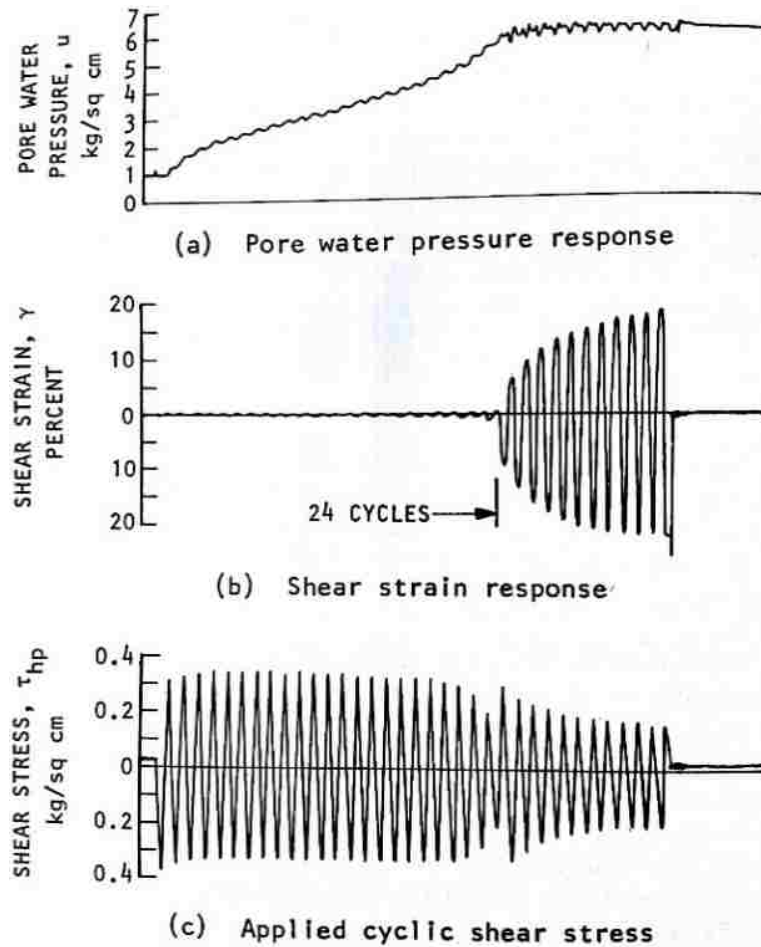


Figure 2-7: Cyclic loading test of loose sand (Seed and Idriss, 1982)

In Niigata, Japan, the Showa bridge and many buildings were severely damaged by earthquake-induced soil liquefaction. Likewise, bridges and roadways in Alaska during the 1964 Alaska earthquake were damaged or destroyed by lateral spread (McCulloch, 1970).

Liquefaction is both destructive to infrastructure and expensive to repair. Figure 2-8 illustrates a surface representation of liquefaction under a pavement (Youd, 1984). Liquefaction only causes significant damage if the earthquake magnitude is large and the soil conditions are just right, otherwise other earthquake hazards will dwarf the impact of liquefaction. The following section will list several liquefaction-induced hazards.

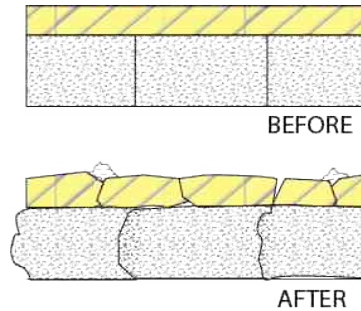


Figure 2-8: Example of ground oscillation, modeled after Youd (1984)

2.3.1 Liquefaction Hazards

Perhaps the most common liquefaction hazard is the sand boil, a phenomenon in which a liquefied soil layer releases pore pressure by cracking through a surface layer and leaving behind a sand volcano or gaping hole. Sand boils are often accompanied by large depressions filled with water and soil from layers that were eroded. Oftentimes, the edges of foundations are perfect exits for water and will have sand boils. See Figure 2-9 for an picture of a sand boil from Kumamoto City that was dark and contained pumiceous materials (Kayen et al., 2017). The dark color of the soil is typical of the Kumamoto volcanically derived soils.



Figure 2-9: Sand boils on side of house in Kumamoto, showing volcanic material that was plastic and pumiceous in origin (Kayen 2017)

A worst-case scenario for liquefaction is a flow liquefaction which is like a slow mudslide. These events are rare but can cause serious damage and may lead to injury, something that is uncommon in soil liquefaction. A similar but less serious phenomenon is lateral spreading, which is when a soil layer under a sloped surface liquefies. Liquefied slopes can spread out laterally for several feet. Eventually the soil stabilizes but retains a lurched slope appearance. Usually any road on top is destroyed and levees are left vulnerable to erosion and collapse. Lateral spread tears apart roads, levees, and hillsides and is expensive and time consuming to repair.

Ground oscillation and settlement is also common where liquefaction occurs (Kramer, 1996). Differential deformation due to loss of bearing capacity leads to ground oscillation, manifesting itself as random cracking and settlement. Large settlement of the ground surface can occur due to displacement of water. When a soil liquefies, the particles rearrange to reach the SSL. Volumetric reconsolidation and the physical exit of water by way of sand boils reduces the void ratio of the soil. Shear failure in the soil due to loss of strength can also manifest itself through ground settlement.

Loss of bearing capacity is another symptom of liquefaction. Excess pore pressure pushes the effective stress of the soil to zero which causes structures to settle and tilt extensively along with the soil around them. Deep foundations can mitigate this risk to the building, though the ground around the structure will still settle. Pile foundations can deform and structures may experience structural damage.

Buoyant rise of buried structures is a telltale sign of liquefaction. Buried pipes and structures are less dense than the soil and will rise to the top of the soil when the soil liquefies. After pore pressures dissipate, the buoyant structures will not have time to sink back into their

original place. Buoyant structures will be torn from their pipe systems and cause ruptures in lifelines. Buried structures have only recently been design for earthquake shaking and liquefaction and will typically need to be replaced, a process that is expensive and disruptive to relief efforts (Kitaura & Miyajima, 1996). Jutting protrusions in pavements are a good indicator of a buoyant structure that has uplifted. Many manholes and pipes have been placed in loosely compacted fill so this phenomenon is often seen in earthquakes.

3 GEOLOGY AND GEOTECHNICS

Geology and geotechnical engineering must both be thoroughly understood to holistically understand a region's soil and history. Such understanding is especially useful in Kumamoto, a geologically complex and young area. Karl Terzaghi, the father of soil mechanics, once said that, "... soils are made by nature and not by man, and the products of nature are always complex... As soon as we pass from steel and concrete to earth, the omnipotence of theory ceases to exist." (Goodman, 1999) A thorough understanding will aid us when retracing the assumptions made by the GEER team (Kayen et al., 2017) and in determining the paucity of liquefaction.

In this section, I will describe the basic geology of Kyushu Island, on which Kumamoto is located. Then, I will describe the Kumamoto Plain and the lively geological processes that have been occurring since the Quaternary Period, followed by the tectonic setting of the region. A large geological map of the study area will be provided at the end of the chapter as Figure 3-12 and Figure 3-13. An interactive version of the map —called GeoNavi —is also available through the Geological Survey of Japan (Naito, 2014).

3.1.1 Kyushu Island

Kyushu Island is a subtropical region with mild winters and warm and humid, but not hot, summers. Rainfall is high and there are two rainy seasons. Kyushu Island is composed of mountains, with the highest peaks at a height of 3,600 m, and the occasional coastal plain (National Environmental Agency, 2018). Kyushu Island is particularly famous for its many

volcanoes, both dormant and active. Several volcanoes such as Unzen, Aso, and Sakurajima are still active and regularly emit ash. Volcanoes and mountains dominate the landscape, and large population centers are located on the coastal plains of the region, away from the mountains. Small villages pocket the landscape, but the mountainous terrain makes large scale development difficult. Volcanism is the most important geological feature of Kyushu Island and has been for the last several million years (Hashimoto, 1991). Kyushu geology can be divided into two segments: the Inner Side and the Outer Side. The Inner and Outer Sides are separated by a mountainous boundary known as the Median Zone, shown in Figure 3-1. The Inner Side faces the Sea of Japan and the older Outer Side faces the Pacific Ocean. The Kumamoto Plain is located on the Inner Side of Kyushu. Many major faults lie across the Median Zone, and there is significant metamorphic rock generation rather than the typical volcanism found throughout the Kumamoto Plain (Hashimoto, 1991).



Figure 3-1: Kyushu Island, Japan with geological Median Line. Image from Google Maps

The geological history of Kyushu Island is storied with many different phases of development. For the reader's benefit, a reference to geological time is provided in Table 3-1 (Alan, 2006). Figures 3-2 through 3-5 illustrate the geological development of the Kyushu region with the Kumamoto Plain highlighted by the yellow box (Hashimoto, 1991). Figure 3-2 shows the initial development of the Median Zone which holds most of the oldest rocks in Kyushu Island. Pre-Cretaceous Period Kyushu Island was composed chiefly of carbonate and marine sediments (Naito, 2014). However, during the Cretaceous Period, the Inner Side started to building-up with non-marine and volcanic sedimentation. The Outer Side started to experience some volcanism but mostly maintained its marine sedimentation (Takai, 1963). Most granites and rhyolites were formed during the Cretaceous and Paleogene Periods.

During the Neogene Period, volcanic sedimentation started on both Inner and Outer Sides of Kyushu Island (Takai, 1963). The Pleistocene Period was eclipsed by a complex mix of volcanism, terrace deposits, and soft and unconsolidated sediments. Large pyroclastic flows from volcanoes, like Mt. Aso, repeatedly coated large areas of Kyushu (Hashimoto, 1991). Coarse clastics, or weathered rocks, are dominant in non-volcanic sediments, but volcanic sediments are intercalated with layers of ash and marine sediments (Hashimoto, 1991). Current day Kyushu is primarily composed of older, weathered volcanic soils called "shirasu" on the Outer Side along with marine sediments and weathered rock. The soils on the Inner Side predominately originate from the massive Mt. Aso volcano. Quaternary Period sediments were few relative to pyroclastic deposition, as illustrated in Figure 3-5.

Table 3-1: Geological time adapted from Geology for Engineers and Environmental Scientists (Alan, 2006)

Era	Period	Epoch	Duration in Millions of Years	Millions of Years Ago	
Cenozoic	Neogene	Quaternary	Holocene		Current
			Pleistocene	3	
			Pliocene	4	3
	Paleogene	Tertiary	Miocene	19	7
			Oligocene	12	26
			Eocene	16	38
Mesozoic	Cretaceous		71	65	
	Jurassic		54	136	
	Triassic		35	190	
Paleozoic	Permian	Pennsylvanian Mississippian	55	225	
	Carboniferous		65	280	
	Devonian			345	
	Silurian		50	395	
	Ordovician		35	430	
	Cambrian		70	500	
			70	570	

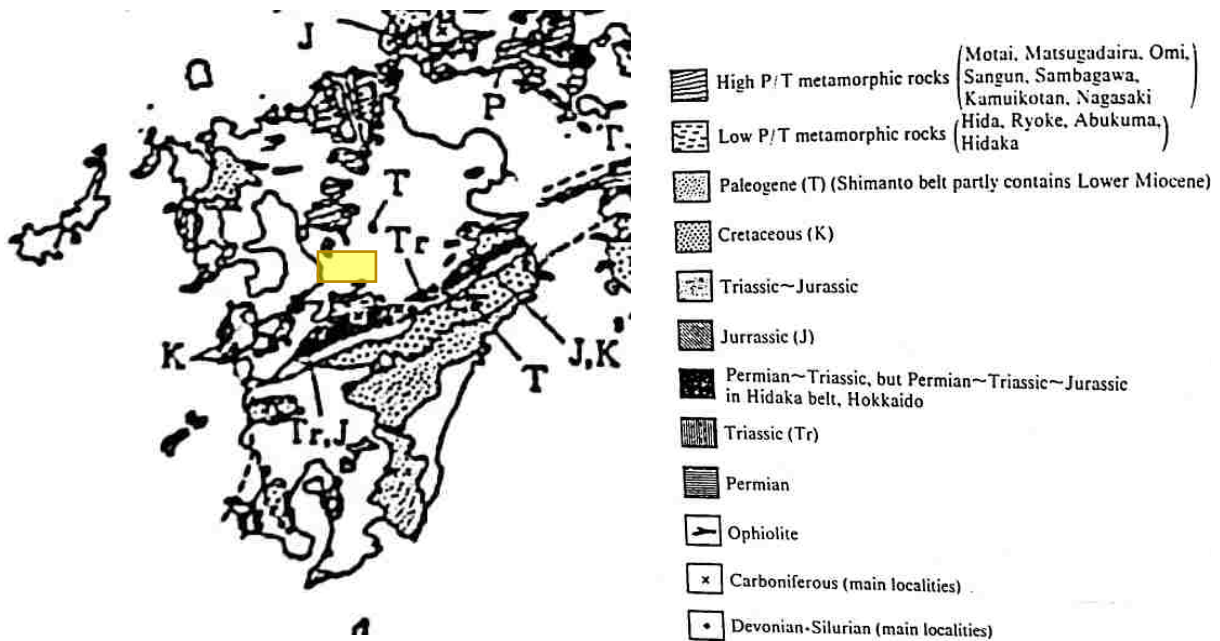


Figure 3-2: Map of Kyushu, Japan: Sedimentary and metamorphic rocks older than Neogene Period. Yellow box shows the boundaries of the study area (Hashimoto 1991)

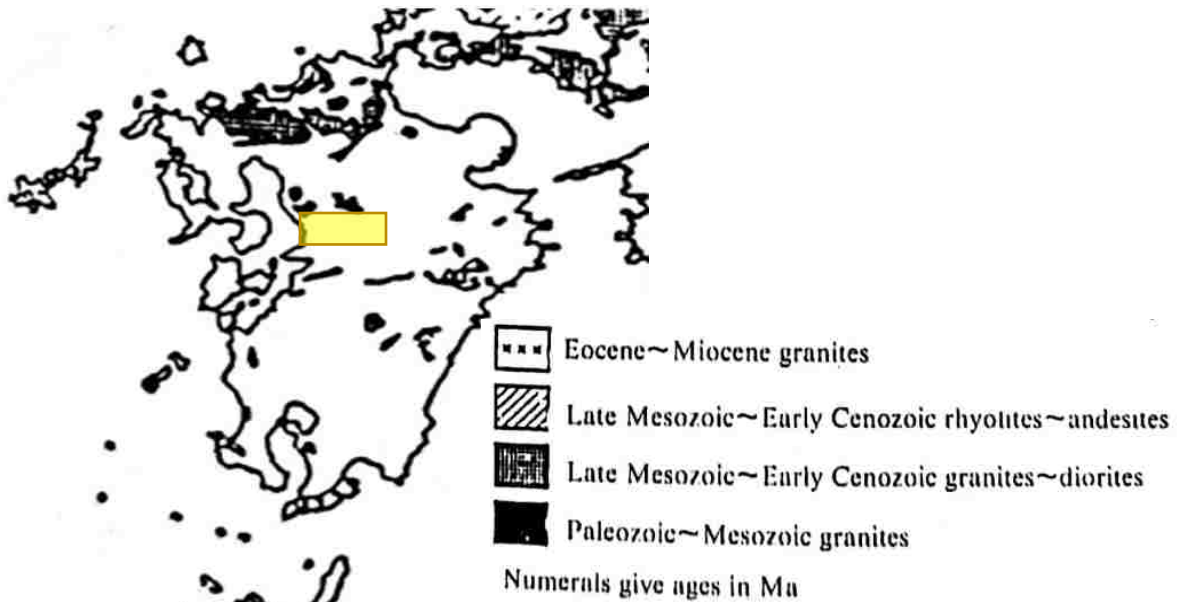


Figure 3-3: Map of Kyushu, Japan: Granites and rhyolites. Yellow box shows the boundaries of the study area (Hashimoto 1991)

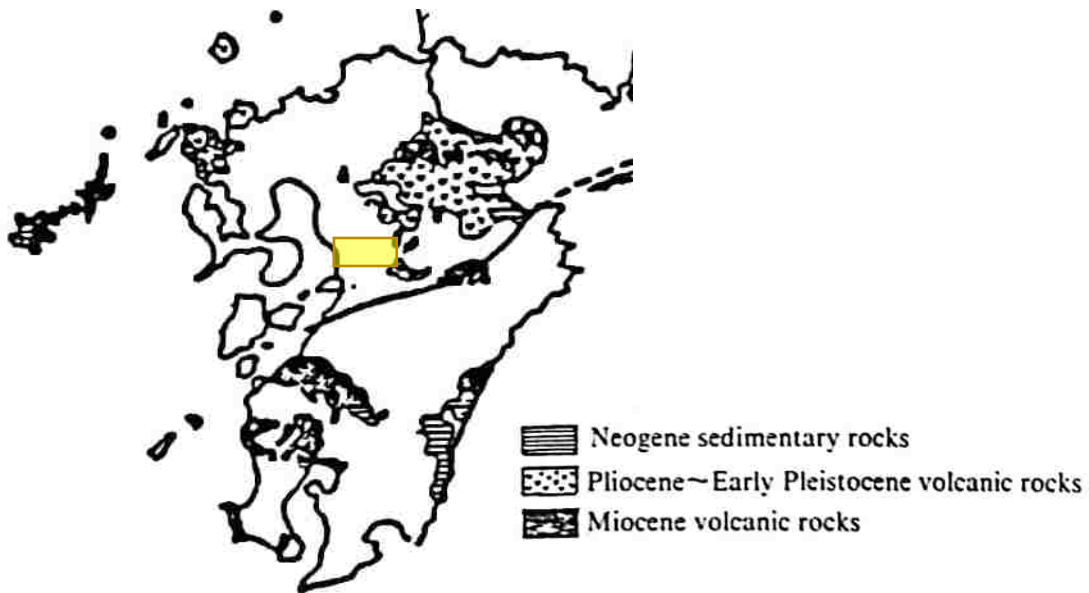


Figure 3-4: Map of Kyushu, Japan: Sedimentary and metamorphic rocks of Neogene Period. Yellow box shows the boundaries of the study area (Hashimoto 1991)

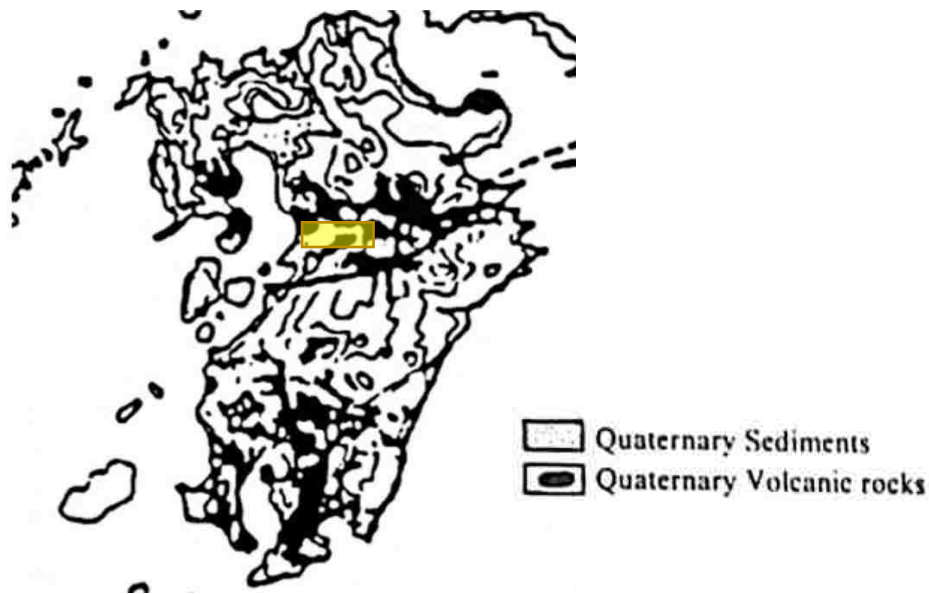


Figure 3-5. Map of Kyushu, Japan: Quaternary Period sediments and volcanic rocks. Yellow box shows the boundaries of the study area (Hashimoto 1991)

3.1.2 The Kumamoto Plain

The Kumamoto Plain is a young alluvial deposit, located between Mt. Aso and Ariake Bay (also known as Shimabara Bay). A general map of the region with major river labels and minor tributaries drawn is provided in Figure 3-6. Kumamoto city receives around 1,000 – 1,500 mm of rainfall per year with an air temperature of 8°C – 30°C in the summer (Kumamoto Prefectural Government, 2009).

High precipitation in the Caldera forms the Shirakawa River which flows down through Kumamoto City. The Midorikawa River and Kase River flow through the southern portion of the plain. The Midorikawa River flows through southern volcanic soils and from the Median Zone, thus carrying metamorphic rock, marine sediments, sandstone, and volcanic sediments (Naito, 2014). Studies by Ideue and Watanabe (2012) confirmed that the gravel beds of the Midorikawa River were composed of welded tuff, a volcanic deposit from the slopes of Mt. Aso. Ideue and

Watanabe (2012) also found a significant amount of sandstone sand along the river banks. The Kase River is an amalgamation of many small streams on the Aso terrace and cuts through some sandstone and mudstone deposits (Naito, 2014). Both the Midorikawa River and Kase River have a considerable amount of non-volcanic alluvium. The Shirakawa, Midorikawa, and Kase Rivers regularly flood and deposit suspended fine clay, silt, sand, and organic matter on the Kumamoto Plain, which is also considered to be a floodplain.

Volcanic ash is easily weathered through flooding and high rainfall. Thus, the plains are filled with weathered volcanic flood sediments. The freshest parent materials are found in the Aso Caldera or on the Aso terraces. Due to the subtropical environment, precipitation and chemical weathering is the primary contributor to the plain due to a short freeze-thaw cycle during the winter in Mt. Aso. In addition to the natural deposition of sediments on the plain, 420 years ago the feudal lord of the city, Kiyomasa Kato, irrigated the plain to create rice paddy fields and altered the natural hydrologic structure of the plain (Kumamoto City, 2015).

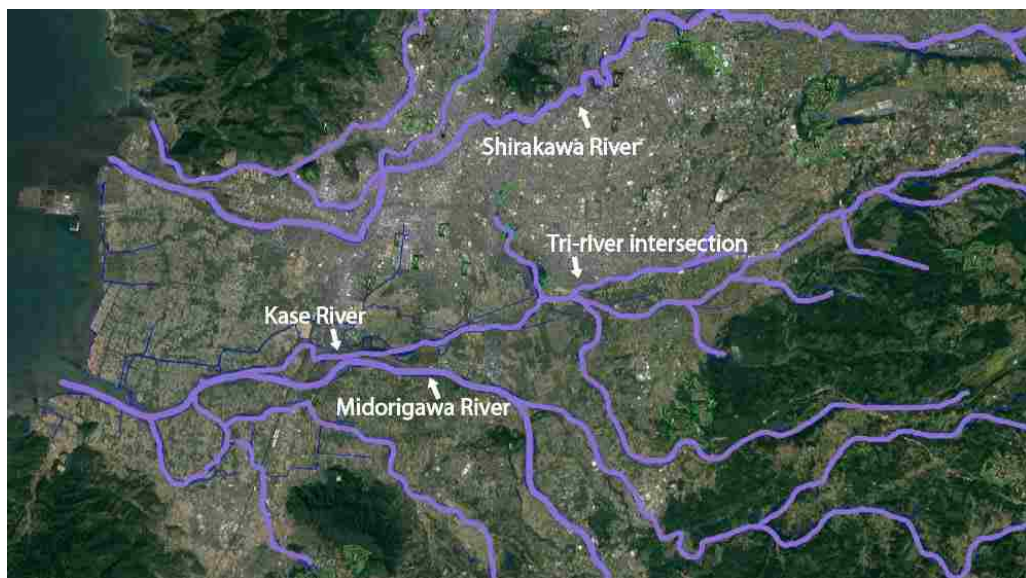


Figure 3-6: Image of the Kumamoto Plain river system, with key rivers labeled, shown in teal (GSI, 2018)

To the west of the Kumamoto Plain is the active volcano Mt. Unzen, separated from Kumamoto by Ariake Bay. Mt. Unzen is active to this day with periodic pyroclastic flows and ash falls. Mt. Unzen only affects the Kumamoto Plain through ash falls from eruptions. The wind flows from west to east, so the soils of Kumamoto may be lightly intercalated with ash from Mt. Unzen. Residents during the 1991 Unzen eruption experienced rainfall mixed with pumice ash (Watanabe et al., 1999).

Ariake Bay, located west of the Kumamoto Plain, previously contained fresh water when sea levels were lower 10,000 years ago (Ariake Bay research group, 1965). Due to rapid sea level rise 6,000 years ago, this area became salinized (Ota et al., 1982). The sudden rise in water level is shown in Figure 3-7 (Ota et al., 1982). The range of this marine deposition is illustrated in Figure 3-8 (Otsubo et al., 1995).

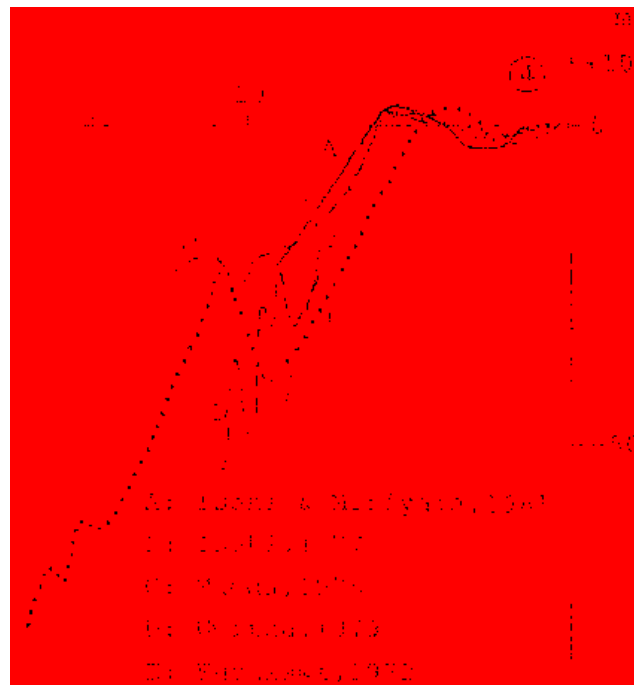


Figure 3-7: Western Japan sea level fluctuations during the last 15,000 years (Ota et al., 1982)

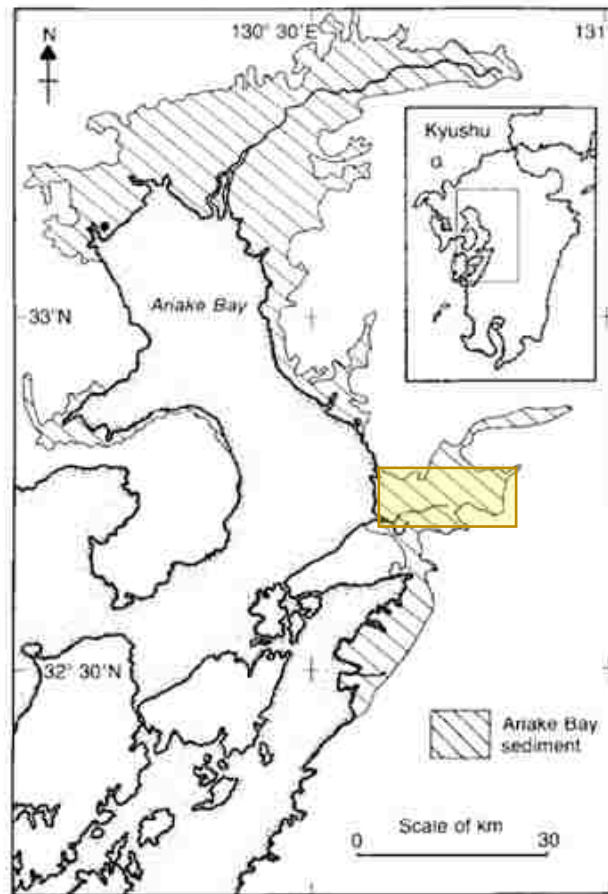


Figure 3-8: Ariake Bay sediments with Kumamoto Plain highlighted. Yellow box shows the boundaries of the study area (Otsubo et al., 1995)

Ariake Bay is filled with smectite quick clays, on top of the Aso-4 pyroclastic flow deposit (Egashira & Otsubo 1982, Katsuaki 2005). For this reason, the western coast of Kumamoto, which is reclaimed land, is rural farmland due to its poor soil foundation. Between 10 to 24 meters underneath the fill material, Ariake clay sediments are found, though at this depth they are less sensitive due to pumping of groundwater and river water leaching of salts (He et al., 2014). Ariake clays are less significant farther away from the bay, as the clay stratum rapidly diminishes in thickness and depth.

The Kumamoto Plain is underlain by massive pyroclastic flow deposits and ash falls from the Aso Caldera. Four massive pyroclastic flows occurred from 300-90,000 years ago and make up the bulk of the ground of the Kumamoto Plain (GSJ, 2018). The alluvial sediments of the latest geological event, Aso-4, composes the bulk of the upper surface of the Kumamoto Plain. The surface manifestations of the Aso-4 pyroclastic flow are shown in Figure 3-9. Most ash fall from Mt. Aso was deposited to the east of the Caldera, but the flows reached past the coast in the west. There are regular ash falls and eruptions, though most of them are minor (Saito, 1968). The last eruption is classified as ongoing and the main cone still emits ash and smoke. There is a regular magma discharge of 1.5 km³/ky, renewing the Aso Caldera with volcanic material. Many pumice layers were deposited at 2,500-year intervals far beyond the edge of the Caldera (Miyabuchi, 2009). The latest major Aso ash fall was in 1979, when tephra damaged crops in three adjacent prefectures including the Kumamoto Plain (Japan Meteorological Association, 2013).



Figure 3-9: Aso-4 pyroclastic flow distribution. Yellow box shows the boundaries of the study area (GSJ, 2018)

Bordering the northern fringe of the Kumamoto Plain is the inactive volcano Mt. Kinpu. Mt. Kinpu is quite old relative to the Kumamoto Plain and is composed of basalt lava, andesite, basaltic andesite lava, and pyroclastic rocks. To the south of the Kumamoto Plain are also a few small inactive volcanoes which have weathered to small hills in present time. These inactive volcanoes are the oldest geological features of the Kumamoto Plain, reaching back to the Mesozoic Period, and are made of marine & non-marine conglomerate. They contribute little to the overall plain stratigraphy. To the southwest of the plain is the Amakusa Island Chain, a peninsula that is composed of andesite, basaltic andesite lava, and pyroclastic rocks.

In the Kumamoto Plain, some of the soils are angular as opposed to the expected rounded particles (Kayen et al., 2017). Rounded particles are typical in alluvial deposits since river transport naturally rounds soil grains. Angular soils are typical with volcanically derived soils due to their glassy material composition which is brittle and fractures easily (Shoji et al., 1993). Volcanic soils will be further discussed in the next chapter.

3.2 Regional Tectonic Setting

The Futagawa-Hinagu fault zone –shown in Figure 3-10 –is the primary tectonic mechanism in the Kumamoto Plain. The fault zone is created from the EW compression of the Philippine Sea plate and the N-S extension of the Central Kyushu rift (Okumura, 2016). The Futagawa-Hinagu fault zone is an unusual extensional system associated with normal faulting and active volcanism (Kayen et al., 2017). The Futagawa and Hinagu faults separate the north movement from the south and have an oblique, strike slip and normal-down-to-north slip movement (Kayen et al., 2017). The Kumamoto Plain is predicted to have a subsidence rate of 0.45 mm/year in the eastern part and 0.90 mm/year in the western part (Ishizaka et al., 1995). See Figure 3-11 for a large-scale plate movement map (Kato et al., 2016).

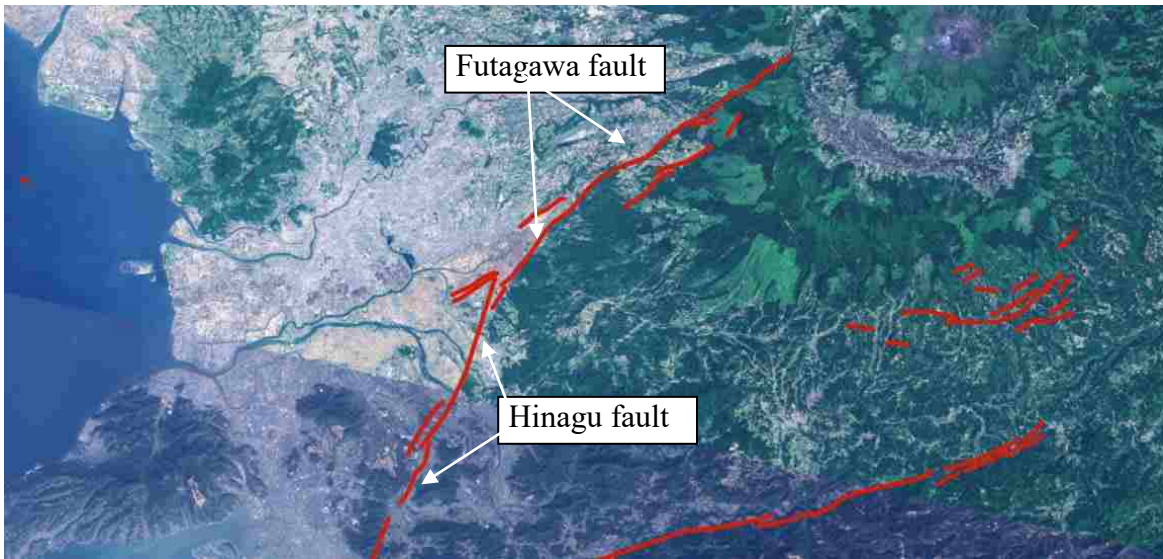


Figure 3-10: Faults near the Kumamoto Plain (GSJ, 2018)

The Kumamoto Plain experienced a major earthquake of seismic intensity five or above in 1889, just after the formation of the Seismological Society of Japan. Seismic intensity is based on the Japanese scale, which is provided in Appendix A-1 (GMA, 2019). Unusual soil alterations from the earthquake, which researchers later concluded was liquefaction, was reported in former river channels and, to a lesser extent, in natural levees. Liquefaction seems to have been a minor concern in the earthquake given the high intensity ground motions. Most damage came from structural collapse and fires (Kuribayashi & Tatsuoka, 1975; Akiyoshi & Fuchida 1998; Wakamatsu, 2000). The most geologically vulnerable zone from this earthquake seems to have been the man-filled former river channels. These river channels were flowing in the central Kumamoto City, near the Kumamoto Castle.

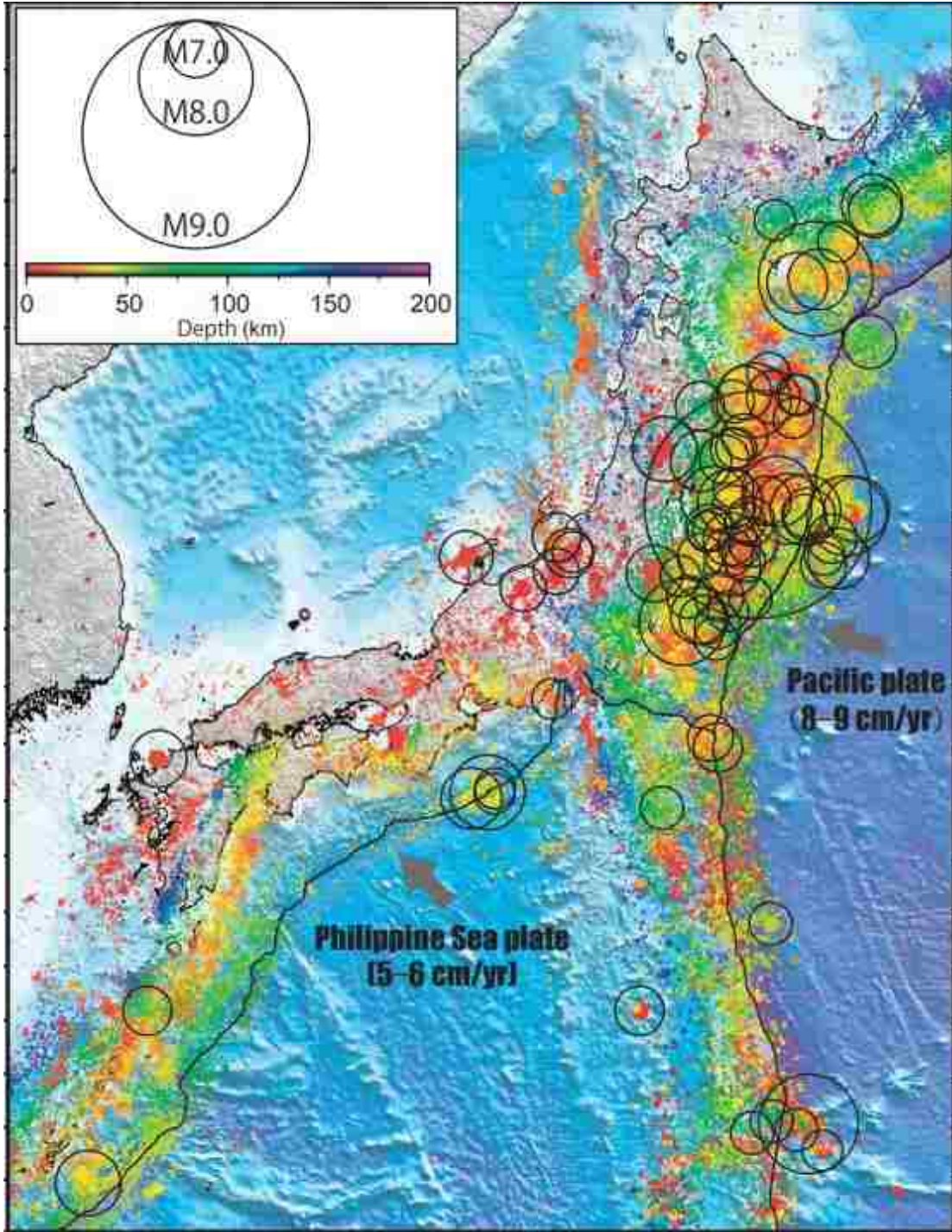


Figure 3-11: Map of Japanese earthquakes and plate movement from 2003 to 2015 (Kato et al., 2016)

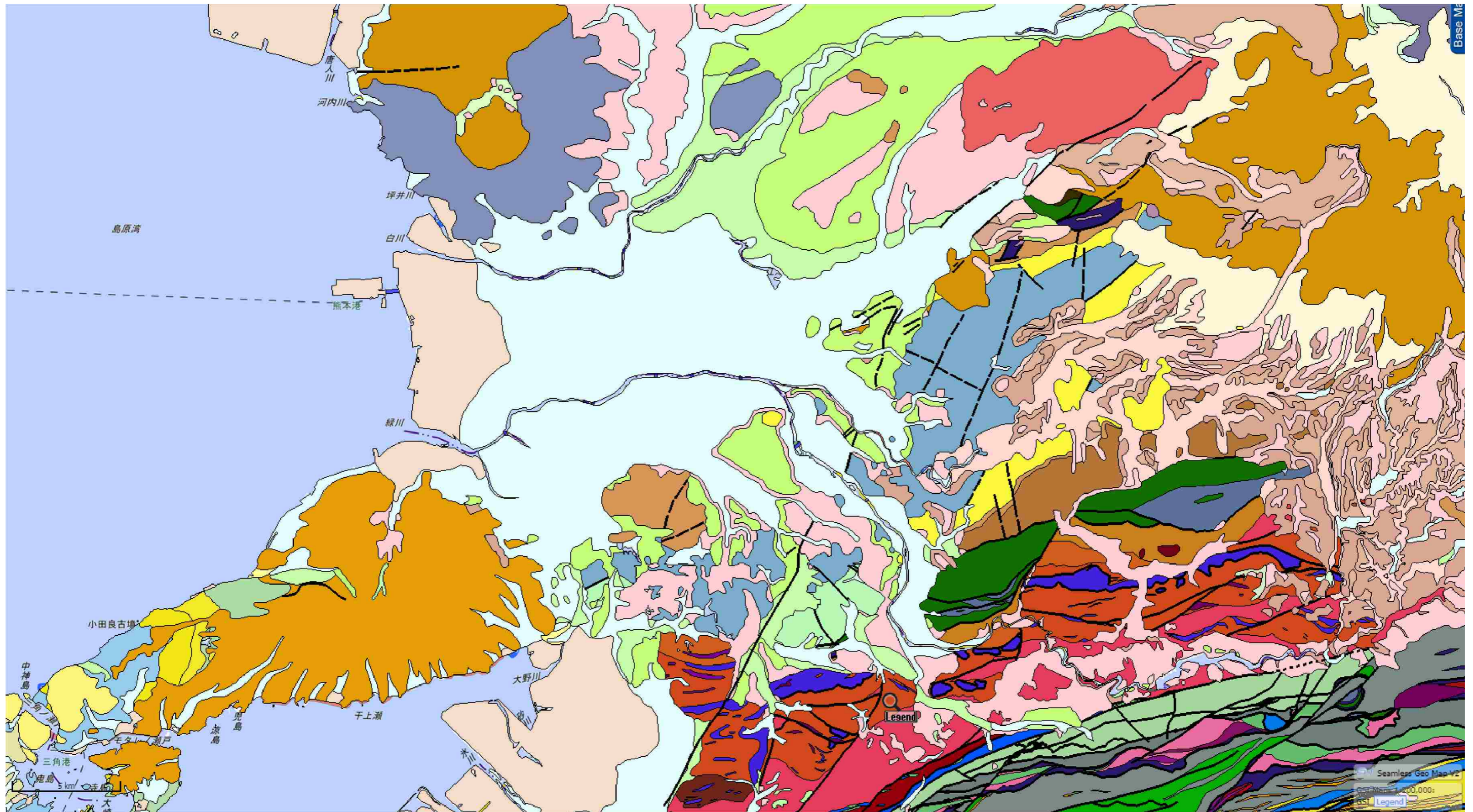


Figure 3-12: Interactive geological map (GeoNavi) showing the Kumamoto Plain, Mt. Aso, and Median Zone (Naito, 2014)



Figure 3-13: Legend of Figure 3-12 geological map (Naito, 2014)

4 VOLCANIC SOILS OF THE KUMAMOTO PLAIN

Volcanic soils and their mineralogical, chemical, and physical properties are a topic outside of tradition geotechnical engineering. In the case of Kumamoto, these soils and their weathered products significantly affect liquefaction susceptibility of the Kumamoto Plain. There is uncertainty regarding the engineering properties of volcanic soils, and even in the field of soil science some soil properties are debated. Volcanic soil research is typically limited to fresh volcanic sediments at shallow depths and soils located far away from major population centers. Fresh volcanic sediments are located adjacent to volcanoes, while volcanically derived soils are located in or near population centers. New Zealand and Japan are the leaders in the field of volcanic ash soil studies due to the abundance of active volcanoes in the respective nations.

This section describes some of the special properties of volcanic soils which will be useful when analyzing data from test sites, described in chapters six and seven. The section will first describe primary materials and then secondary materials found in the Kumamoto Plain.

4.1 Primary Materials of the Kumamoto Plain

The parent materials of the Kumamoto Plain are pyroclastic flow deposits, welded tuff, andesite basalt, and ash fall with the addition of mudstone, metamorphic rocks, and sandstone for the southern half of the Kumamoto Plain (Naito, 2014; Matsumoto, 1963; Ogo et al., 2018; and GSJ, 2018). These primary materials form an angular matrix with volcanic glass forming the

infill. Many other minerals may also be mixed into this matrix. Sandy loam top soils of the Kumamoto Plain are composed of primary materials of non-colored volcanic glass, plagioclase, plant opal, and pumice with secondary materials of allophane with a relatively high amount of organic matter (Kano et al., 1965).

4.1.1 Soil Crushability

The GEER team (Kayen et al., 2017) and other researchers (Bhattacharya et al., 2018; Mukunoki et al., 2016) who examined sand boils found pumiceous materials or volcanic deposits in the ejecta. Pumice and volcanic glasses are crushable soils that tend to have high shear resistance, angularity, and resistance to liquefaction compared to similar silica-based soils (Liu et al., 2015). Volcanic soils in general are crushable and exhibit lower resistances than for silica sands with similar relative density (Miura et al., 2003; Orense et al., 2012; Suzuki & Yamamoto, 2004). Soil crushability is most significant for coarse grained soils such as sand and gravel. Thick strata of sands are found near the surface of the Kumamoto plain (Mukunoki et al., 2016) and so soil crushability may be a significant concern when testing the soil.

Several studies have been done on crushable soils and their impacts on conventional liquefaction initiation testing procedures (Lazcano, 2010; Wesley et al., 1999; Orense & Pender, 2012; Orense & Pender, 2013; Orense et al., 2014). Orense et al. (2014) found that SPT and CPT testing under-predicted a crushable soil's resistance to liquefaction. SPT and CPT testing is a dynamic test where large strains are exerted upon the soil which crushes the soil and gives lower resistance values than they actually exhibit in-situ. For this reason, the relationship between cone/hammer resistance, relative density, and liquefaction are not reliable for a pumiceous sand.

4.2 Secondary Materials of the Kumamoto Plain

Allophane and imogolite clays are found in the topsoil of the Kumamoto Plain (Kano et al., 1965) and are the youngest weathered products of volcanic soils in the Kumamoto Plain.

Allophane and imogolite are underlain by halloysite. Old weathered clays are either kaolinite or Ariake Bay quick clays. A brief summary of secondary clay formation will be discussed in this section.

Initially, volcanic ash soils can weather to either non-allophanic or allophanic material. In high rainfall and drainage areas, primary material desilication occurs, which leads to the formation of 2:1 Al/Si allophane and its cousin, imogolite (Giesecking, 2012). If the soil is not well drained, the silicates are not able to leech out of the material, and the secondary constituents of the volcanic ash soil may become smectite (Giesecking, 2012). In other cases, less desilication results in the formation of halloysite or 1:1 Al/Si allophane. These relationships are shown in Figure 4-1 (Parfitt et al., 1983).

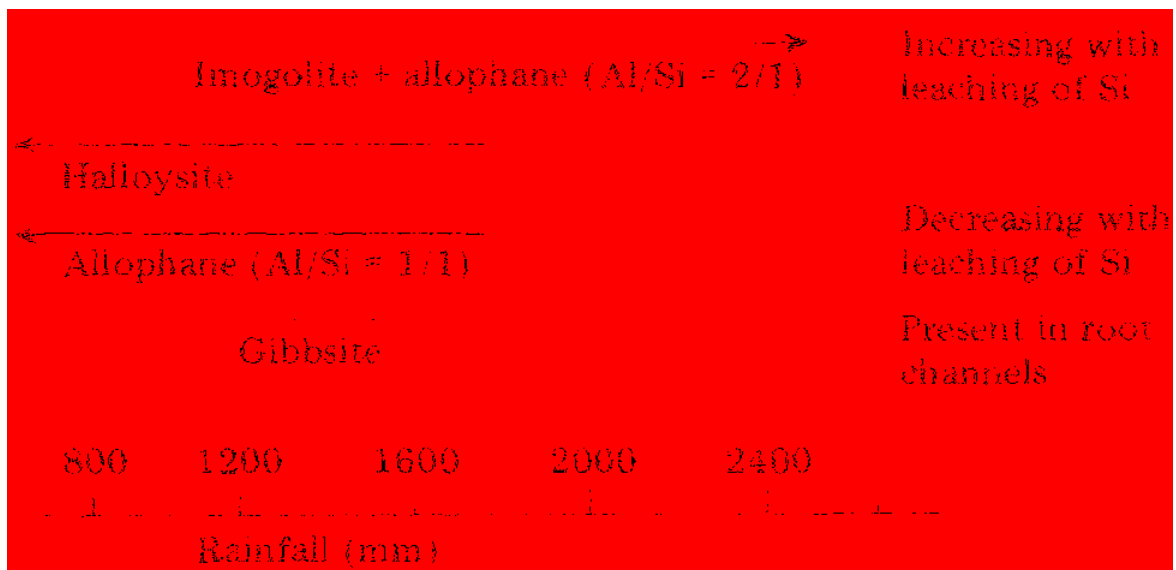


Figure 4.1: Formation of different volcanic secondary materials by rainfall (Parfitt et al., 1983)

4.2.1 Allophane and Imogolite

Allophane is a non-crystalline, colloidal, aluminosilicate with $\text{SiO}_2/\text{Al}_2\text{O}_3$ ratios between one and two. Allophane may seem amorphous but has shapes like hollow spheres, though there is still some variation depending on type and location of the soil (Henmi & Wada, 1976).

Allophane is extremely small even for a clay making it difficult to determine its exact structure. With time, allophane starts to conglomerate and form imogolite tubes. Imogolite is a colloidal, jelly-like clay with a tubular structure found with allophane (Yoshinaga & Aomine, 1962). The structure and harmonization of allophane and imogolite is shown in Figure 4-2 (Henmi & Wada, 1976). Notice the dots (allophane) interbedded in the tubes (imogolite).

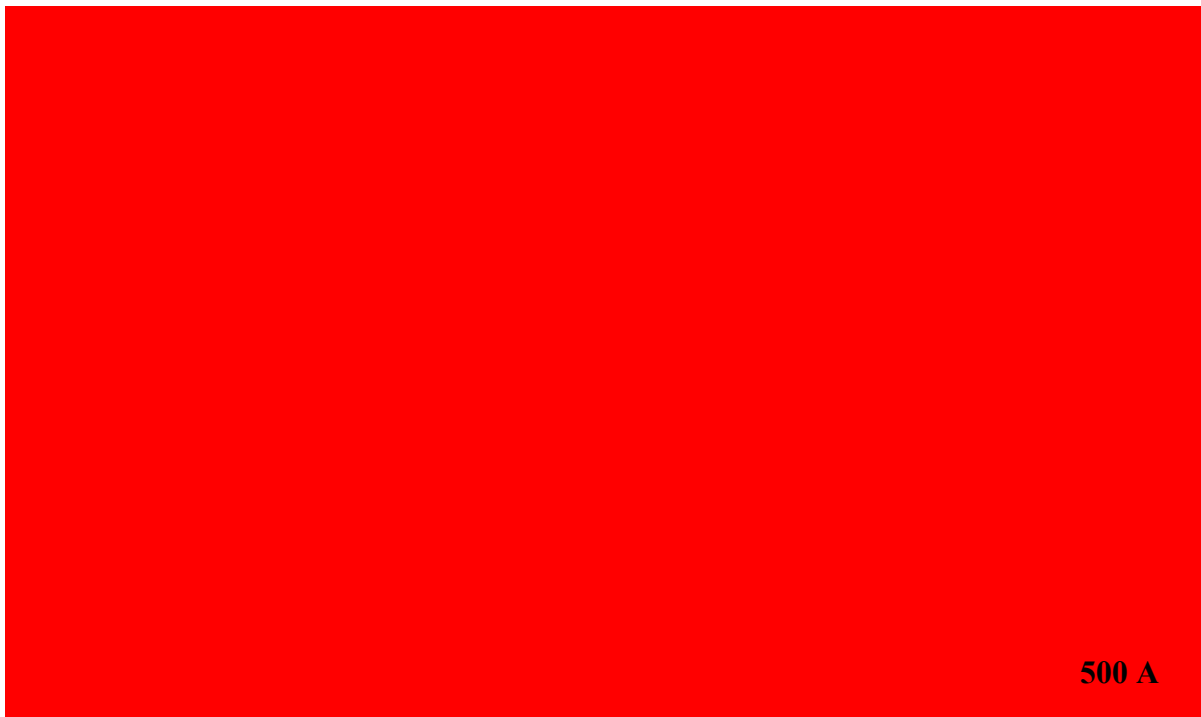


Figure 4-2: Allophane and imogolite (Henmi & Wada, 1976)

A unique feature of highly allophanic soil is its texture. Allophane feels slippery, greasy, and soapy to the touch and is distinct from the feel of montmorillonite, kaolinite, or halloysite.

The higher the water content, the greater the greasy feel and the cohesion. Allophane can hold a high-water content in the 150 to 200% range due to the hollow nature of the microscopic soil structure (Shoji et al., 1993). Allophanic clays have a bulk density between 2.5-2.7 g cm⁻³, which is similar to other minerals (Shoji et al., 1993). Allophane and imogolite wet mineral density can vary between 1.8 to 2.9 making it difficult to determine allophane and imogolite presence just by measuring particle density (Maeda et al., 1977).

The area directly east of the Kumamoto Plain is composed of allophanic clays as depicted in Figure 4-3 (Saigusa & Matsuyama, 1997; Takahashi & Shuji, 2002). Allophanic clays refer soils that form allophane, imogolite, and halloysite, as opposed to smectite. Note that this image only accounts for parent material deposits of volcanic materials, not for any weathered constituents as would be found in the Kumamoto Plain.

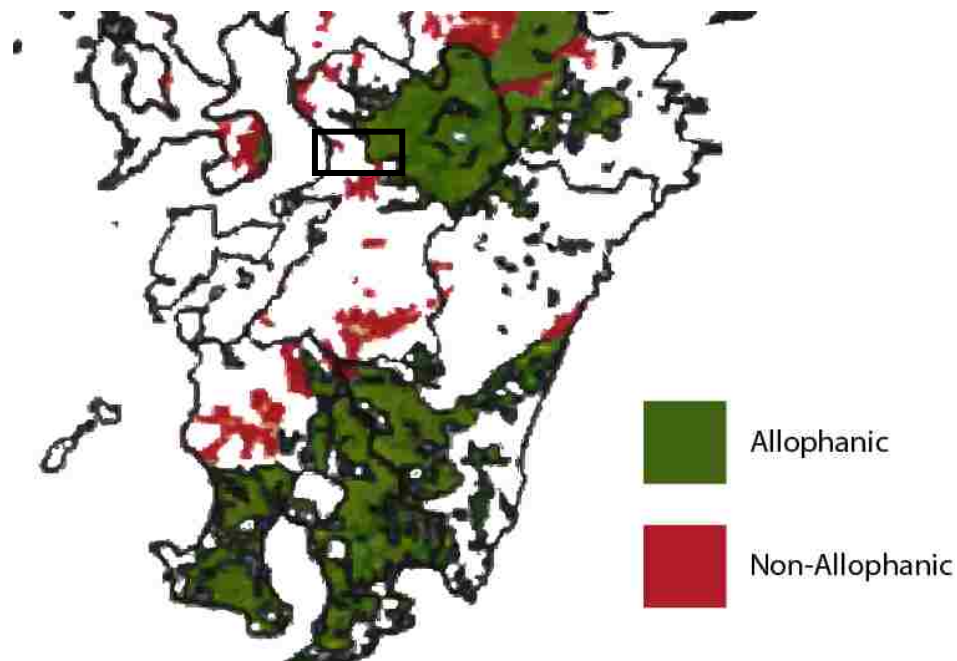


Figure 4-3: Allophanic and non-allophanic clay distribution for direct deposits for Kyushu Island. Box shows the boundaries of the study area (Saigusa & Matsuyama, 1997; Takahashi & Shuji, 2002)

4.2.2 Halloysite

Halloysite is the resilication and recrystallization of allophane and imogolite and has properties more akin to typical clays (Wada 1987). A picture of halloysite is shown in Figure 4-4 (Nagasawa, 1978). Halloysite is sticky like any other typical clay, rather than soapy and greasy like allophane.

Halloysite is tubular and is formed from the spheres and strands of allophane and imogolite. Halloysite starts out hydrated, with water inside the structure, just like allophane. With time and heat, the water inside the structure may evaporate and the halloysite may become meta-halloysite (Giesecking, 2012). Once meta-halloysite unrolls completely, it becomes a kaolinite clay.

Halloysite formations seem to have no strong correlation with depth or time (Nagasawa, 1978; Sudo, 1954). The age of the youngest hydrated halloysite found in Kyushu was in the Aso Caldera, at a depth of two meters, deposited around 9,000 years ago. A comparison volcanic soil in Southern Kyushu was tested and the halloysite there was found at a depth of 2.5 meters and was determined to have been deposited over 30,000 years ago (Aomine & Miyauchi, 1963). Aomine & Miyauchi (1963)'s research prove just how differently two similar soils will weather chemically. Generally, allophane is close to the surface, while halloysite is deeper down. Halloysite is less plastic than allophane and water content and Atterberg limits become much less extreme with the increased presence of halloysite as shown in Figure 4-5 (Wesley, 2973).



Figure 4-4: Halloysite image with scale lines representing 0.5 μm (Nagasawa 1978)

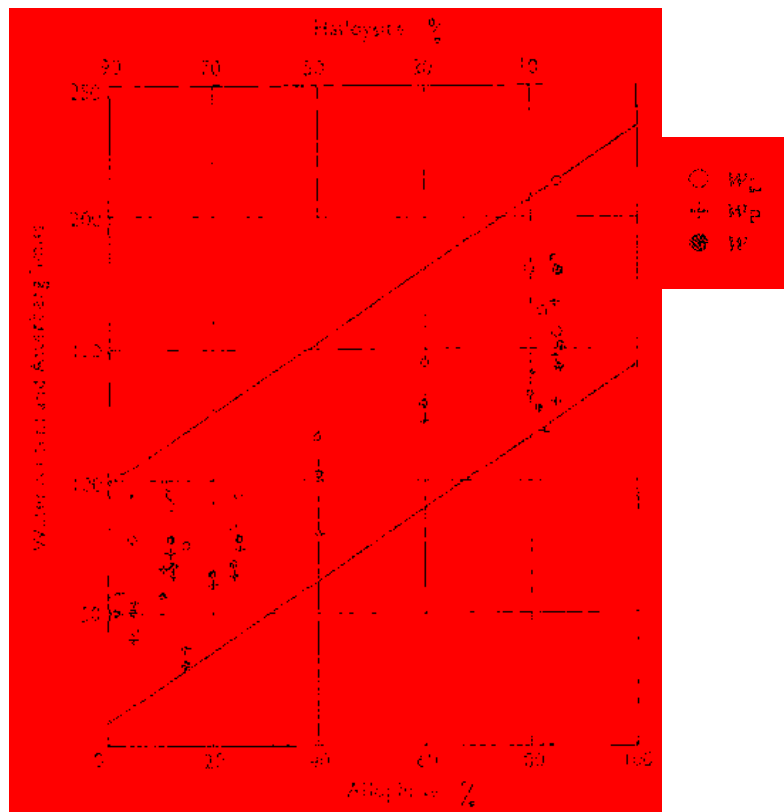


Figure 4-5: Increase in water content and Atterberg limits with increasing allophane content (Wesley 1973)

4.2.3 Organic Contents of Allophanic Soils

Volcanic soils also possess an affinity for organic matter and are typically layered in with organic matter (Shoji et al., 1993). Both non-allophanic and allophanic soils are referred to as andosols in Japan. The word andosol comes from the Japanese word “*An*” meaning black and “*do*” meaning soil. Young Andosols with low allophane content have a color that is dictated by parent material and organic matter (Shoji et al., 1993). Andosol low particle density is due to the porous nature of the material, which helps to develop non-crystalline materials and soil organic matter (Shoji et al., 1993). Dark black soils from sand boils were commonly encountered in Kumamoto, which is indicative of volcanically derived soil and represents ash and organic material in the soil (Kayen et al., 2017). Black colored andosols compose the top layer of the Kumamoto Plain, with increasing thickness the closer to the Aso Caldera.

4.2.4 Allophanic Soil Sensitivity to Laboratory Testing Procedures

Allophanic soils suffer irreversible changes when dried. Figures 4-6 through 4-8 depict the changes to various engineering index properties due to drying of allophanic soils, depending on whether they are allophane or halloysite dominant (Wesley, 1973; Yamazaki and Takenaka, 1965). The severity of the drying effect is extreme for allophane dominant soils but less so for halloysite dominant soils. Air-dried halloysite will have minor changes to Atterberg limits and gradation but will still result in usable data. Air-dried allophane will result in unusable data due to the extreme change in soil index properties. The above challenges encountered when testing volcanic soils must be accounted for when performing geotechnical analysis.

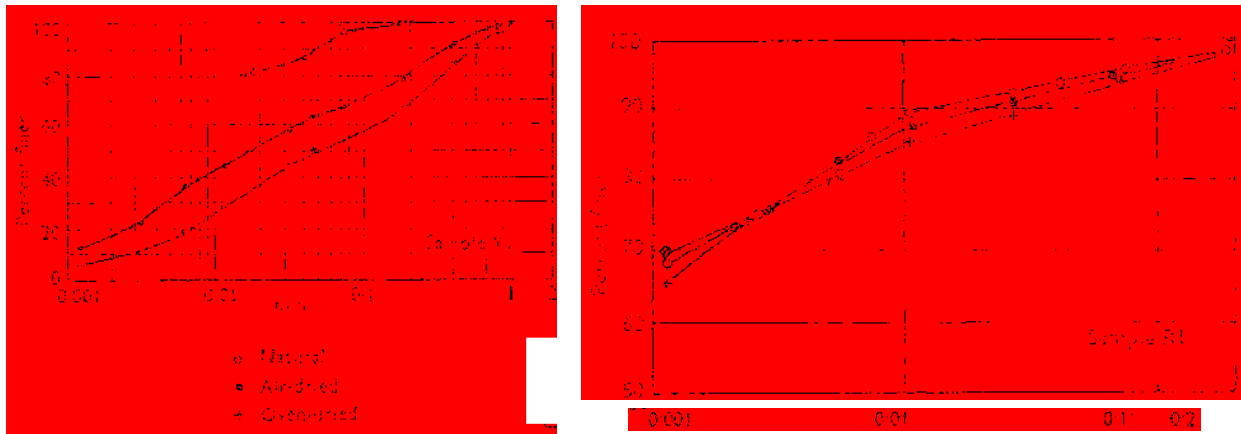
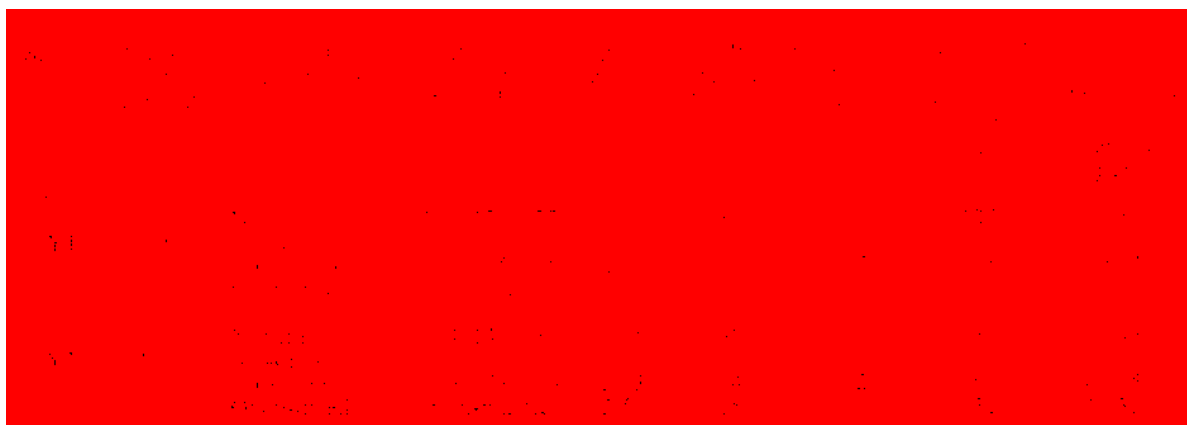


Figure 4-6: Effects of drying on allophanic soil grain size distribution. Y1 (left) is allophane dominant while R1 (right) is halloysite dominant soils. Altered from (Wesley 1973)



Sample	SI	Condition	Liquid Limit (%)			Plasticity Index	Shrinkage (%)			Shrinkage Ratio
			LL ₂₅	LL ₅₀	LL ₇₅		Sh ₂₅	Sh ₅₀	Sh ₇₅	
R1	51	Natural	76	36	40	2.78	95	73	37	1.313
		Air-dried (n=9)	71	35	36	2.78	95	73	35.5	1.340
		Oven-dried	59	33	26	2.74	95	71	30.5	1.430
R2	51	Natural	94	53	42	2.76	98	77	51.5	1.084
		Air-dried (n=21)	85	51	34	2.76	98	84	48	1.135
		Oven-dried	61	41	20	2.73	98	82	39	1.260

Figure 4-7: Index properties differences based of test condition. First two samples (Y1 & Y2) are allophane dominant soils and the last two samples (R1 & R2) are halloysite dominant clays. Altered from (Wesley 1973)

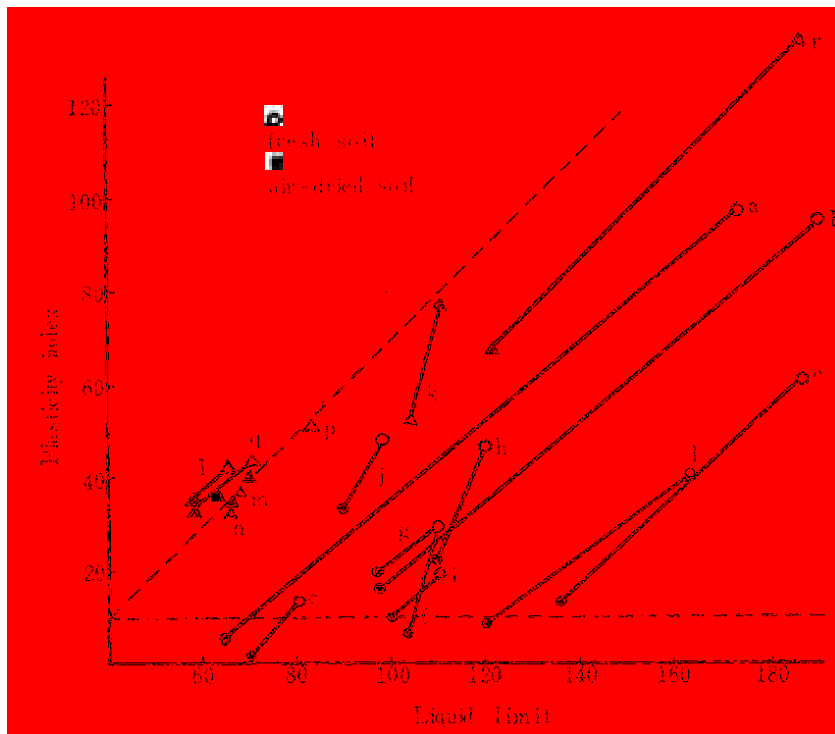


Figure 4-8: Effects of soil drying on volcanic soil plasticity (Yamazaki & Takenaka, 1965)

5 THE 2016 EARTHQUAKE SEQUENCE

The 2016 Kumamoto Earthquake sequence occurred during April of 2016, beginning with two large foreshocks of moment magnitude 6.2 and 6.0. These foreshocks caused substantial damage and primed the area for the 7.0 moment magnitude mainshock. Many aftershocks occurred, but these paled in comparison to the foreshocks and mainshock. The three main earthquakes each had high intensity ground motions with recorded PGAs ranging from 0.2g to 1.2g. Ground motions and accelerations were accessed on publicly available Japanese strong-motion seismograph networks (K-NET, KiK-net).

The Japanese reported moment magnitude is slightly different from the USGS reported magnitude. The Japanese use a model specifically tuned to the region to compute the magnitude, while the USGS give magnitudes that are useful in comparing the earthquake to other earthquakes around the globe (USGS, 2019). For this research, the USGS calculated moment magnitude will be the default, though some of the figures provided by the Japanese are labeled with the Japanese measured local magnitude.

5.1.1 Foreshocks

There were two large foreshocks of moment magnitude 6.2 and 6.0. In Japanese local magnitude they were 6.5 and 6.4. The locations relative to the Kumamoto Plain are given in Figure 5-3. The first foreshock occurred on April 14th at 21:26 local time. The location of the

focus was approximately 32.74 N 130.81 E at a depth of 11 kilometers (Kayen et al., 2017). The first foreshock faulting mechanism was a right lateral strike slip with a maximum recorded PGA around 1.08g. The second foreshock occurred on April 15th at 00:03 local time. The location of the focus was approximately 32.70 N 130.78 E at a depth of seven kilometers (Kayen et al., 2017). The maximum recorded PGA was lower at 0.81g. Figure 5-1 summarizes the PGA with epicentral distance for both foreshocks.

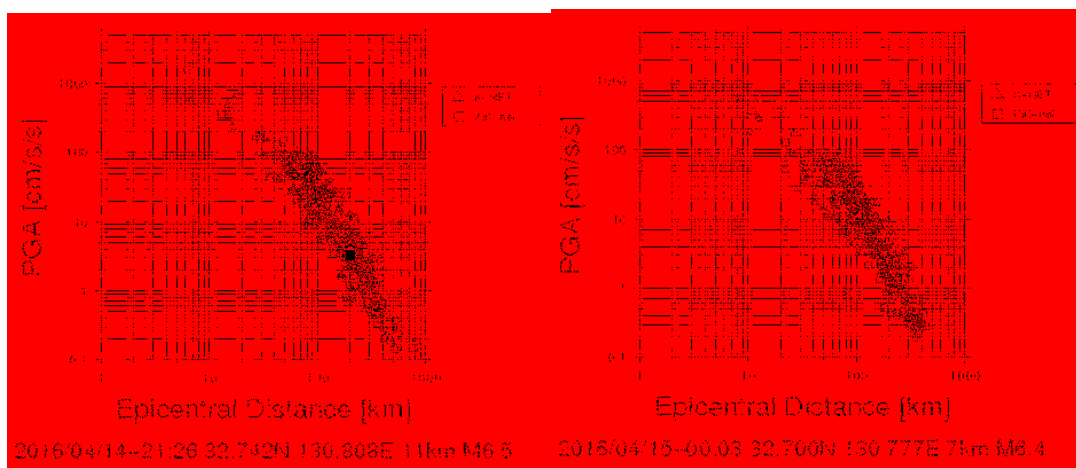


Figure 5-1: Foreshock PGA with epicentral distance. Left: M 6.2. Right: M 6.0

5.1.2 Mainshock

The mainshock of moment magnitude 7.0 (7.3 Japanese local magnitude) occurred on April 16th at 01:25 local time, at a location of 32.75N 130.76E and a depth of 12 kilometers (Kayen et al., 2017). There were frequent aftershocks following the main shock, and it is theorized that many small inactive faults were reactivated (Kato et al., 2016). Figure 5-2 shows PGA with epicentral distance. The maximum PGA is similar to the first foreshock, but the ground motions for areas further away than 10 km are significantly higher for the mainshock. Thus Kumamoto City, the Aso Caldera, and the Kumamoto Plain were most affected by the

mainshock. Accelerations and seismic intensity are shown in Table 5-1 with Japanese seismic intensity (See Appendix A-1). Figure 5-3 shows recording station locations and the earthquake epicenters relative to the Kumamoto Plain. Intensities of six and higher are characterized by difficulty in standing during the shaking with most indoor furniture toppling over and structural components such as walls sustaining damage and, in some cases, failing (JMA, 2019). Figure 5-4 shows the velocity and acceleration at Mashiki Town, and Figure 5.5 shows the acceleration response spectrum for the station located closest to the Kumamoto City.

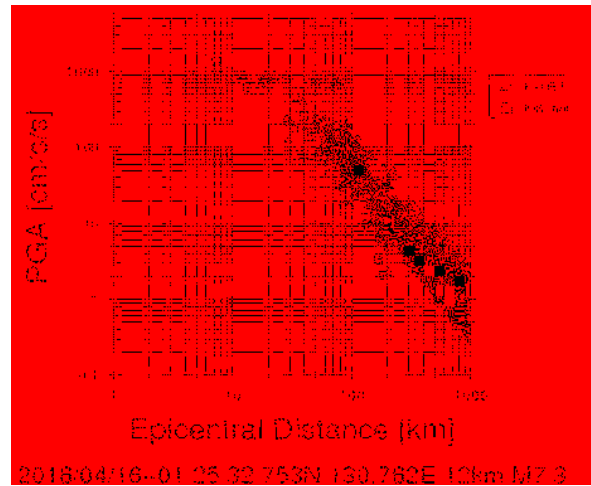


Figure 5-2: Mainshock PGA with epicentral distance

Table 5-1: Acceleration recordings for various stations

Station	Latitude	Longitude	Max Acc (g)			Intensity
			N-S	E-W	U-D	
KMMH16	32.797	130.82	0.67	1.18	0.89	6.5
KMM008	32.688	130.658	0.66	0.79	0.43	6.2
KMM006	32.793	130.777	0.84	0.63	0.54	6
KMM009	32.686	130.986	0.79	0.65	0.19	5.7
KMMH03	32.998	130.83	0.80	0.23	0.41	6.1
KMM011	32.617	130.865	0.61	0.61	0.26	5.6
KMM005	32.876	130.877	0.54	0.49	0.40	5.7
KMMH14	32.635	130.752	0.47	0.41	0.55	5.7
KMM007	32.827	131.123	0.28	0.43	0.31	5.3
KMM004	32.932	131.121	0.27	0.35	0.27	5.5

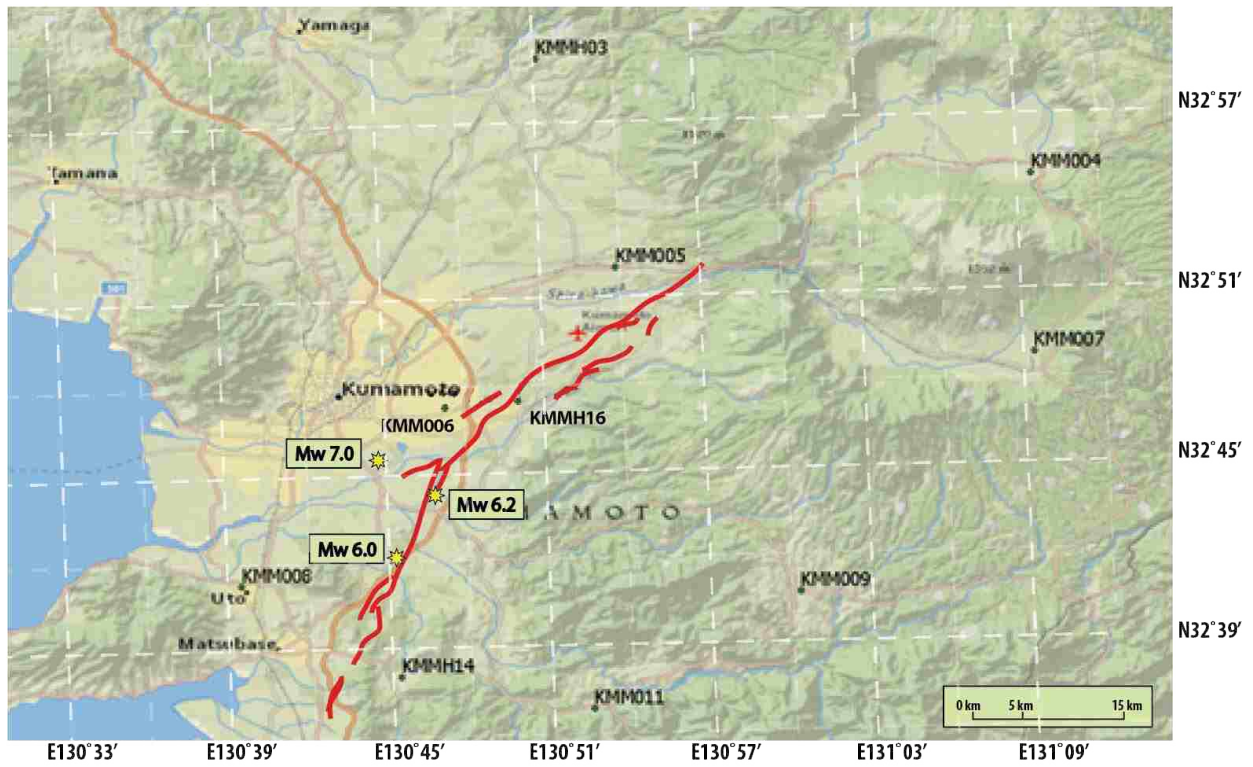


Figure 5-3: Locations of seismic stations listed in Table 3-1.

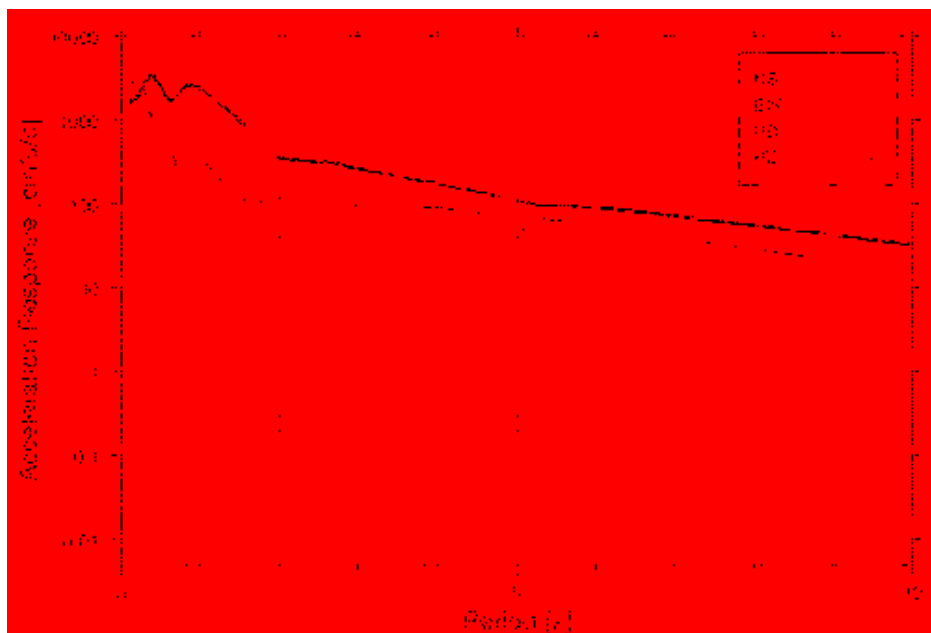


Figure 5-4: Velocity and acceleration response spectrum of Mashiki (KMMH16)

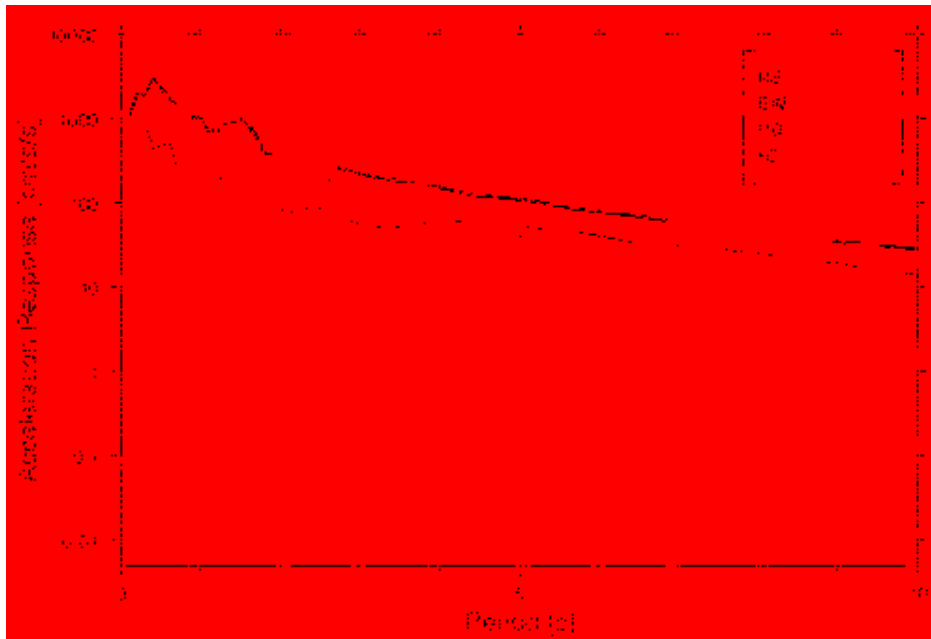


Figure 5-5: Acceleration response spectrum of location directly east of Kumamoto City (KMM006)

5.2 General Damage After the Event

Kumamoto City was lightly damaged from the earthquake and performed exceptionally well given the high ground motions. Modern structures performed well and the most significant structural damage was non-critical cracking of large buildings in the downtown area. Kumamoto Castle experienced major structural damage and many of its castle walls collapsed, which comes as no surprise given its age and lack of earthquake countermeasures.

The populated area nearest to the fault, Mashiki Town, suffered catastrophic damage. Unfazed modern structures were juxtaposed with completely collapsed older wooden homes. The strong ground motions can be attributed to the soft soils of the plain, which amplified the ground motions. A map of the soil amplification for the Kumamoto Plain is given in appendix A-3 (J-SHIS, 2009). The soil amplification map assumes that engineering bedrock has a shear wave velocity of 400 m/s and determines if ground motions are amplified above this value or

dampened below it. The Kumamoto Plain had amplification factors of two and above, while the mountains surrounding the plain had factors of one and less.

5.3 Liquefaction Damage Summary

The 2016 Kumamoto Earthquake ground motions were more than sufficient to provide ample CSR intensity and duration for liquefaction in the Kumamoto Plain. Because the shaking was so strong and the resulting liquefaction so minor, there must be other factors that hindered liquefaction. Figure 5-6 shows a Kumamoto City liquefaction hazard map, which shows the entire plain being at an extremely high (-) risk (2016). A few areas were classified as extremely high (+) risk, which is the highest hazard risk possible on the hazard map.

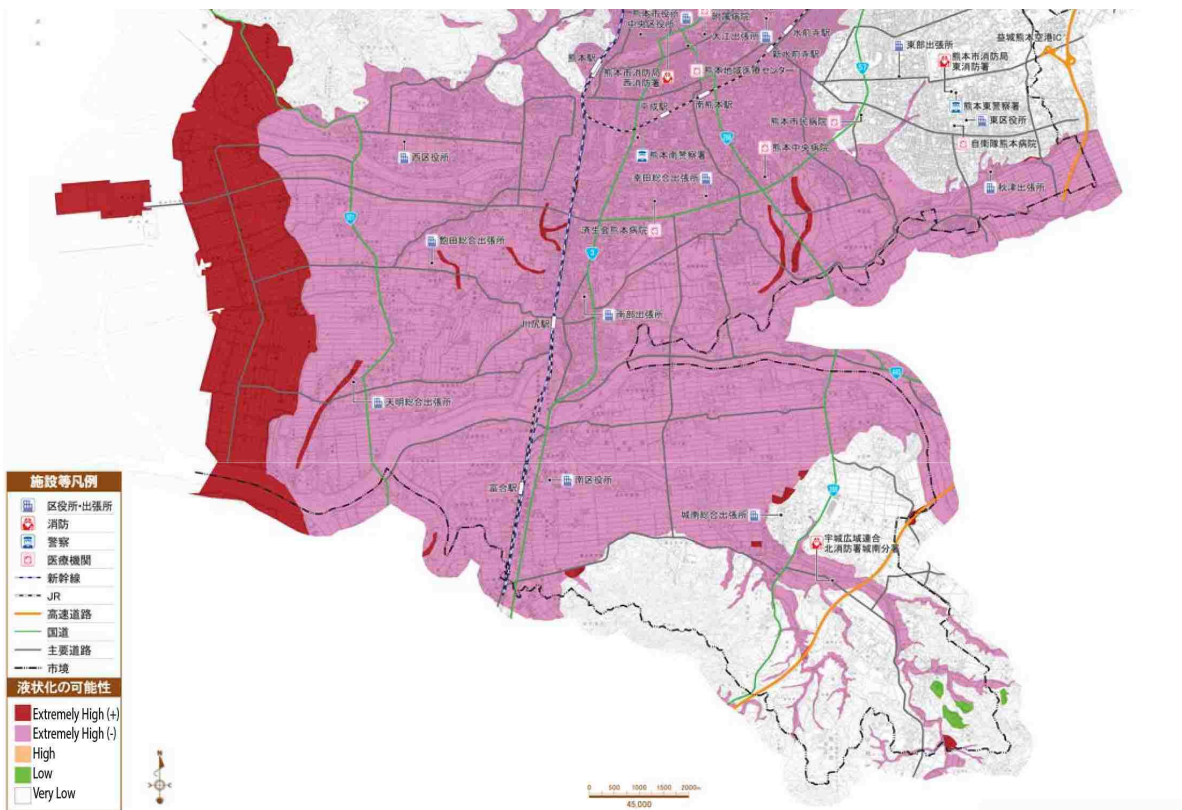


Figure 5-6: Kumamoto City liquefaction hazards map (Kumamoto City, 2014)

Three areas of the Kumamoto Plain experienced liquefaction and are illustrated in Figure 5-8 (altered from Mukunoki et al., 2016). Zone 1 was liquefaction along the outlet mouths of the coastal rivers and on the manmade island on the coast. Zone 2 was liquefaction in narrow strips of land and one large liquefied strip which is hypothesized to be a former river channel. Zone 3 was liquefaction sporadically pocketing floodplains and levees and manifesting as sand boils and fissures.

One of the difficulties in accurately determining liquefied sites was the over-reliance on aerial photography to determine liquefaction. While useful, some aerial indications of liquefaction overstated the areas of actual liquefaction. For example, decomposing rice stalks were mistaken for sand boils, as were puddles of water, and even shadows of buildings. Japanese farmers often recycle old crops for fertilizer and pile them up in rice fields after harvest around October (see Figure 5-7). As shown in Figure 5-8, there was significant liquefaction as determined by aerial photography, but field surveys showed less frequency of liquefaction (Mukunoki et al., 2016; Kayen et al., 2017; Goda et al., 2017).



Figure 5-7. Harvested rice stalks being used to fertilize a field in Japan (Nippon, 2014)

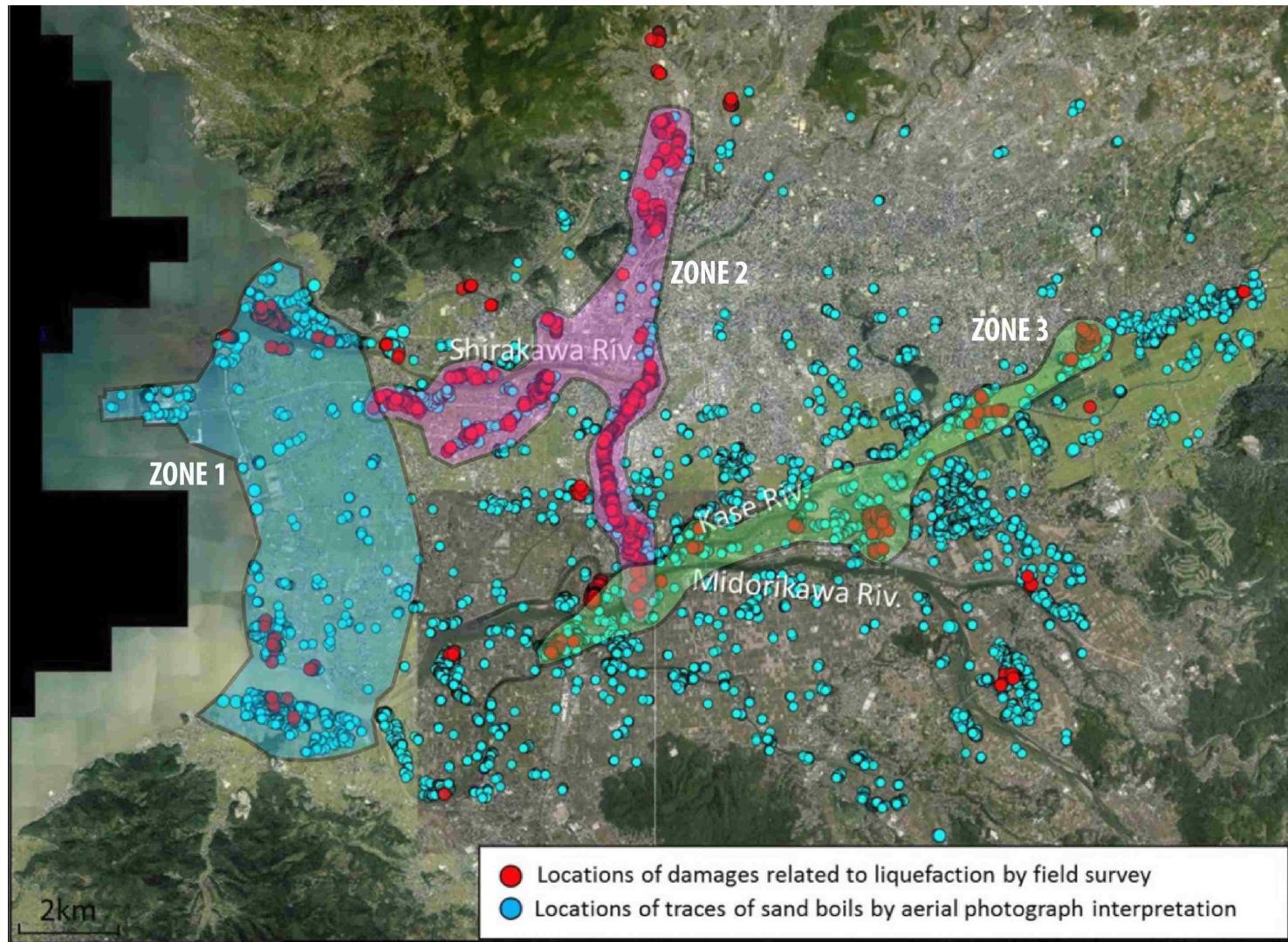


Figure 5-8. Field survey and aerial photograph interpretation of liquefaction damage in the Kumamoto Plain with zones of interest marked. Altered from (Mukunoki et al., 2016)

Mashiki Town, which experienced the strongest ground motions, had liquefaction suspected damages but very few surficial manifestations of liquefaction (NZSEE 2016). Minor liquefaction of backfilled pipes and manholes occurred in some neighborhoods around Mashiki (Kiyota et al., 2016). In general, liquefaction damage in the Kumamoto Plain ranged from minor to none. The alluvial soils were expected to have significant liquefaction but experienced mostly sporadic minor liquefaction (Kayen et al., 2017). The few zones that experienced moderate or frequent liquefaction will be explained in more detail below.

5.3.1 Zone 1: Man-made Island and Coastline of West Kumamoto

The coastal region of the Kumamoto Plain is filled with loosely compacted fill composed of sand and silty sand, underlain by Ariake Bay clays. The area's development is limited to residential homes and small businesses given the poor foundational attributes of the soil. The reclaimed land had little to no liquefaction due to its high fines content and low to medium plasticity (determined from publicly available boring logs), even though the soil is thought to be mostly sand. The soil is soft and mixed with many sea shells; the soil is likely composed of recycled sea bed materials. The estimated peak ground acceleration is around 0.5g. This area of the Kumamoto Plain was predicted to have severe liquefaction as shown in Figure 5-6 (Kumamoto City, 2014).

Sediment deposition zones at the mouths of the Shirakawa and Midorikawa Rivers both liquefied. Sands are deposited on the beach and coast, while silts and clays are pushed out to settle on the sea bed. Publically available boring logs show mostly medium sand and fine sand layers. The sediment deposition zones at the mouths of the Shirakawa and Midorikawa Rivers contain sea walls and have been heavily altered over time and was likely engineered with clean sands and gravels. Liquefaction was expected at these locations given a large enough earthquake.

The man-made island to the west of the Kumamoto Plain experienced irregular liquefaction and settlement. The island was built over a thick layer of marine silt and clay with three meters of surcharge sand left on top, which is hypothesized to have liquefied (Kayen et al., 2017). Sensitive clay properties may have contributed to the settlement as well as the liquefaction, though research in this field is sparse (Torrance & Ohtsubo, 1995; Ohtsubo et al., 1982). Not all areas of the island were overlain by the three meters of surcharge sand which would explain the irregular liquefaction. Like the mouths of the Shirakawa and Midorikawa Rivers, this area liquefied as expected.

5.3.2 **Zone 2: Ancient River Channels in Kumamoto City**

Several ancient river channels liquefied in Kumamoto City, in line with accounts of the 1889 Kumamoto Earthquake, which describe ancient river channels near the castle liquefying (Akiyoshi & Fuchida, 1998). The largest N-S liquefaction channel, shown in Figure 5-9, has no official records indicating it was a former river channel. Ultimately, the Japanese Ministry of Land, Infrastructure, Transport and Tourism has concluded that the area was an ancient river that was filled in during the Edo Period, roughly 400 years ago (MLIT, 2017). Boring logs of areas on the liquefied strip show poorly graded sand and medium sand, which is opposed to the high plasticity and fines content indicated in boring logs located near, but not on, the liquefied strip (Enomoto & Kubo, 2016; Matsumoto & Hidetoshi, 2016). The material of this liquefied strip appears to be fill material, and this is supported by historical markers that mention a bridge in the area and a large irrigation channel which runs down the ancient river's length. Ancient maps and a land classification map also convey the possibility of a river. Available historical evidence strongly suggest that this area is an ancient river (Bhattacharya et al., 2018; Kayen et al., 2017;

Mukonoki et al., 2016). There were two other ancient river channels located to the west of the major N-S liquefied strip and one to the north as well.



Figure 5-9: N-S liquefied river channel with liquefied sites (Wakamatsu et al., 2016)

5.3.3 Zone 3: Rivers to the South of Kumamoto

Liquefaction along the levees and fields of the Shirakawa River was mostly absent which reflects the dominant influence of volcanic soils. Levees and fields along the Kase and Midorikawa Rivers showed much more minor liquefaction, which reflects the influence of the other non-volcanic deposits.

Only one lateral spread was encountered by the GEER team, though a few cases of lateral spreading were located by Japanese researchers (Kayen et al., 2017; Kiyota et al., 2017). Lateral spread was neither severe nor widespread, and most levee damage can be attributed to ground motions and general subsidence. Lateral spreading that occurred in Kumamoto was minor compared to other lateral spread events in Japan, such as the 2011 Tohoku, 1995 Kobe, and the 1964 Niigata Earthquakes (Hamada, 1992; Ishihara, 1999; Tokimatsu et al., 2013). In fact, most levee damage was repaired within a few weeks after the earthquake and was not observed by the GEER team (Kayen et al., 2017; MLIT, 2017). The dearth of lateral spread is astounding given the many miles of waterways and alluvial sand deposits in the Kumamoto Plain. Figures 5-10 and 5-11 summarize levee damage as recorded by the Japanese Ministry of Land, Infrastructure, Transport and Tourism (MLIT, 2017).

Japanese researchers found extensive liquefaction at the intersection of the three rivers: the Yakata, Kiyama, and Akizu. (Kiyota et al., 2017). These three rivers converge to form the Kase River, which flows through the Kumamoto Plain between the Shirakawa and Midorikawa Rivers. The area at the river convergence had a residential neighborhood that experienced moderate liquefaction induced tilting of homes. One lateral spread occurred over a small section of the Akizu River and was confirmed to be due to a man-filled river channel in the area (Kiyota et al., 2017). Over the last 40 years, many of the rivers in the Kumamoto Plain, and especially the Kase River, have been rerouted and engineered for flood protection. For example, many rivers used to meander but have been widened and straightened in the present day. Due to major river alterations, recycled fill material seems to have been used to refill the old river channels. Overall, liquefaction in the southern Kumamoto Plain was limited to instances of minor liquefaction on levees with most minor liquefaction occurring on adjacent rice fields and neighborhoods.





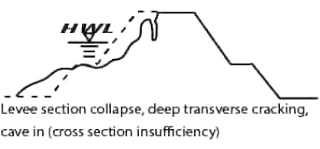
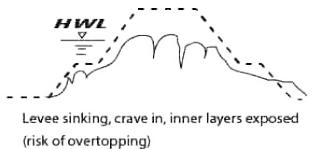
Failure form	Failure mechanisms	Remaining function	Supposed failure mechanism from Kumamoto earthquake	Midorikawa river system				Shirakawa	Sum
				Midorikawa	Hamatogawa	Kasegawa	Mifune		
I  Longitudinal crack above HWL (High water line)	-Fill material strength insufficient, strength reduction	-As long as there aren't cracks all along the top of the levee, the levee can generally function as normal	There is a longitudinal crack which does not reach the H.W.L (High water line)	31	2	11	6	7	57
II  Longitudinal crack below HWL	-Fill material strength insufficient, strength reduction	-Taking into account the crack width and depth, judge to see if it will remain functional. -If levee functionality is compromised, use temporary preventive measures. -If only part of the levee is judged to be compromised, temporarily reinforce the levee.	There is a longitudinal crack which does reach the H.W.L	1	0	0	0	0	1
III  Transverse crack above HWL	-Fill material strength insufficient, strength reduction -Transverse structural material loosening	-Unless the entire top of the levee is cracked, the levee is still functional.	There is a transverse crack which does not reach the H.W.L	15	5	19	8	11	58
IV  Transverse crack below HWL	-Fill material strength insufficient, strength reduction -Transverse structural material loosening -Expansion of water	-The levee is no longer considered functional. -The fill material must be tested for strength, and the ground surface for soil liquefaction.	There is a transverse crack which does reach the H.W.L	0	0	0	0	0	0
V  Levee section collapse, deep transverse cracking, cave in (cross section insufficiency)	-Fill material strength insufficient, strength reduction -Fill material section liquefaction -Fill material saturation -Ground strength	-The levee is no longer considered functional. -The fill material must be tested for strength, and the ground surface for soil liquefaction.	On either the inside, outside, or both sides of levee there is a significant change, cracks reaching the H.W.L	4	0	1	0	0	5
VI  Levee sinking, cave in, inner layers exposed (risk of overtopping)	-Fill material strength insufficient, strength reduction -Fill material liquefaction -Ground strength insufficient,	-The levee is no longer considered functional. -The fill material must be tested for strength, and the ground surface for soil liquefaction.	On the entire levee there is significant subsidence, cracks reaching the H.W.L	4	0	0	0	0	4
Anything not involving a river dike, parapet, or embankment				12	1	4	3	26	46
SUM				67	8	35	17	44	171

Figure 5-10: MLIT damage survey for levees (MLIT, 2017)

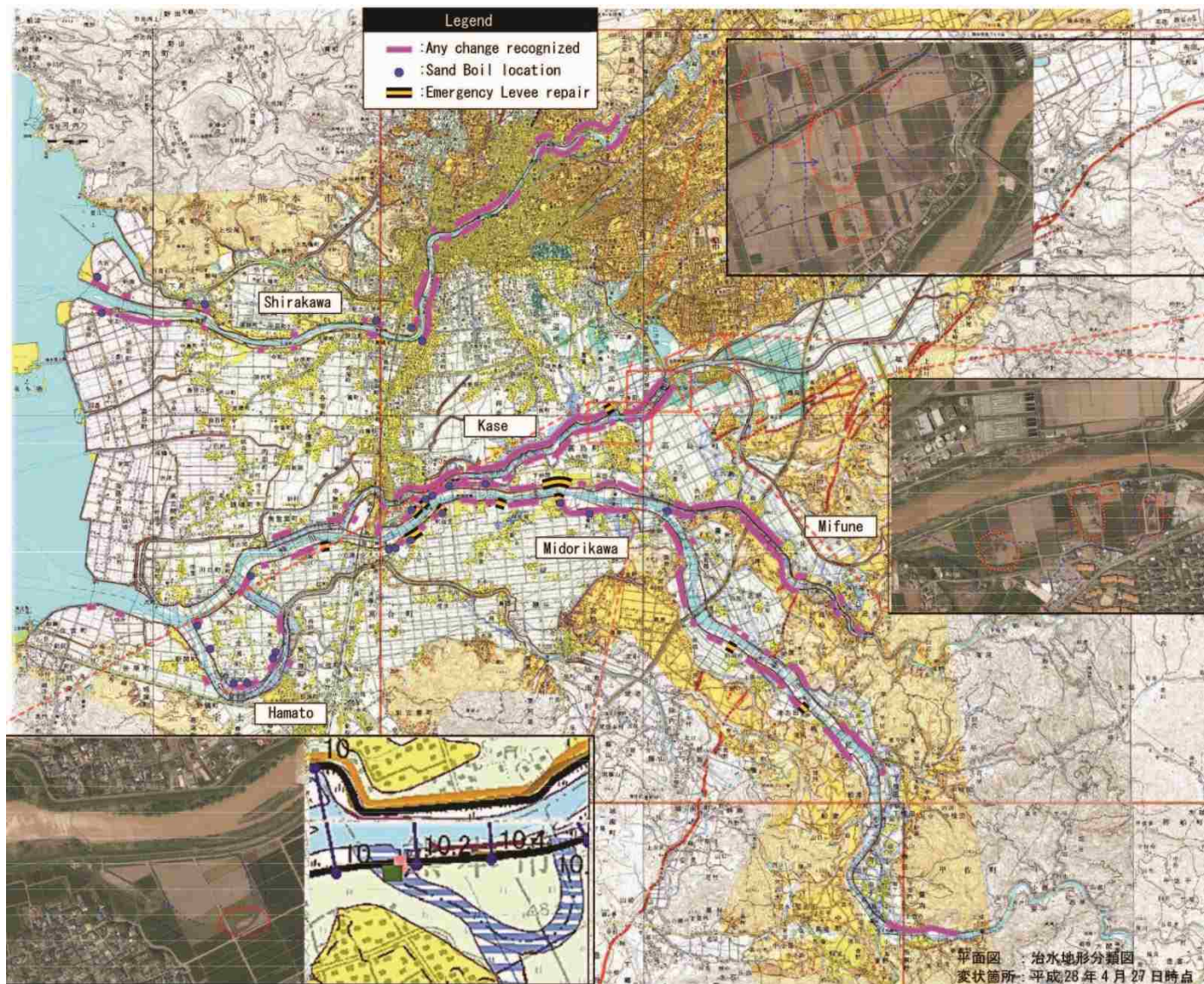


Figure 5-11: Lateral spread and levee cracking locations, altered from MLIT (2017)

6 LIQUEFACTION SUSCEPTIBILITY AND INITIATION OF SELECT SITES

We mounted a field expedition to Kumamoto in the spring of 2017 to test specific sites with current liquefaction initiation criteria. We ultimately chose four sites to test which balanced research merit with our limited budget and difficulty in acquiring drilling permission. This chapter will explain the methods used to test each site and then give the results of each site in detail. The four test sites are given in Figure 6-1.

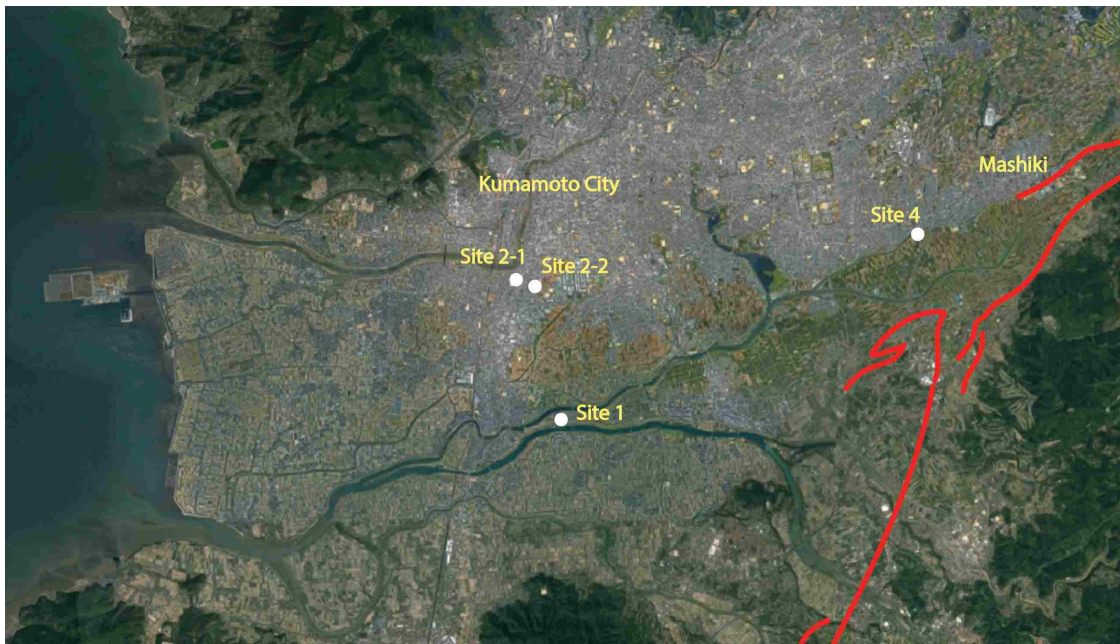


Figure 6-1. Kumamoto Plain with test sites and faults located

6.1 Methods of Testing

Each test hole was chosen with confirmed liquefaction sites nearby or present at the location. Sites 2-1 and 2-2 were chosen to test zone 2, the liquefied river channels. Sites 1 and 4 were chosen to test zone 3, the liquefied levees and fields in the south of the Kumamoto plain. Each site had an Standard Penetration Test (SPT), Cone Penetration Test (CPT), and laboratory testing of soil samples. SPT and CPT testing was done in adjacent holes. Tokyo Soils and Research was contracted to perform the field work, and we supervised the work throughout the trip. Site 2-1 also had undisturbed samples taken by piston sampler, which were shipped to the University of Colorado for cyclic triaxial testing. I processed all the data and analyzed the sites to determine their liquefaction potential. A PGA of 1.0 was used for sites 1 and 4, and a PGA of 0.5 was used for sites 2-1 and 2-2. These are consistent with observed ground motions as reported in chapter 5. A seismic slope stability analysis was performed at site 4 to compare the degree of liquefaction with the potential for slope failure.

Tokyo Soils and Research performed the SPT testing with a semi-automatic drop device, which has a hammer efficiency estimated to be 78% (Skempton, 1986). Borings were classified on the spot by the Japanese field engineers and were later translated. The SPT blow count data was analyzed with the Boulanger and Idriss (2014) criteria to determine liquefaction susceptibility. The Idriss and Boulanger (2012) method was not performed due to its use of rod length, which was not recorded during the SPT testing. SPT logs were not re-updated with the laboratory results, but I added the laboratory results to the data using the Unified Soil Classification System (USCS). The laboratory results are shown in highlighted boxes on the boring logs. The original boring logs are available in Appendix B.

Tokyo Soils and Research performed the CPT testing. I processed the raw data and analyzed the sites for liquefaction susceptibility using the program Cliq. I used the Idriss and Boulanger (2012), Youd et al. (2001), Robertson (2009), and the Boulanger and Idriss (2014) methods. Only the Youd et al. (2001) results will be displayed in the text. A summary of the other methods will be shown in the following section. The CPT data was analyzed both with and without thin layer corrections, but the results exhibited only trivial differences. The results without the thin layer correction will be presented. The Kumamoto Plain does not have any strong interbedded layering at the sites we tested. In addition to liquefaction initiation, I computed predicted lateral spreading and vertical settlement. I determined the probability of surficial manifestations of liquefaction as classified by Ishihara (1985) which analyzes the degree of earthquake shaking and the thicknesses of liquefied material and resistant surficial layers. I created Liquefaction Potential Index (LPI) charts for each site (Iwasaki, 1978). LPI charts are useful in determining the probability of damaging liquefaction but are unreliable in predicting liquefaction and in utilization for lateral spread sites (Maurer et al., 2014). A similar chart for the Liquefaction Severity Number (LSN) is provided. The LSN predicts the degree of damage at a site using CPT readings (Van Ballegooy et al., 2014). Both the LPI and LSN will be provided in the following chapter, as a comparison between different CPT methods.

Tokyo Soils and Research air-dried the soils before testing for their Atterberg limits. The plasticity tests that were conducted on Kumamoto soils likely underestimated the true soil plasticity. There would be a minor difference in the measured versus true plasticity because most of the clays are halloysite. The grain size and Atterberg limits should be reasonable enough to use in analysis, because allophane rich clays should only be located at the top of the soil profile. Halloysite soils, as discussed in chapter 5, are much less susceptible to air-drying effects. Figure

6-2 shows typical volcanic soil Atterberg limits with Figure 6-3 showing measured Atterberg limits from our test sites (Rao, 1996). Halloysite soils are parallel to and near the A line (Wesley, 1973). When adjusting for the moderate change in plasticity, the values from our test sites correspond nicely to halloysite.

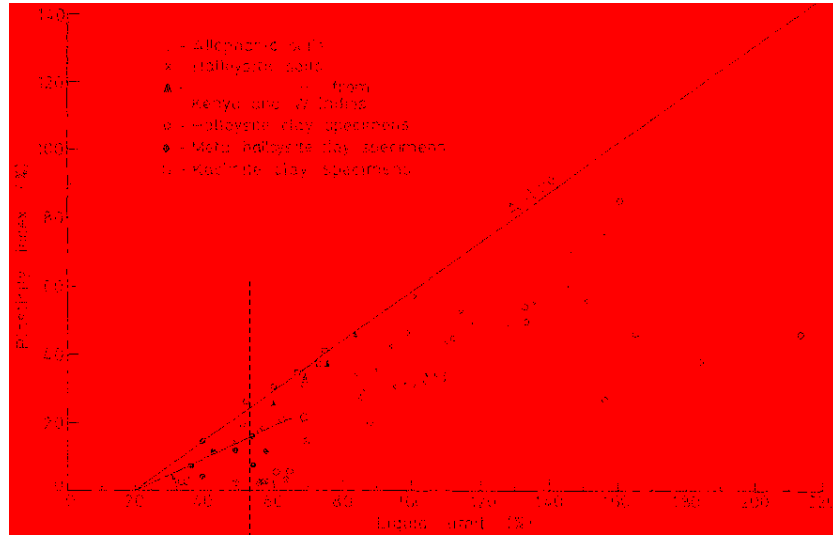


Figure 6-2: Typical Atterberg limits for volcanic soils (Rao, 1996)

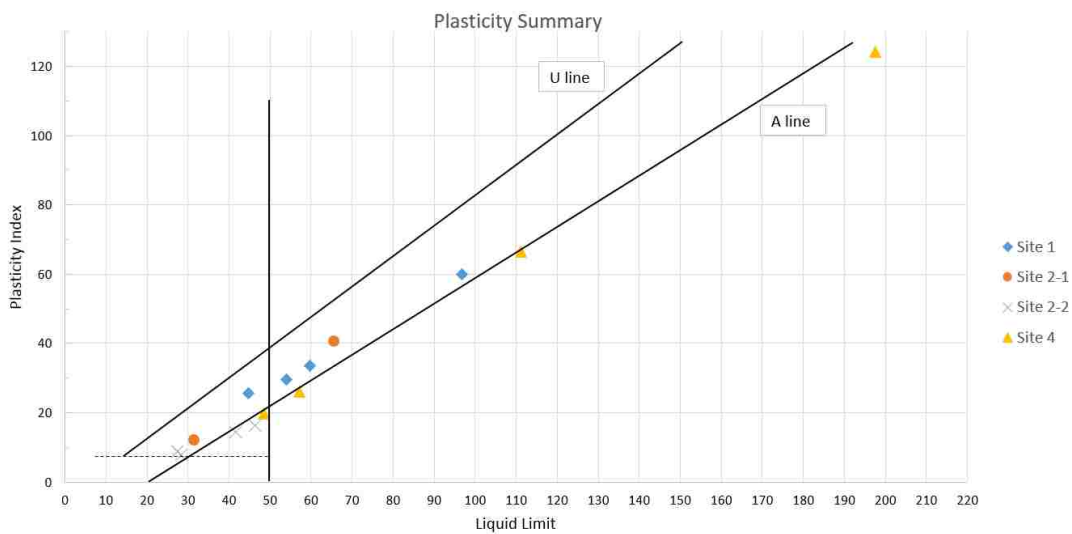


Figure 6-3: Atterberg limits summary chart

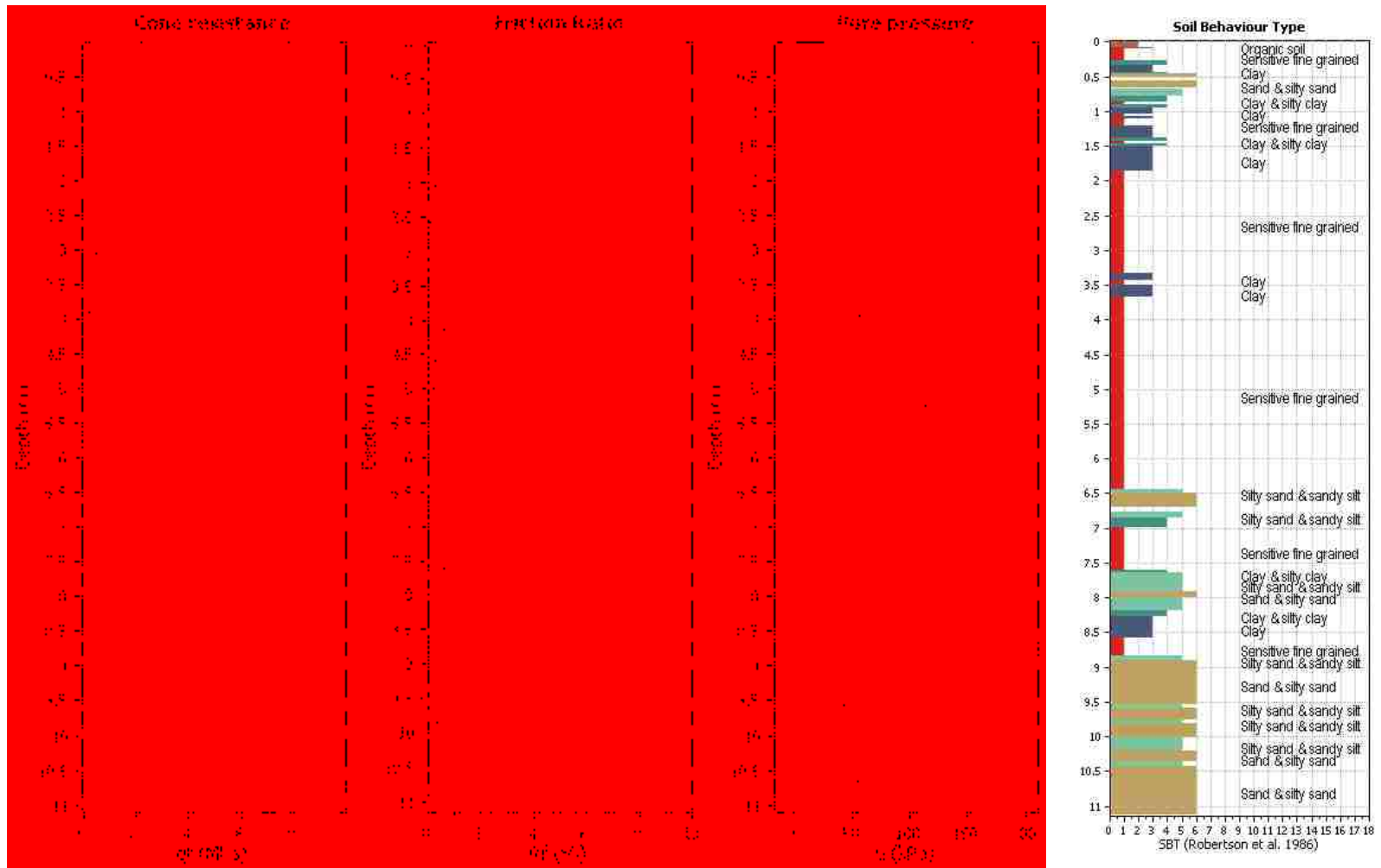


Figure 6-5. Site 1 CPT readings and SBT

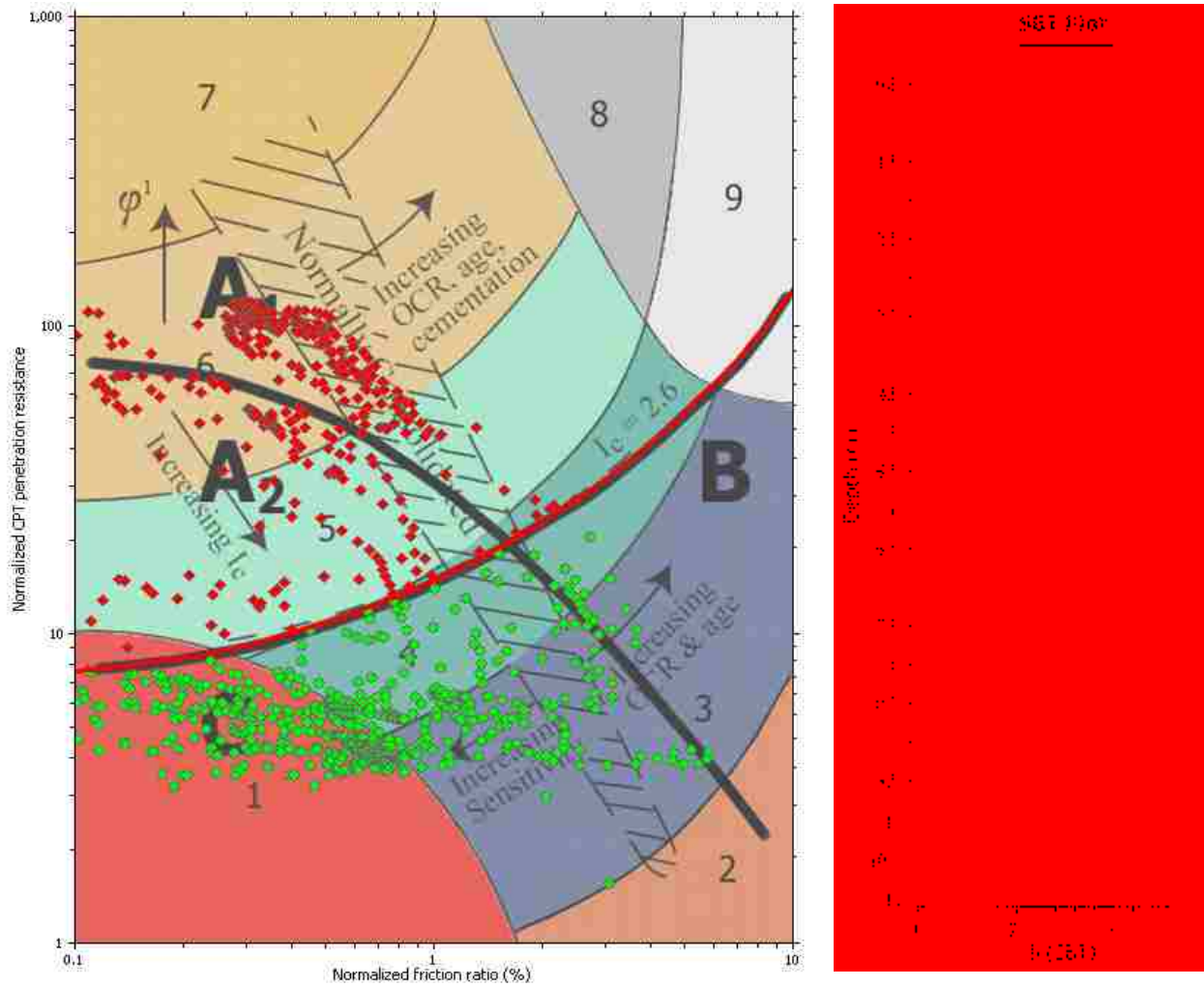


Figure 6-6. Site 1 normalized CPT penetration resistance plotted against normalized friction ratio and I_c with depth

6.2.1 Geomorphology

The Inubuchi village is built on a natural levee and the farmland is built on a flood plain. A geomorphological map and locations of liquefaction are shown in Figure 6-7. The boring log shows that the natural levee is extremely soft and plastic which explains its resistance to liquefaction. The soft clay deposits should not be the Ariake Bay deposits, since the deposits are located deeper down. Local boring logs suggest that the rice fields are layered with sand, gravels, and fill materials. Major river course alterations that occurred during the 1960s and 1970s in Kumamoto significantly altered the natural sediments of the plain due to loose deposition of excess soil. See Figure 6-8 for before and after pictures.

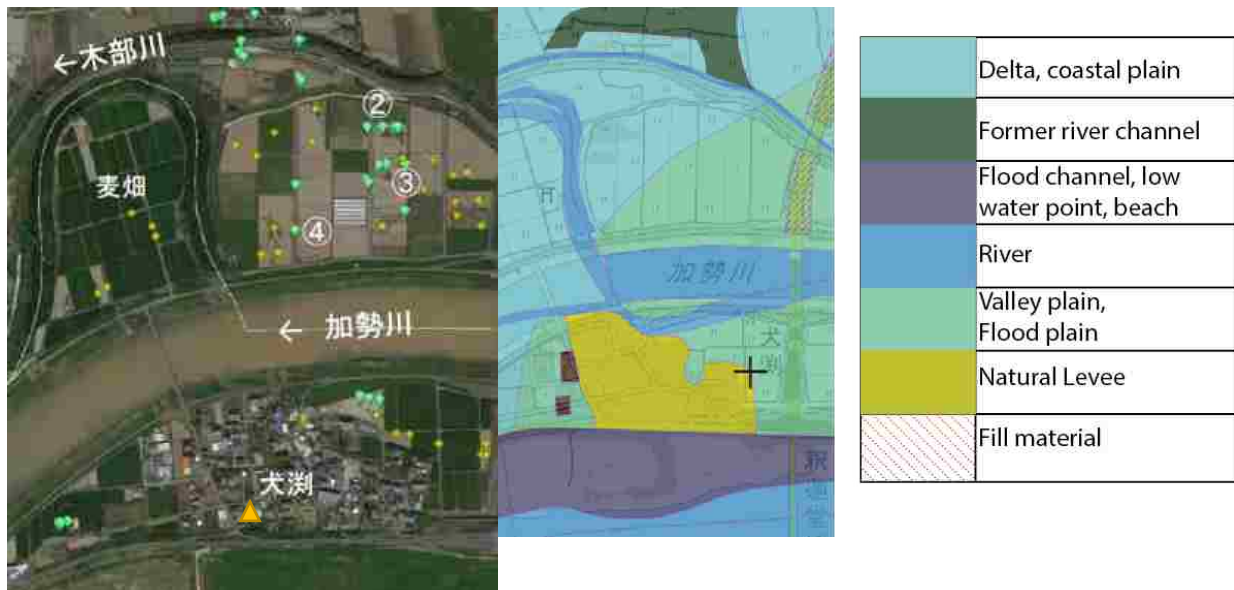


Figure 6-7: Map of liquefied locations with triangle representing boring location and geomorphological land classification map (Wakamatsu et al., 2016; GSI, 2018)



Figure 6-8: Before (1960s) with estimated modern day river course and after (2016) picture (GSI, 2018)

6.2.2 SPT Susceptibility and Initiation Analysis

I did not perform an SPT analysis because none of the site material was susceptible to liquefaction due to high fines content along with high soil plasticity, according to the Boulanger and Idriss (2004) and Bray and Sancio (2006) criteria. The water table was at a depth of one meter from the surface. Fine grained and plastic material dominated the entire profile with the only sand being present at the bottom of the test hole, as expected, due to the underlying pyroclastic deposits. Laboratory testing indicated that these sands were too plastic to liquefy.

6.2.3 CPT Liquefaction Susceptibility and Initiation

I performed a CPT initiation analysis to contrast the results of the SPT analysis. The results of the CPT analysis are shown in Figure 6-9. My analysis predicts liquefaction occurring at the deeper sand layers at an interval of 9 to 11 feet. My analysis also predicted 12 cm of settlement. Little to no surficial manifestation of liquefaction is indicated, based on the Ishihara chart (1985) shown in Figure 6-10.

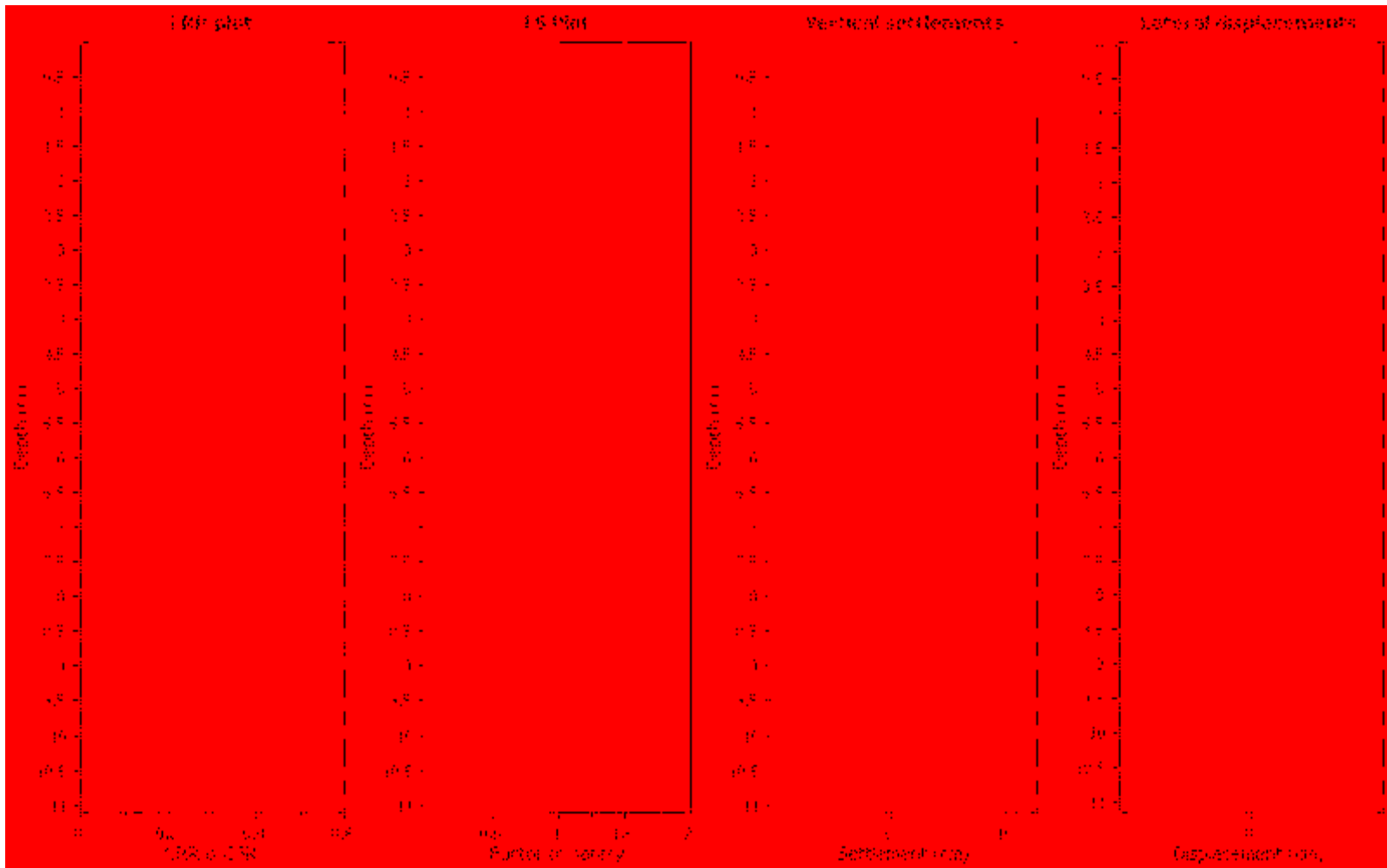


Figure 6-9: Site 1 liquefaction analysis using Youd et al. (2001)

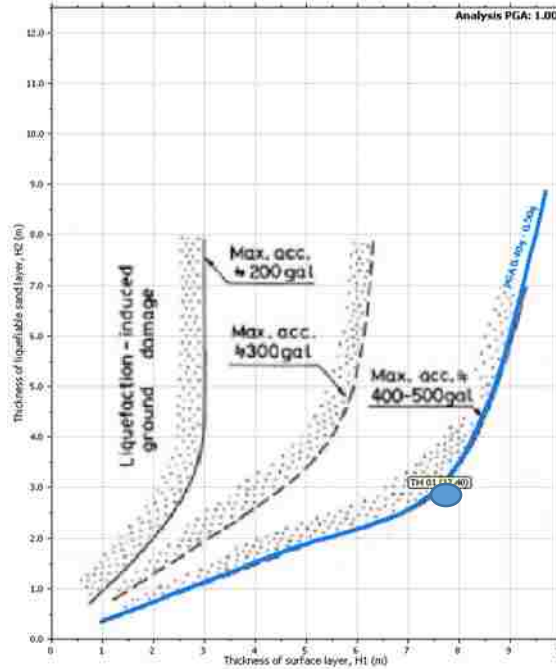


Figure 6-10. Site 1 surficial manifestation of liquefaction (Ishihara, 1985)

6.3 Site 2-1: Downtown Kumamoto with Severe Liquefaction

Site 2-1 is located in a recently urbanized area of Kumamoto City. The coordinates are 32° 46' 11.73" N, 130° 41' 33.90" E. Since the last 50 years, this area has turned from residential farmland to the suburbs of Kumamoto City. The site lies between a large collector street and a heavily traveled arterial street. Site 2-1 lies in the middle of a gravel parking lot, over the location of an old home that was demolished due to liquefaction damage. The liquefaction was among the worst that was observed in Kumamoto following the 2016 Earthquake sequence (Kayen et al., 2017). Figure 6-11 summarizes the boring log data and Figure 6-12 summarizes the CPT data. Figure 6-13 illustrates the normalized CPT penetration resistance plotted against normalized friction ratio and I_c with depth for site 2-1.

Site 2-2 was located on the liquefied channel zone, discussed in chapter 5. The sands were poorly graded, which was consistent with other soil profiles along the liquefied strip (Enomoto & Kubo, 2016; Matsumoto & Hidetoshi, 2016)

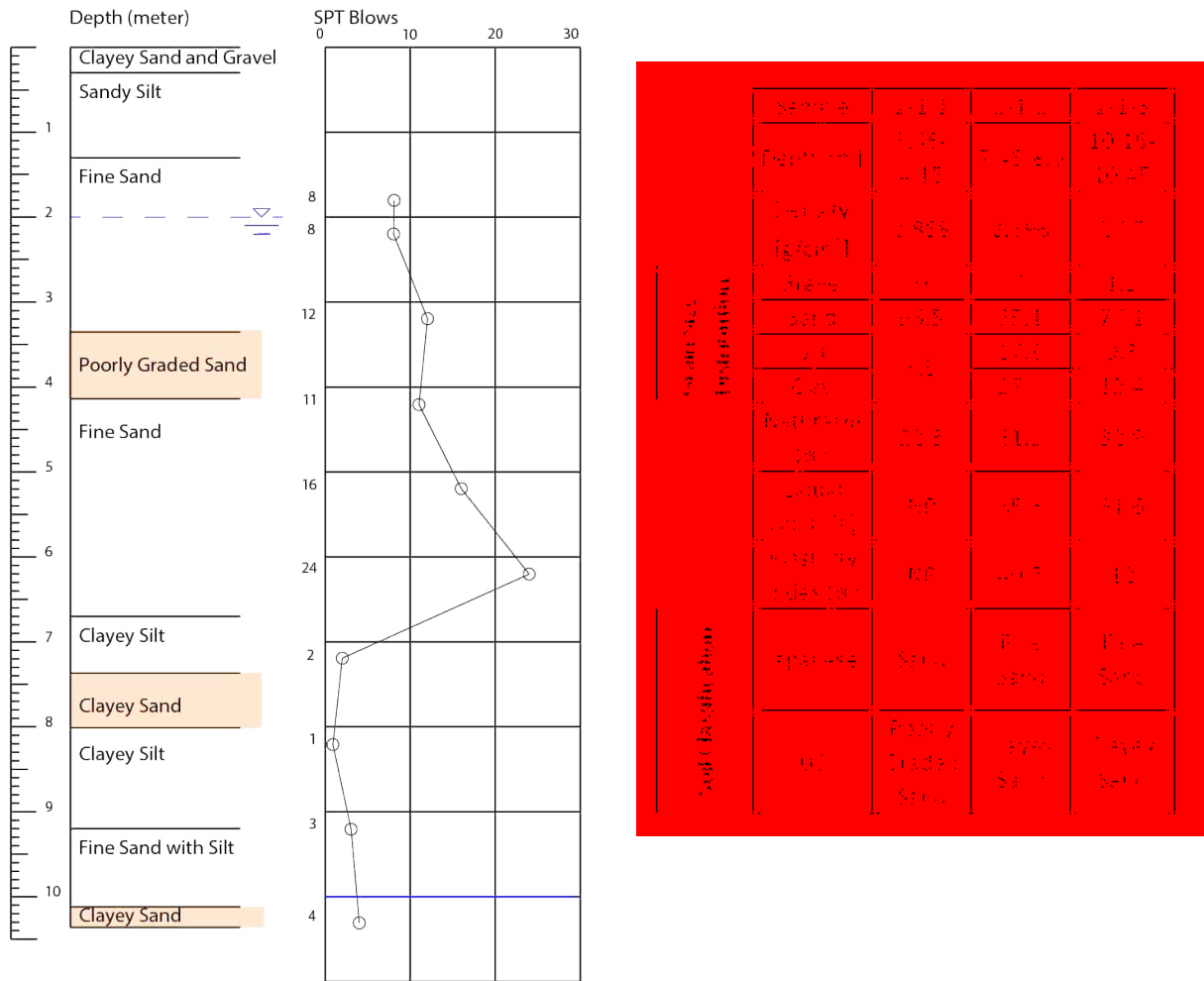


Figure 6-11: Site 2-1 SPT counts, soil layering, and laboratory test results

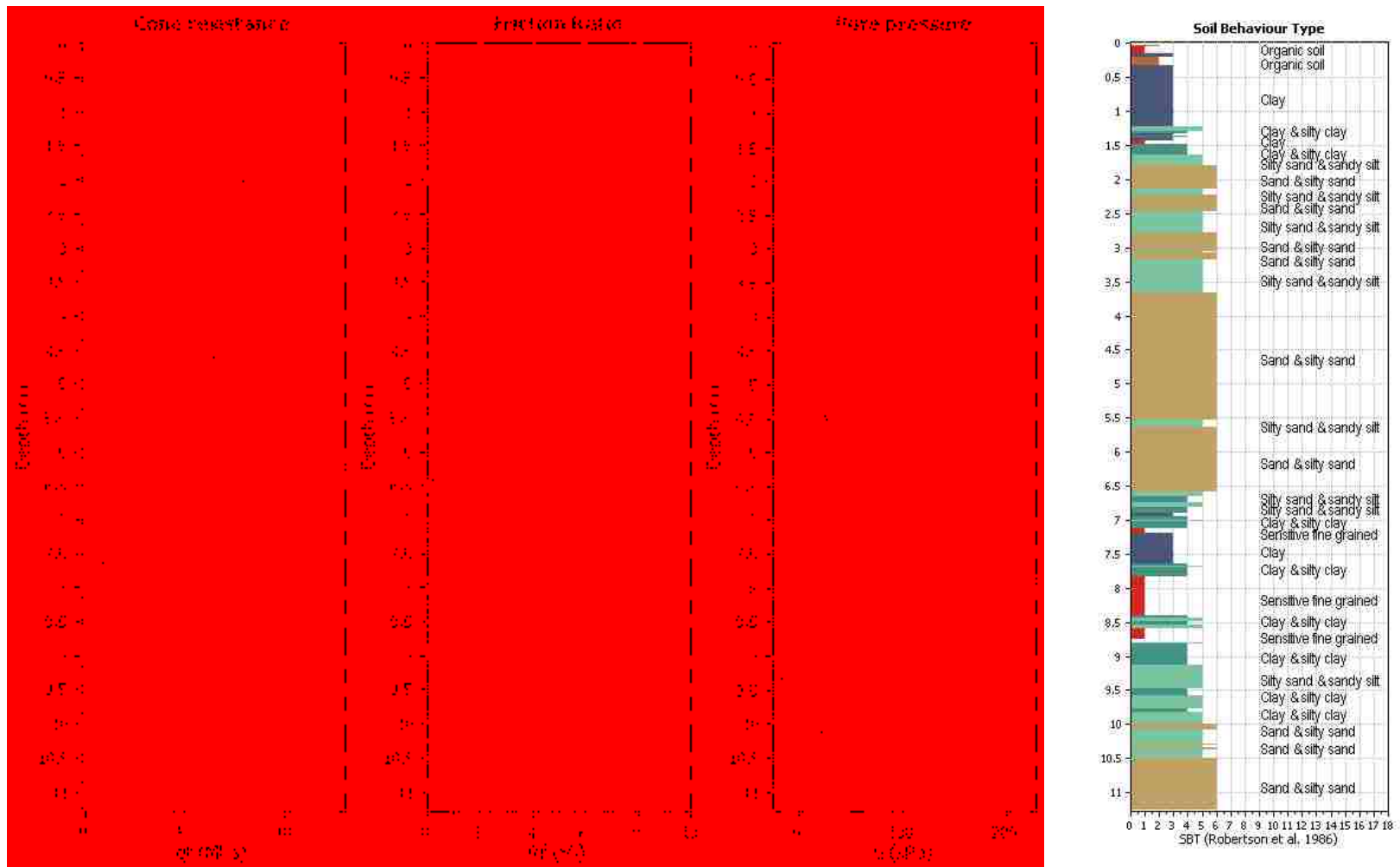


Figure 6-12. Site 2-1 CPT results and SBT

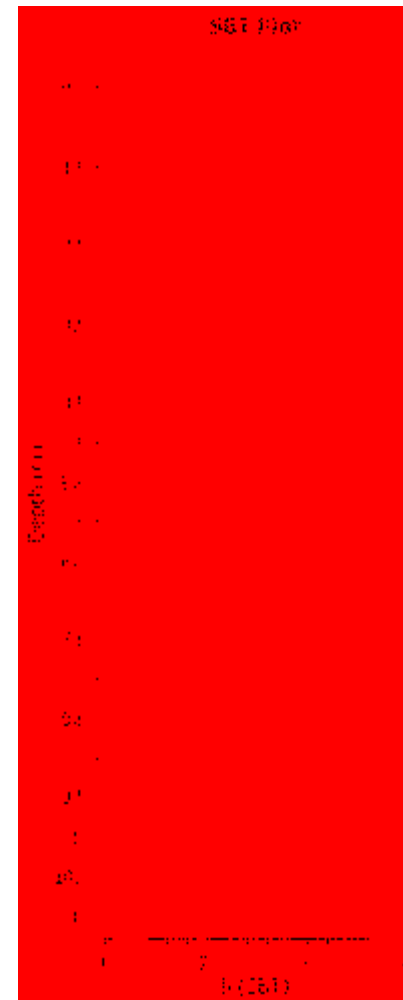
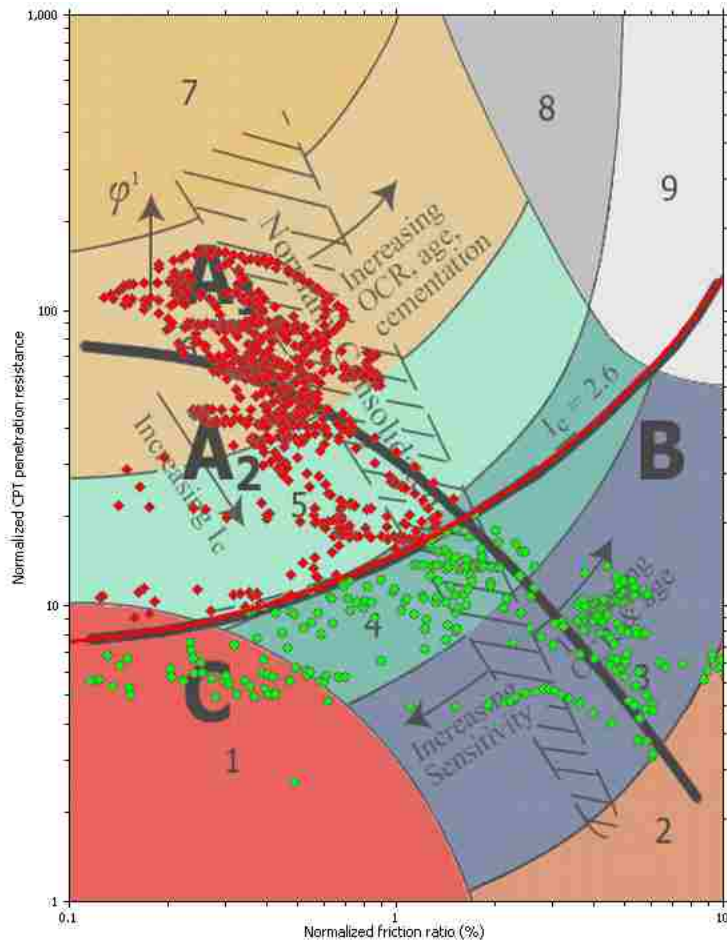
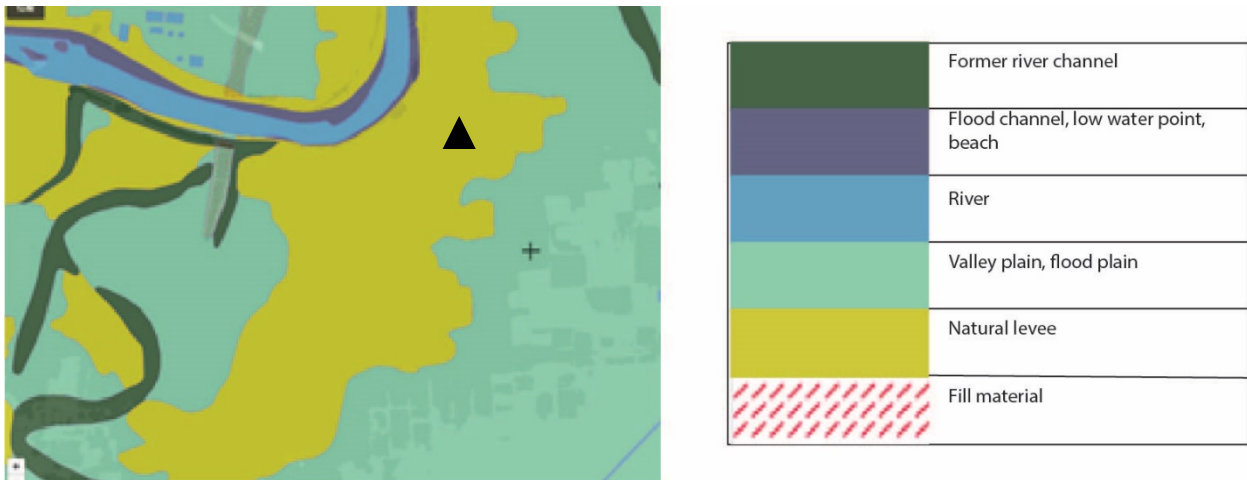


Figure 6-13: Site 2-1 normalized CPT penetration resistance plotted against normalized friction ratio and I_c with depth

6.3.1 Geomorphology

This area is deeply underlain by silts and clays, probably highly weathered byproducts of the Aso-4 pyroclastic flow and Ariake Bay clays. Above these fine grained materials is a five-meter layer of poorly graded sand which is unusual and does not appear to be naturally placed. Sands in the Kumamoto Plain almost always have a significant amount of fines present. Other nearby boring logs off the liquefied strip show sand layers with a large amount of fines present. On top of this poorly graded sand is a one-meter volcanic ash fall deposit. The uppermost layer of Site 2-1 is naturally deposited through ash falls and flood sediments. Figure 6-14 shows the land classification map.



Figures 6-14: Geomorphological land classification map of site 2-1 with site 2-1 indicated by the triangle (GSI, 2018)

6.3.2 SPT Susceptibility and Initiation Analysis

I performed an SPT analysis at this site which predicts the poorly graded sand layer would liquefy. The results are shown in in Table 6-1. Around 3.5 meters of sand was expected to

liquefy for this area. The poorly graded sand has low blow counts and zero plasticity, which makes it highly susceptible to liquefaction.

Table 6-1: Site 2-1 SPT analysis using Boulanger and Idriss method (2016)

Depth interval	Material	PI	FC	N	$N_{1(60cs)}$	$CRR_{M,\sigma'v}$	$CSR_{M,\sigma'v}$	FS (SPT)
0-.5	Sand	#N/A	#N/A	#N/A	#N/A	#N/A	0.33	#N/A
.5-1	Silt	#N/A	#N/A	#N/A	#N/A	#N/A	0.32	#N/A
1-1.5	Silt	#N/A	#N/A	#N/A	#N/A	#N/A	0.32	#N/A
1.5-2	Sand	0	3.5	8	17.27	0.21	0.32	#N/A
2-2.5	Sand	0	3.5	8	15.93	0.19	0.34	0.48
2.5-3	Sand	0	3.5	12	21.74	0.28	0.37	0.62
3-3.5	Sand	0	3.5	12	20.92	0.26	0.39	0.56
3.5-4	Sand	0	3.5	11	18.64	0.22	0.41	0.46
4-4.5	Sand	0	3.5	11	17.99	0.21	0.42	0.43
4.5-5	Sand	0	3.5	16	24.66	0.34	0.44	0.65
5-5.5	Sand	0	3.5	16	24.00	0.32	0.45	0.60
5.5-6	Sand	0	3.5	24	34.30	1.25	0.45	2.13
6-6.5	Sand	0	3.5	24	33.61	1.08	0.46	1.85
6.5-7	Sand	0	3.5	24	32.97	0.95	0.46	1.63
7-7.5	Sand	40.7	44.9	2	8.36	0.11	0.47	#N/A
7.5-8	Sand	40.7	44.9	2	8.28	0.11	0.47	#N/A
8-8.5	Sand	40.7	44.9	1	6.91	0.10	0.47	#N/A
8.5-9	Sand	40.7	44.9	1	6.87	0.10	0.47	#N/A
9-9.5	Sand	12	21.7	3	8.43	0.11	0.47	#N/A
9.5-10	Sand	12	21.7	4	9.56	0.12	0.47	#N/A

6.3.3 CPT Susceptibility and Initiation Analysis

My CPT analysis predicts seven meters of liquefied soil and 25 cm of settlement, shown in Figure 6-15, which is much more severe liquefaction than the SPT results. Tokimatsu et al. (2018) recorded an average of around 15 cm of settlement for a building of this size in this location of the Kumamoto City. There was surficial manifestation of liquefaction at this site and this is properly predicted in Figure 6-16 (Ishihara, 1985).

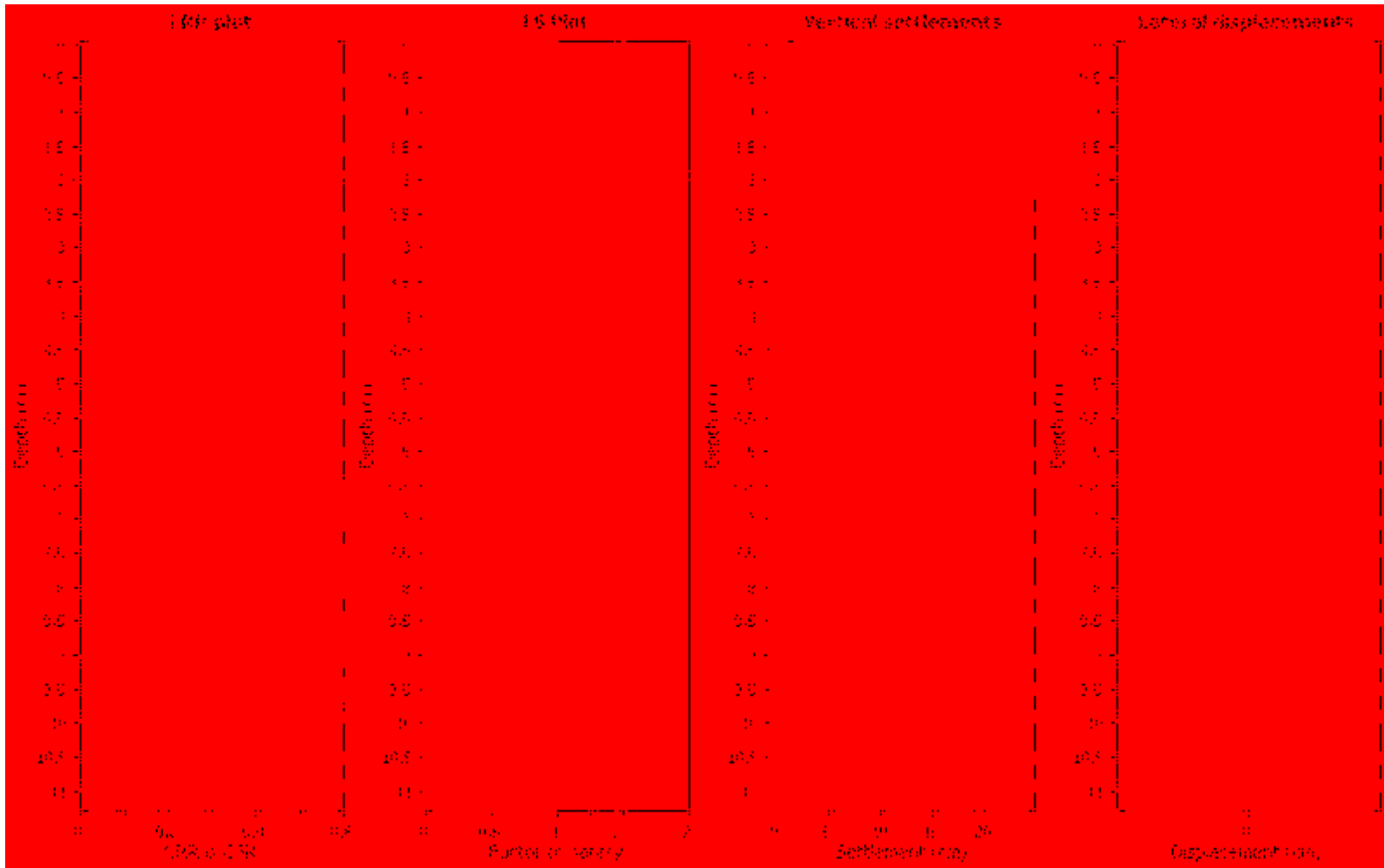


Figure 6-15: Site 2-1 liquefaction analysis using Youd et al. (2001)

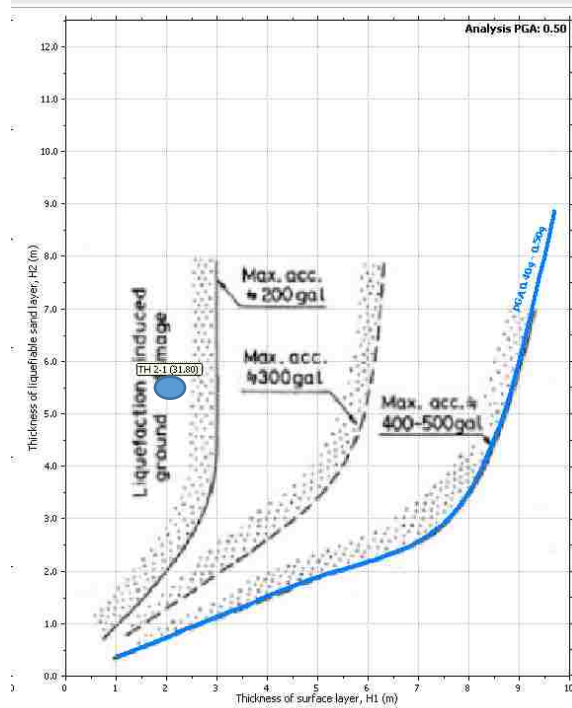


Figure 6-16. Site 2-1 surficial manifestation of liquefaction (Ishihara, 1985)

6.4 Cyclic Triaxial Testing of Samples at Site 2-1

Dr. Shideh Dashti and her Ph. D. student, Mahir Badanagki, who were joint participants on the research for this earthquake, were given undisturbed soil samples from site 2-1 for cyclic triaxial testing. Unfortunately, the undisturbed samples were dried out, requiring them to be remoistened and reconstituted in the laboratory. This would result in lower plasticity measured for halloysite fines present in the sample. The poorly graded sand was non-plastic, however, so the results for that point are more accurate. Reconstituted samples have lower liquefaction resistance than in situ but Yagi (2003) suggests that in-situ cementation of volcanic soils hinders liquefaction and that reconstitution of samples significantly changes soil properties.

We used isotopically consolidated, undrained tests to evaluate soil stiffness degradation and excess pore water generation with an applied cyclic loading frequency of 1 Hz. The summary results of the tests are shown in Figure 6-17 below. The red star indicates the CSR and equivalent cycles measured during the strongest event in Kumamoto. The average CRR line is slightly higher than this point indicating that many soils were close to liquefying. In general, the samples showed a high degree of resistance to liquefaction triggering.

Due to the drying and reconstitution of the samples, these results would need to be validated with additional testing at the site. The results do seem, however, to line up with the SPT and CPT results.

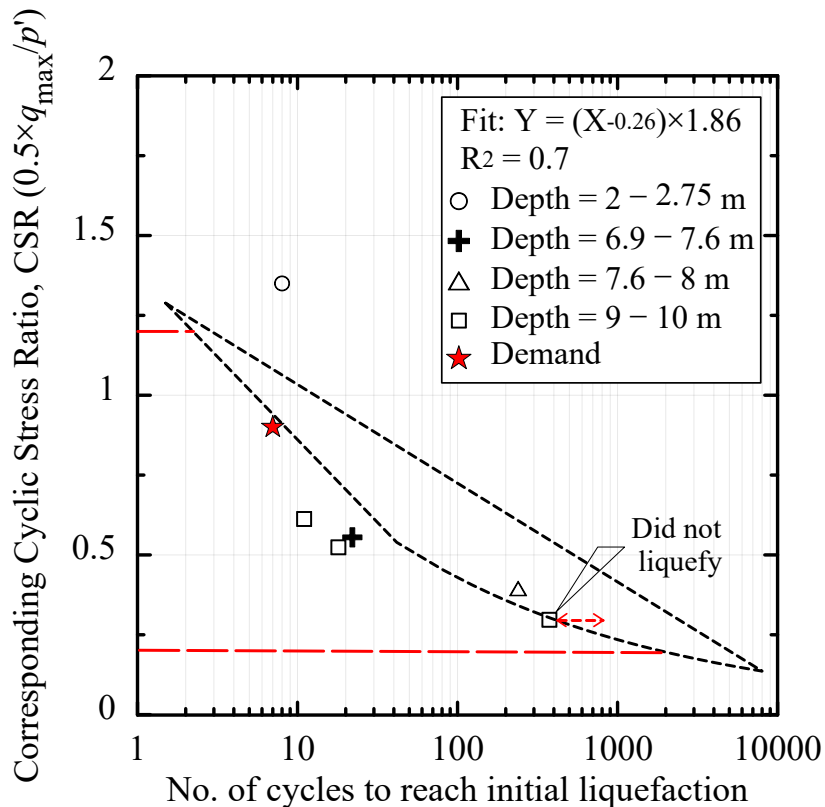


Figure 6-17: CSR vs. Number of cycles obtained experimentally on Kumamoto samples

6.5 Site 2-2: Downtown Kumamoto with no Liquefaction.

Site 2-2 location is about 250 feet to the west of site 2-1, coordinates of 32° 46' 11.88" N, 130° 41' 29.39" E. Site 2-2 is located in a residential area in a small gravel parking lot. No liquefaction was observed in this parking lot and only minor liquefaction was observed in this neighborhood at a sandy field in a nearby elementary school. Site 2-2 is not located on the liquefied strip of land. Figure 6-18 summarizes the SPT data and Figure 6-19 summarizes the CPT data. Figure 6-20 illustrates normalized CPT penetration resistance plotted against normalized friction ratio and I_c with depth.

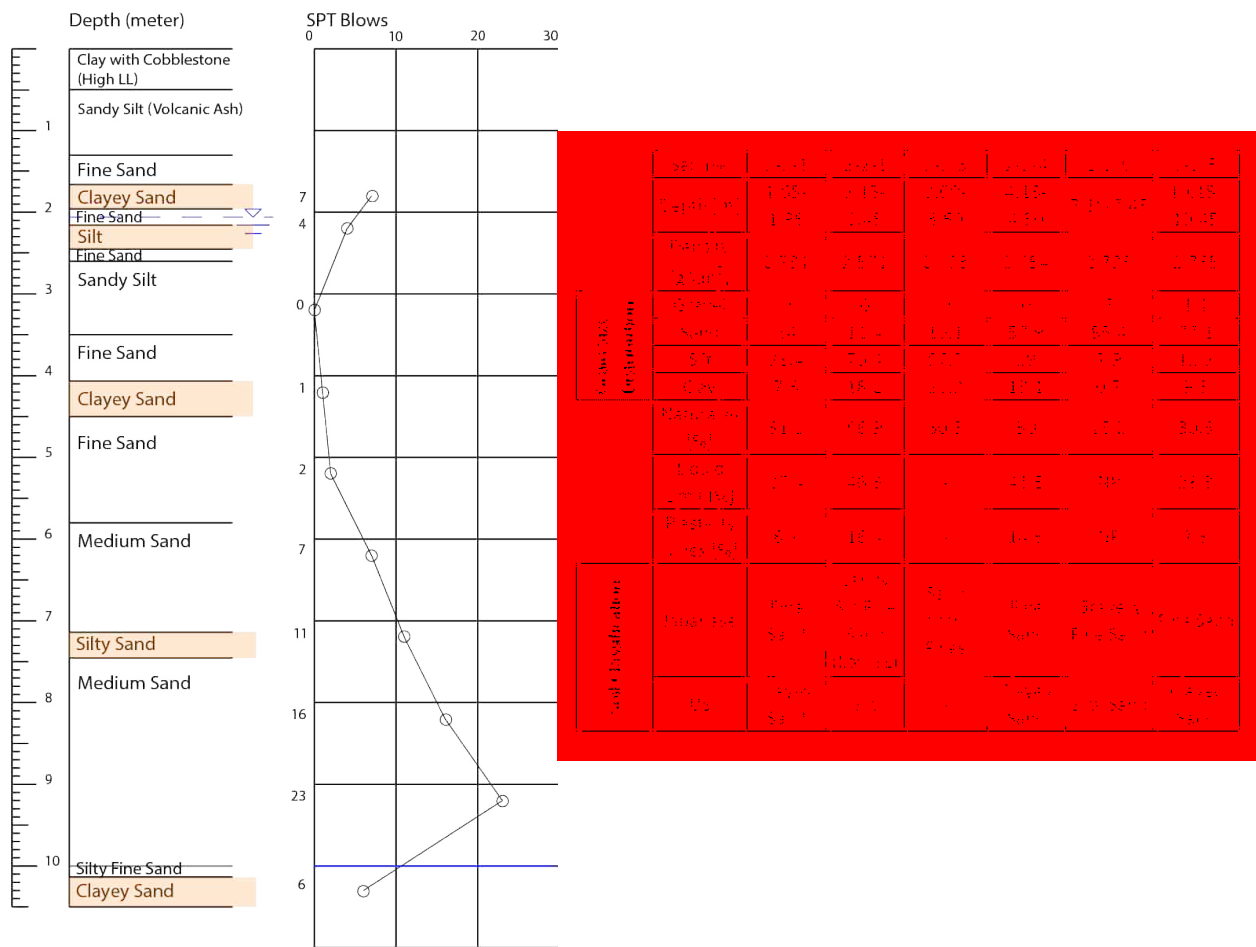


Figure 6-18: Site 2-2 SPT counts, soil layering, and laboratory test results

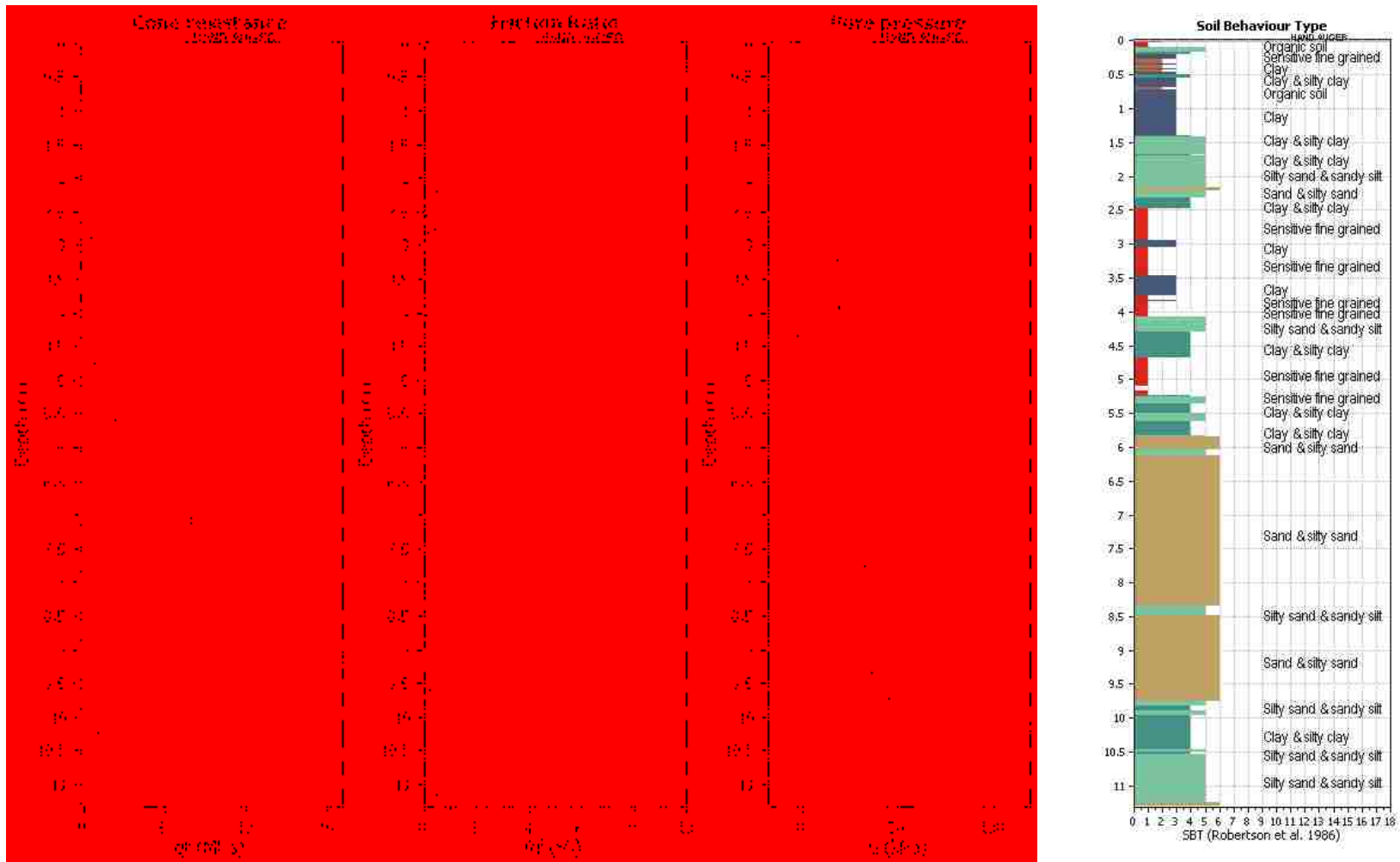


Figure 6-19. Site 2-2 CPT results and soil behavior classification

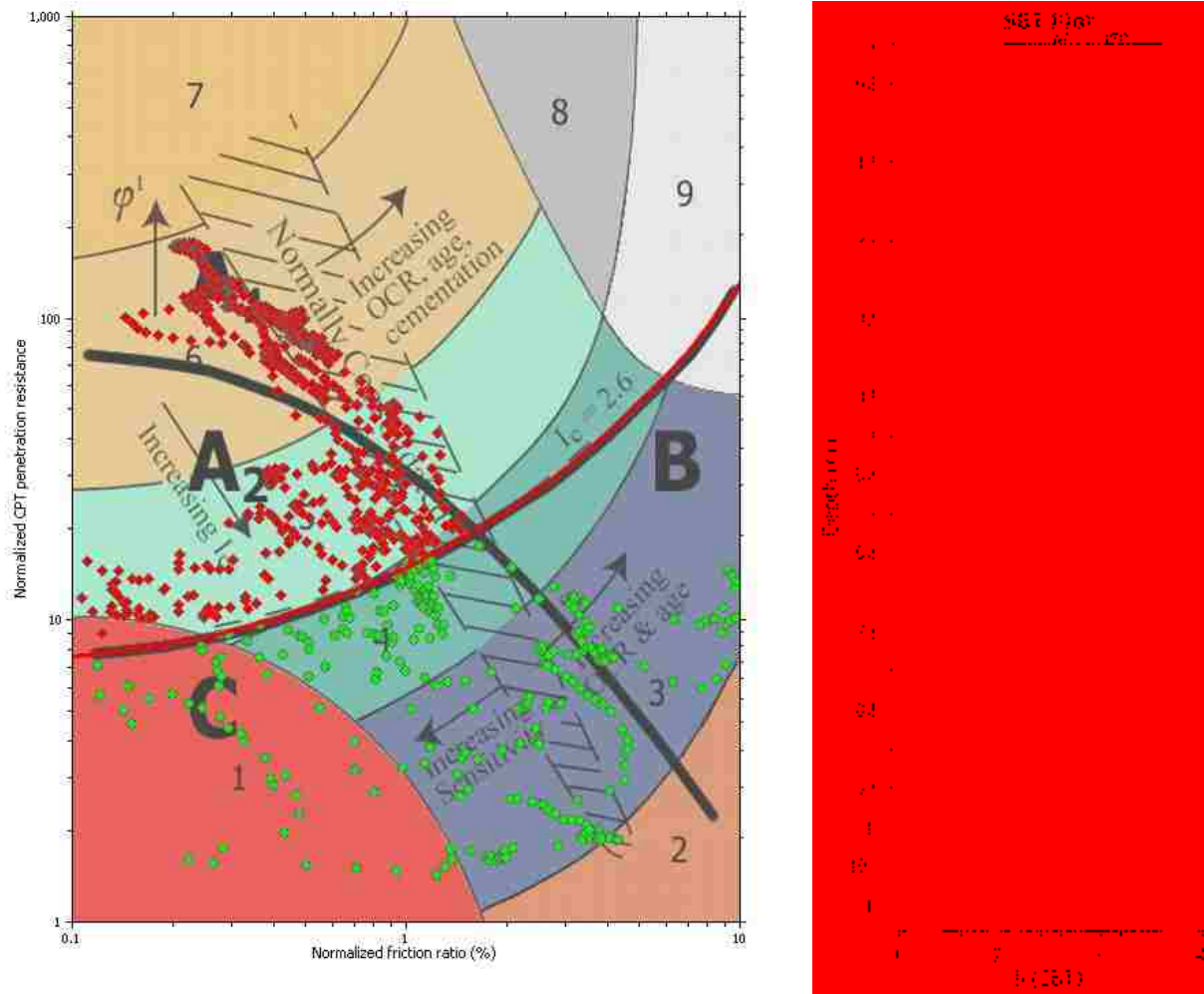


Figure 6-20: Site 2-2 normalized CPT penetration resistance plotted against normalized friction ratio and I_c with depth

6.5.1 Geomorphology

The deeper layers above the Aso-4 flows and Ariake Bay clay sediments are composed of four meters of silty sand mixed with some gravel. Above this is a layer of clayey sand about two meters thick. This site is also located on a natural levee and seems to have naturally deposited material throughout the soil profile.

6.5.2 SPT Susceptibility and Initiation Analysis

I performed an SPT analysis, shown in Table 6-2, which predicts four meters of liquefaction occurring in the silty sand layer. The GEER team (Kayen et al., 2017), however, reported no observed liquefaction at this site. Due to the dry preparation of the soil samples, plasticity in the silty sand layer shown on the boring log is probably higher than results indicate. Unfortunately, only one sample was retrieved between a depth of four and ten meters, at a depth of seven meters. The SPT analysis of the site over-predicted liquefaction.

Table 6-2: Site 2-2 SPT analysis using Boulanger and Idriss method (2016)

Depth interval	Material	PI	FC	N	$N_{1(60cs)}$	$CRR_{M,\sigma'v}$	$CSR_{M,\sigma'v}$	FS (SPT)
0-.5	Clay	#N/A	#N/A	#N/A	#N/A	#N/A	0.33	#N/A
.5-1	Silt	#N/A	#N/A	#N/A	#N/A	#N/A	0.32	#N/A
1-1.5	Silt	#N/A	#N/A	#N/A	#N/A	#N/A	0.32	#N/A
1.5-2	Sand	8.7	36	7	20.28	0.25	0.32	#N/A
2-2.5	Sand	8.7	36	4	13.69	0.17	0.34	#N/A
2.5-3	Silt	16.4	88.6	4	13.29	0.16	0.37	#N/A
3-3.5	Silt	16.4	88.6	0	5.52	0.10	0.39	#N/A
3.5-4	Silt	16.4	88.6	0	5.52	0.10	0.41	#N/A
4-4.5	Sand	14.5	42.1	1	7.35	0.11	0.43	#N/A
4.5-5	Sand	14.5	42.1	1	7.27	0.11	0.44	#N/A
Table 6-2: Continued								
5-5.5	Sand	14.5	42.1	2	8.79	0.12	0.45	#N/A

5.5-6	Sand	14.5	42.1	2	8.67	0.12	0.46	#N/A
6-6.5	Sand	0	8.6	7	10.90	0.13	0.46	0.27
6.5-7	Sand	0	8.6	7	10.58	0.13	0.47	0.26
7-7.5	Sand	0	8.6	11	15.73	0.17	0.47	0.35
7.5-8	Sand	0	8.6	11	15.34	0.17	0.47	0.34
8-8.5	Sand	0	8.6	16	21.52	0.25	0.47	0.48
8.5-9	Sand	0	8.6	16	21.08	0.24	0.47	0.47
9-9.5	Sand	0	8.6	23	29.62	0.53	0.47	0.98
9.5-10	Sand	0	8.6	23	29.14	0.50	0.47	0.93
10-10.5	Sand	7.8	21.8	6	11.90	0.13	0.46	#N/A

6.5.3 CPT Susceptibility and Initiation Analysis

I performed a CPT analysis, shown in Figure 6-22, which predicts around seven feet of liquefaction and 25 cm of predicted settlement. The GEER (Kayen et al., 2017) reported no settlement at this site. The Ishihara (1985) plot predicts significant surficial liquefaction as shown in Figure 6-21, which was not observed at the site.

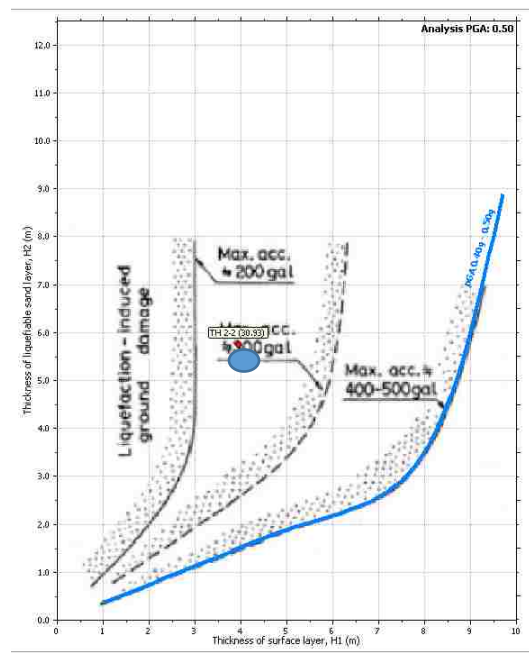


Figure 6-21. Site 2-2 surficial manifestation of liquefaction (Ishihara, 1985)

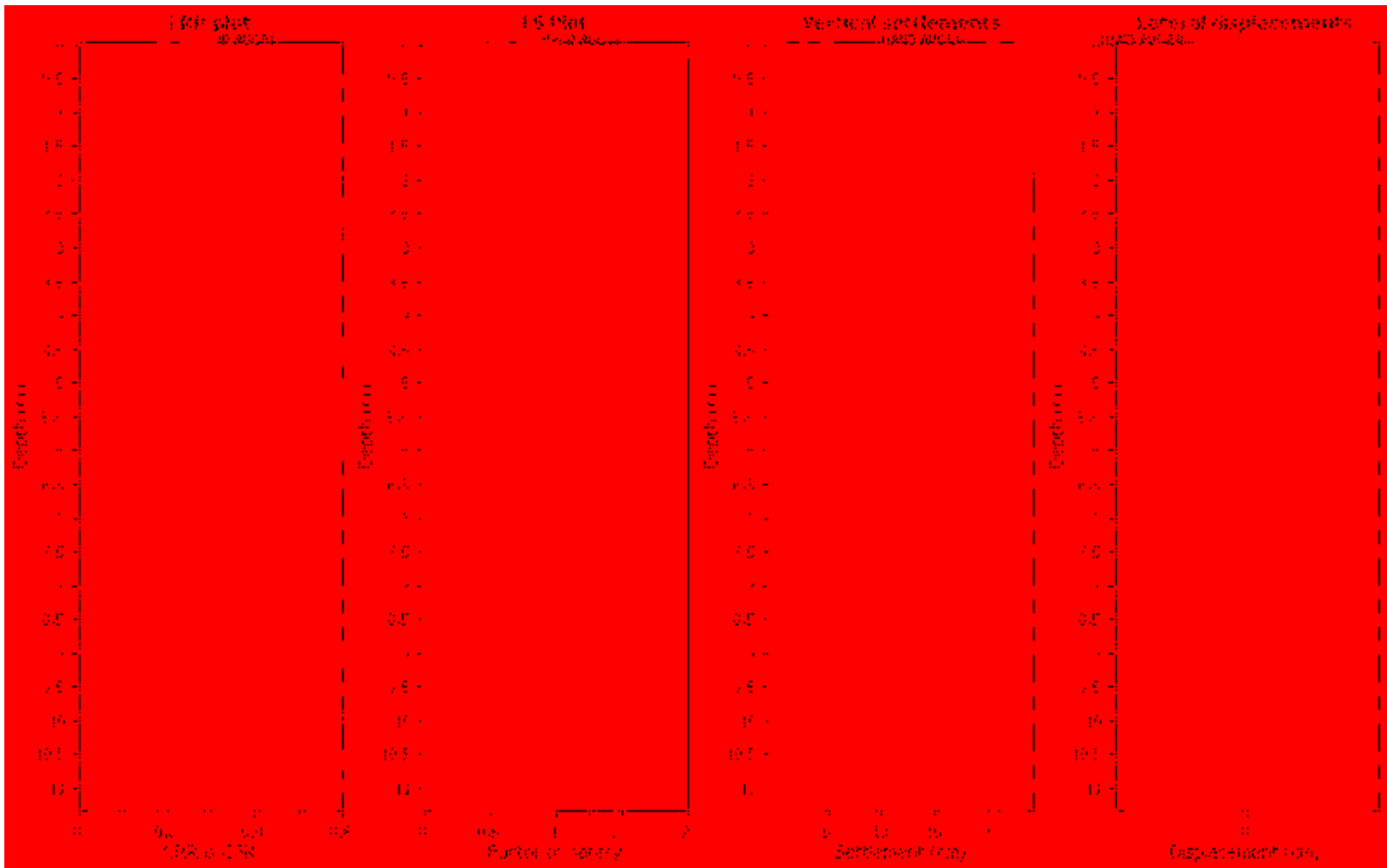


Figure 6-22: Site 2-2 liquefaction analysis using Youd et al. (2001)

6.6 Site 4: Levee Located Near the Epicenter with Minor Liquefaction

Site 4 is the farthest away from Kumamoto City, and lies nearly at the terraces of Mt. Aso. Site 4 lies just west of Mashiki and experienced very high ground motions. The coordinates are 32° 44' 17.44" N, 130° 42' 2.47" E. Site 4 is located on a former river channel on the Akizu River that has now been transformed into a backyard farming plot. The GEER (Kayen et al., 2017) team reported lateral spread like cracking, and minor fissures and sand boils, and minor liquefaction in the neighborhood to the north. Movement towards the river, however, was not confirmed. Figure 6-23 is the SPT summary and Figure 6-24 is the CPT summary. Figure 6-25 illustrates normalized CPT penetration resistance plotted against normalized friction ratio and I_c with depth. Site pictures are shown in Figure 6-26.

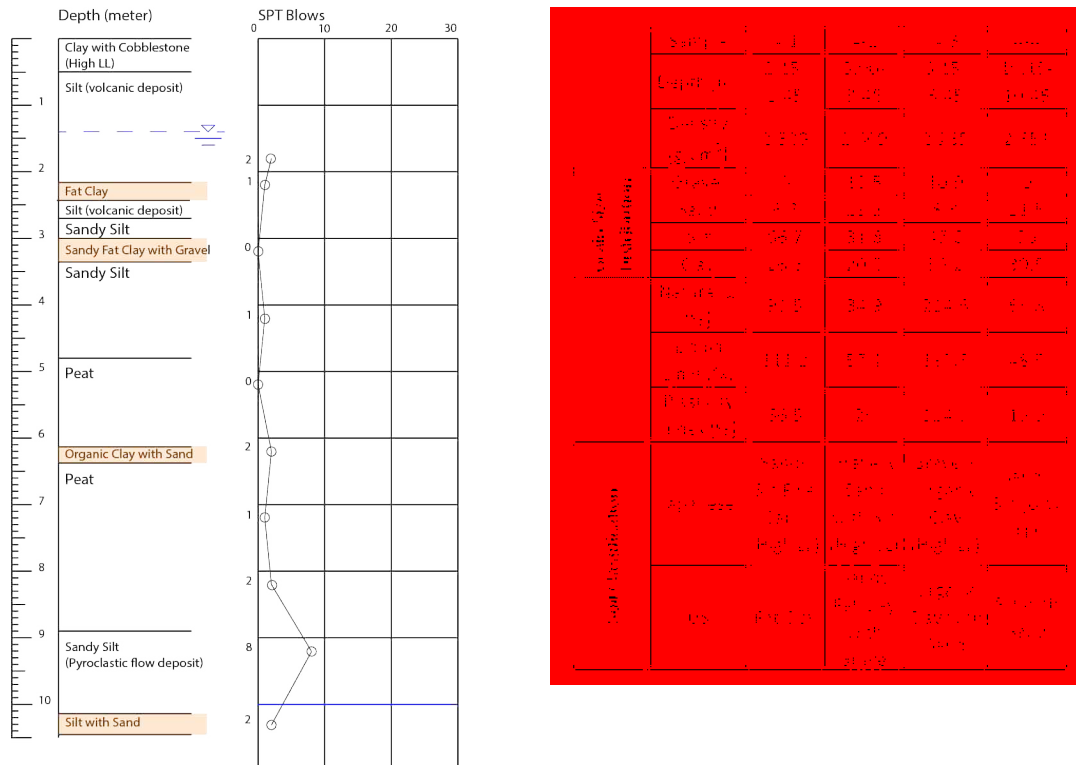


Figure 6-23: Site 4 SPT counts, soil layering, and laboratory test results

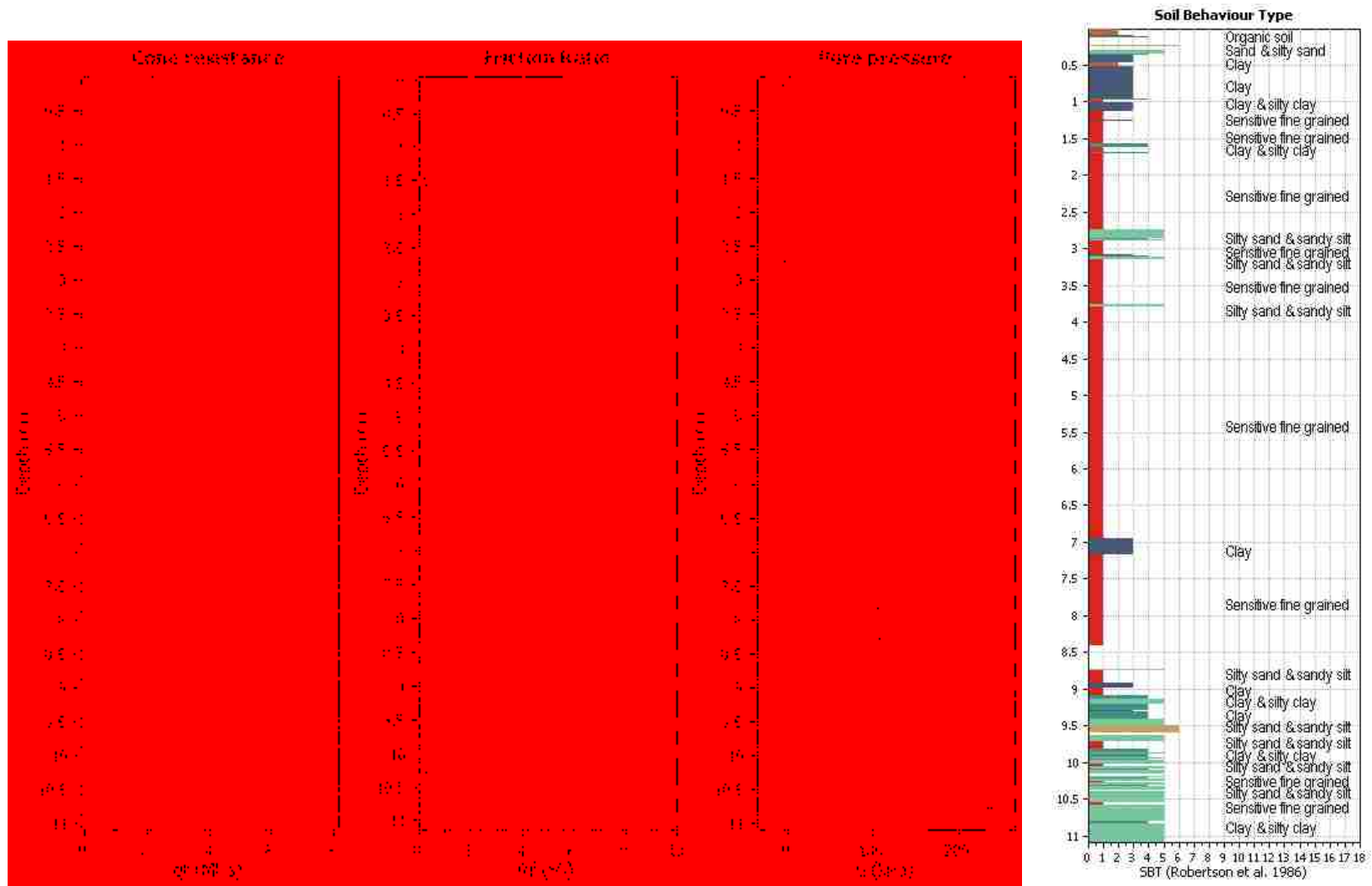


Figure 6-24. Site 4 CPT results and soil behavior classification

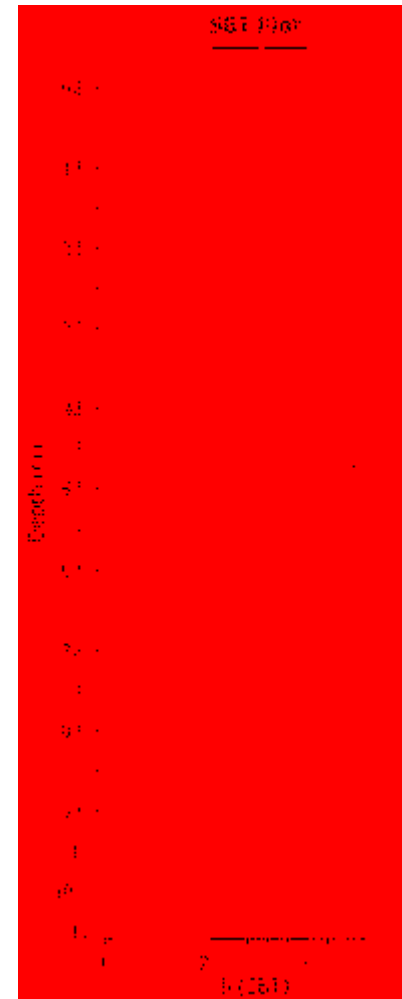
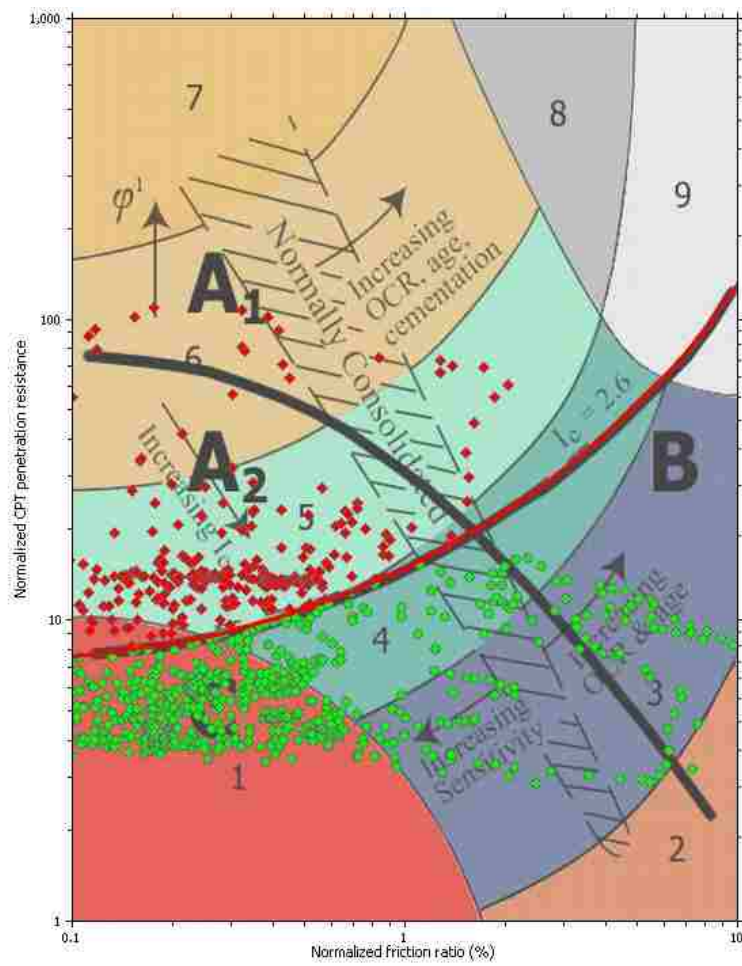


Figure 6-25: Site 4 normalized CPT penetration resistance plotted against normalized friction ratio and I_c with depth



Figure 6-26. Hypothesized lateral spread at site 4 and observed fissures and ejecta (Kayen et al., 2017)

6.6.1 Geomorphology

Because of the proximity to the Aso terraces, the soils are more heavily influenced by the Aso Caldera. At a depth of nine meters is the Aso-4 pyroclastic flow deposit, which at this proximity to the Caldera is relatively near to the surface compared to other sites on the Kumamoto Plain. Above this flow deposit is a thick layer of peat. Above the peat is a fresh deposit of volcanic sediment. The river has been extensively altered in the last 40 years, being widened and redirected. Figure 6-27 shows the geomorphology of the region and Figure 6-28 shows the new and old river layout. Recycled materials from the adjacent floodplain were used to fill in this area and were most likely clayey and organic, making compaction difficult. The soil is not suitable for homes, and the area has been turned into a large neighborhood farming plot and a bus stop. In addition, this area is likely highly anisotropic when it comes to soil profile and composition.



Figures 6-27: Geomorphological map of site 4 (GSI, 2018)



Figure 6-28: Present day picture of area 2016 (left) and 1970 (right) (GSI, 2018)

6.6.2 SPT Analysis

I did not perform an SPT analysis as all soils were either too plastic or too organic to liquefy. Other nearby sites may have had minor liquefaction, but our testing indicated otherwise for this test hole. The original, sandy pyroclastic layer at the bottom was also too plastic to liquefy. Although geological reports summarize the pyroclastic flow material as a sand, this sandy material seems plastic and non-susceptible to liquefaction.

6.6.3 CPT Analysis

I performed a CPT analysis, given in Figure 6-30, which predicts around three meters of liquefaction, 17 cm of settlement, and 120 cm of lateral spreading. My analysis shows that no surficial manifestation of liquefaction would have occurred, based on the chart in Figure 6-29 (Ishihara, 1985). The GEER (Kayen et al., 2017) reported minor surficial liquefaction.

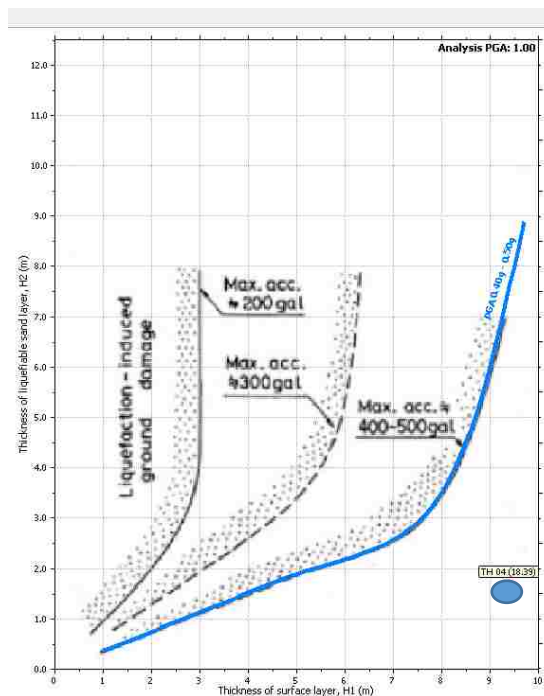


Figure 6-29. Site 4 surficial manifestation of liquefaction (Ishihara, 1985)

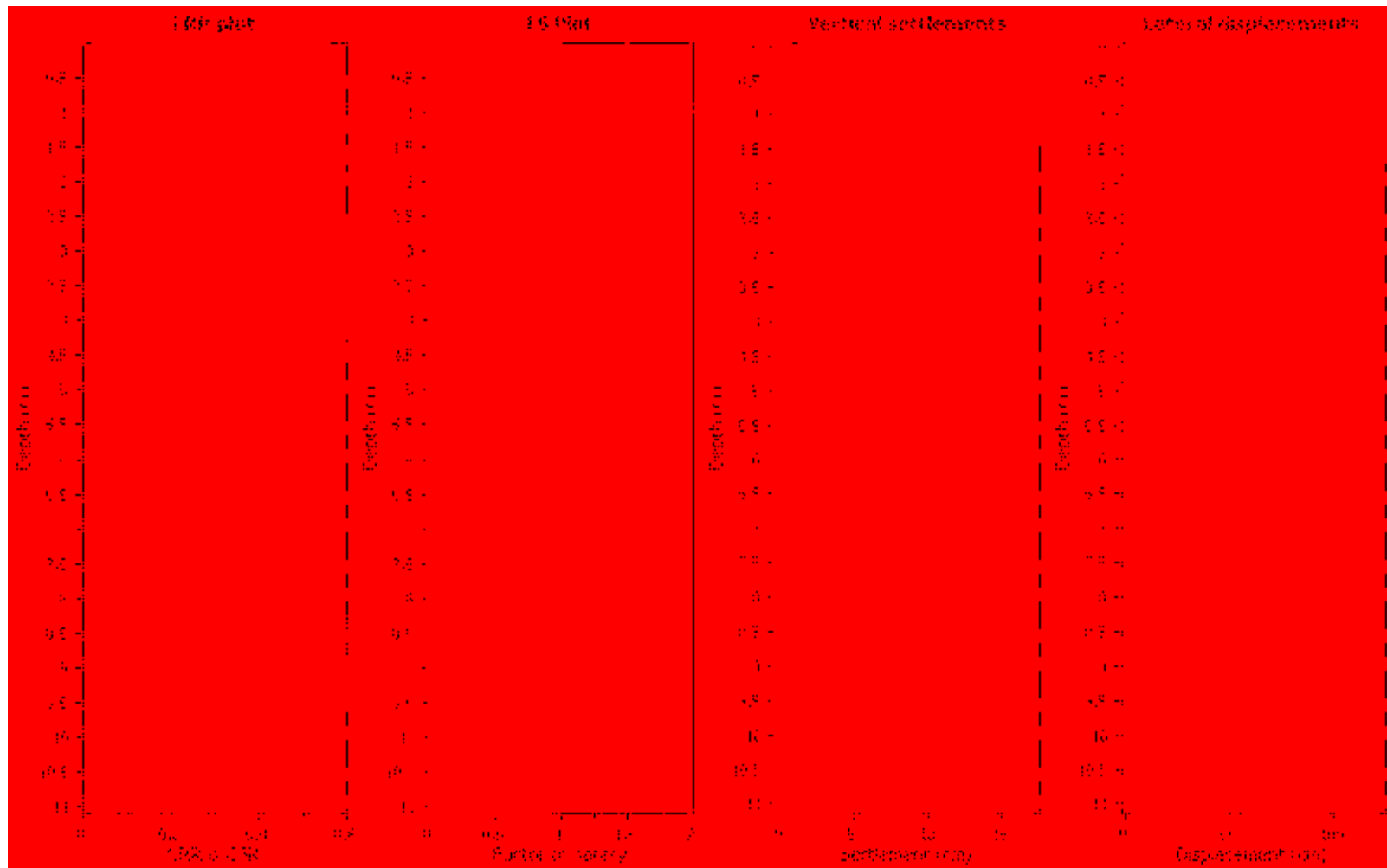


Figure 6-30: Site 4 liquefaction analysis using Youd et al. (2001)

6.7 Slope Stability Analysis of Site 4

The GEER team (Kayen et al., 2017) observed small sand boils and cracking that were theorized to be lateral spreading at site 4. Due to the organic and very weak foundational strength of the site, I performed a slope stability analysis using Slide, provided by Rocscience, to analyze the site for earthquake-induced slope displacements. A horizontal seismic coefficient of 0.425 was used in direction of failure which allows for up to 1.0 meters of lateral displacement with a factor of safety of 1.0. The seismic coefficient of 0.425 was computed using charts explained in Hynes-Griffin and Franklin (1984). A PGA of 1.0 g was used and is reasonable considering the maximum PGA of 1.18 that occurred just a kilometer to the east of the site. The slope angle was measured to be around 16 degrees. I calculated general soil properties from the text, Embankments on Organic Soil (Hartlen & Wolski, 1996) and equations from Low et al. (2010).

Equations 6-1 through 6-3 are the fundamental equations used to compute material properties. Figure 6-31 and Figure 6-32 give the slope stability analysis for a rotational failure. Figure 6-33 and Figure 6-34 give the slope stability analysis for a block failure. Figures 6-31 through 6-34 have estimated material properties listed. Block failure was plausible given the underlying pyroclastic flow deposits, which create a uniform pumice sand foundation. Both rotational failure and block failure had slope limits set at the approximate location of cracking observed by the GEER team (Kayen et al., 2017).

The slope factor of safety computed using the Bishop simplified procedure went from 2.612 to 0.422 for a rotational failure mechanism and from 2.325 to 0.325 for a block failure mechanism, indicating slope failure. The rotational and block failure plane aligned relatively well with the observed cracking which is shown on the slope stability plots (Kayen et al., 2017).

My analysis suggests that the organic soil would likely have failed along the pyroclastic flow layer during the high intensity shaking. The denser pyroclastic flow layer served as an ideal slip plane for slope failure. The small sand boils and ejecta were likely due to the volcanic sand till near the surface of the soil, just under the surficial clay layer. Many levees in Kumamoto experienced subsidence and cracking due mainly to the weak foundational strength of the soils combined with seismic loading and minor liquefaction (Kyushu Regional Development Bureau, 2012 & 2017). The highly organic contents of site 4 are probably unique to just site 4, but weak foundational material and a dense stratum of sand may be the cause of the cracking of levees and embankments across the Kumamoto Plain. Site 4 experienced a unique combination of shallow seismic slope failure and localized lateral spreading. The GEER team correctly identified this site as a lateral spread (Kayen et al., 2017), though the shallow seismic slope failure was probably the greater factor behind the cracking, which was observed throughout the levees and embankments of the Kumamoto Plain (MLIT, 2017).

$$N_{KT} = 13.4 + 6.65 \cdot w_L \quad N_{KT} \leq 15.2 \quad (\text{Larsson and Mulabdic, 1991}) \quad 6-1$$

w_L = Water content in %

$$\tau_{fu} = \frac{q_T - \sigma_{vo}}{N_{KT}} \quad (\text{Hartlen \& Walski, 1996}) \quad 6-2$$

q_T = Corrected cone tip resistance

σ_{vo} = Initial vertical stress

N_{KT} = Cone factor

$$\tau_{fu} = c + \phi' \quad (\text{Hartlen \& Walski, 1996}) \quad 6-3$$

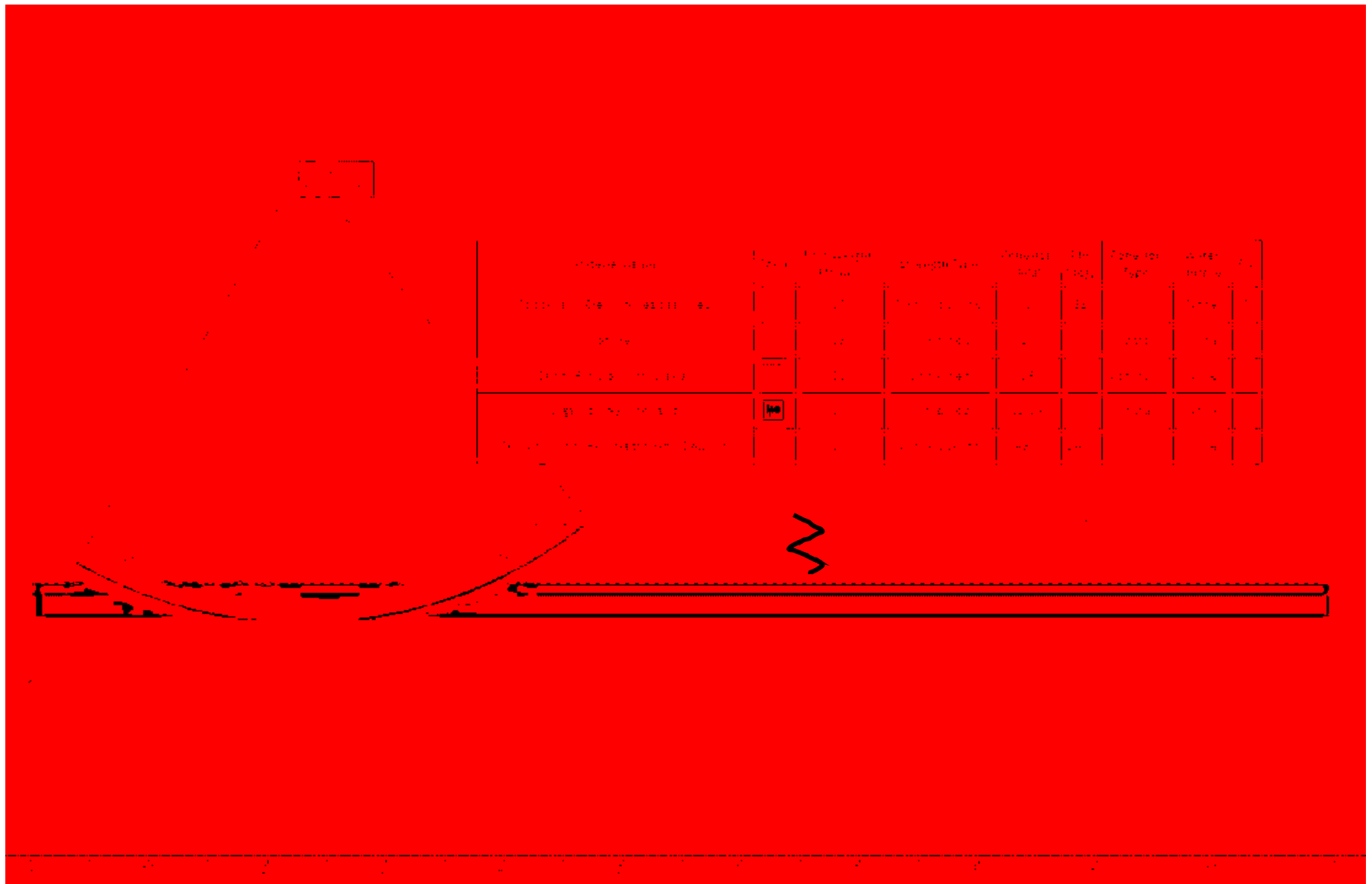


Figure 6-31: 2.612 factor of safety with rotational failure mechanic with static loading



Figure 6-32: 0.422 factor of safety with rotational failure mechanic with seismic loading

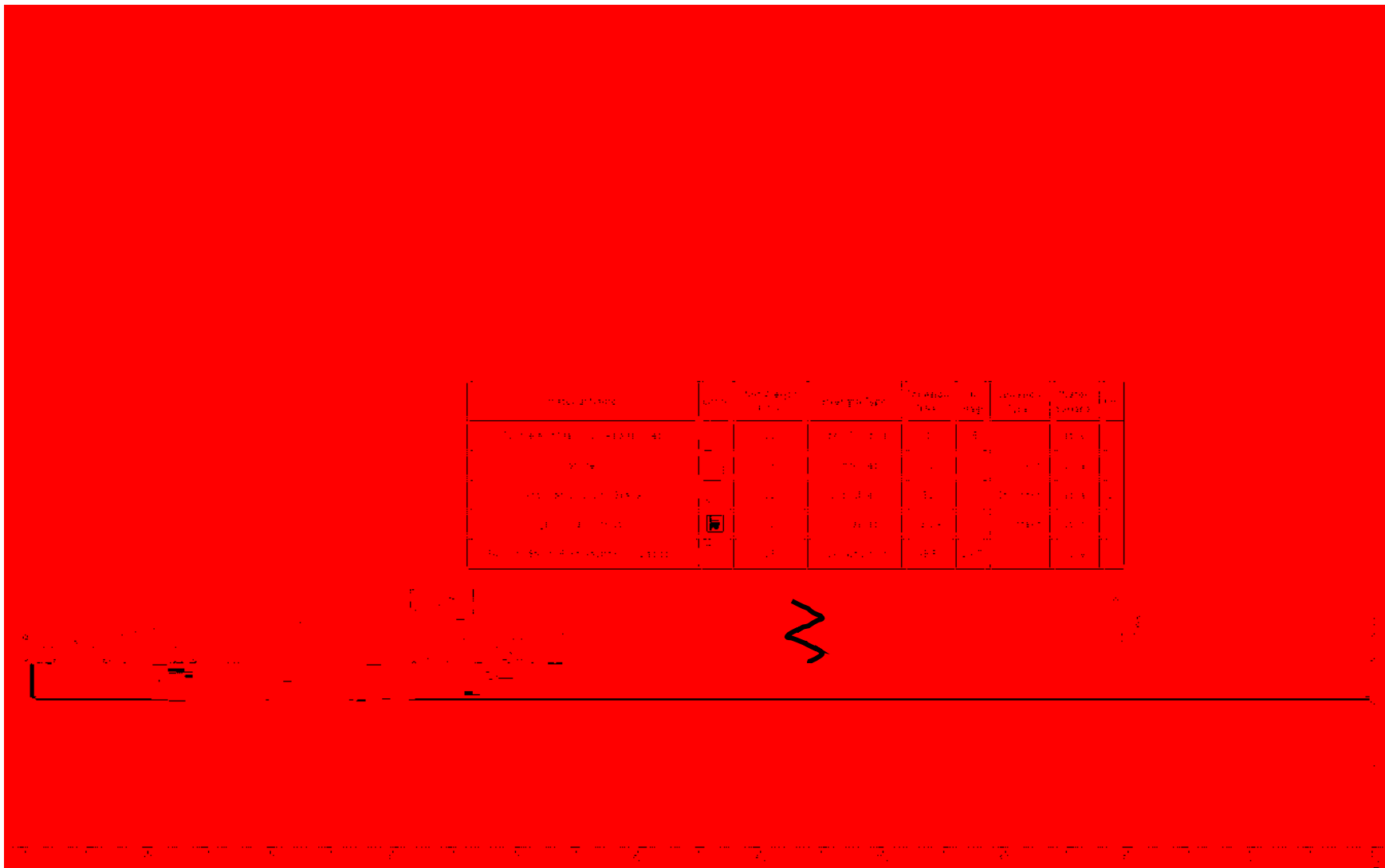


Figure 6-33: 2.323 factor of safety with block failure mechanic with static loading

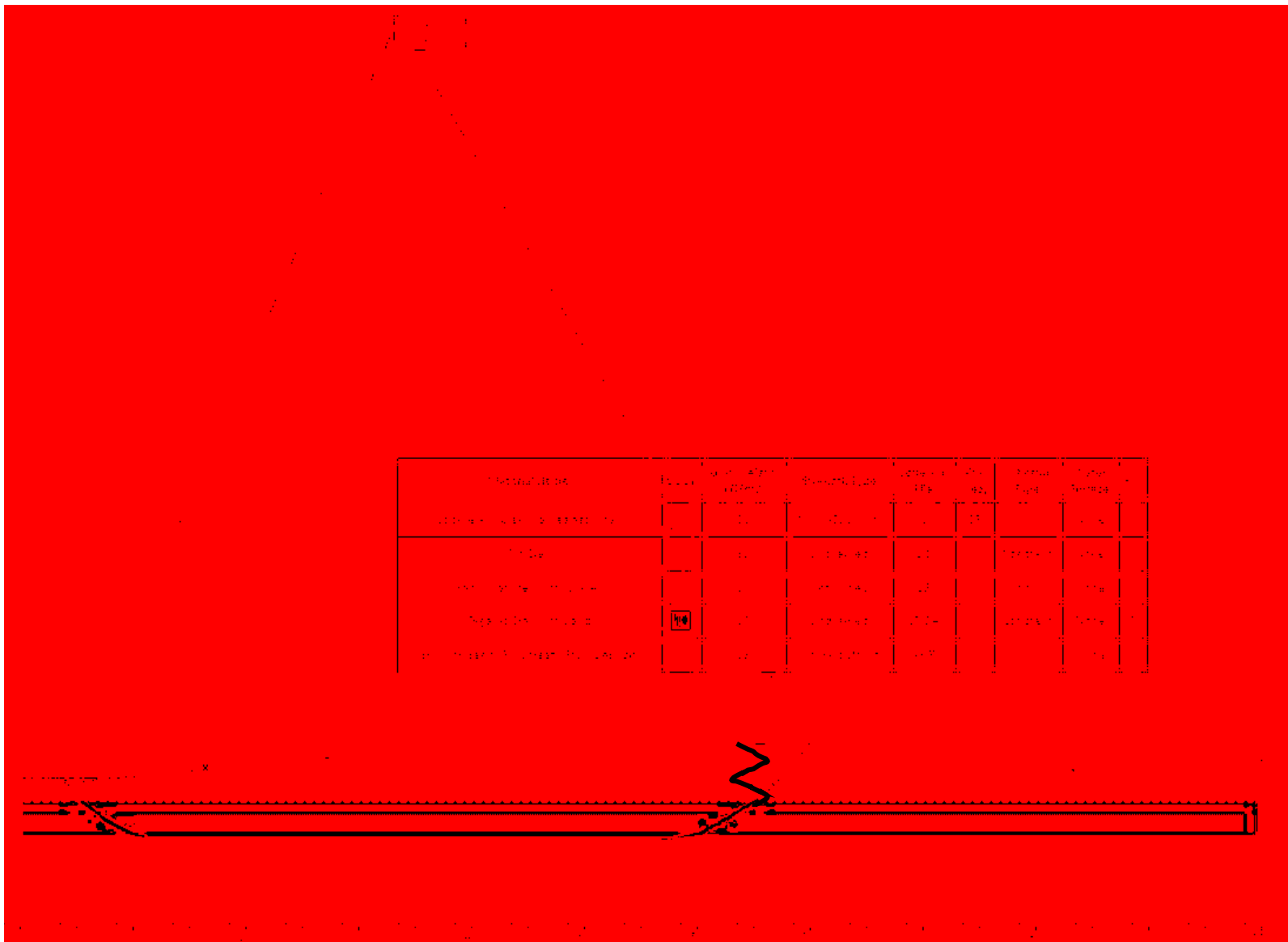


Figure 6-34: 0.325 factor of safety with block failure mechanic with seismic loading

7 DISCUSSION OF RESULTS

This chapter will discuss liquefaction in the Kumamoto Plain, based on publicly available boring logs and the results of the field tests in the previous section. I will compare several different methods of CPT-based liquefaction analyses to see if there are discrepancies between the various methods. I will also discuss the impact of regional geomorphology on liquefaction and misinterpretation of boring logs.

7.1 SPT-based Analysis with Boulanger and Idriss (2014)

The Boulanger and Idriss (2014) liquefaction initiation procedure properly predicted site 2-1 liquefaction, but was overly conservative for site 2-2, where liquefaction did not seemingly occur. There may have been some soil grain crushing which led to low blow count readings, though this needs to be confirmed with mineralogical testing. The greatest advantage of SPT testing was in the sample retrieval, which allowed for relatively accurate determination of fines content and soil plasticity.

7.2 CPT-based Analysis Methods Comparison

I compared the Youd et al. (2001), Idriss & Boulanger (2012), Robertson (2009), and Boulanger and Idriss (2014) CPT liquefaction analyses using Cliq. Note that Idriss and Boulanger (2012) is the same as the Idriss and Boulanger (2008) in the charts below. Youd et al.

(2001) is the same as the Robertson (NCEER 2001). The LPI and LSN are given for all the sites with different methods in Figures 7-1 and 7-2. Predicted settlement and lateral spread are given for all the sites with different methods in Figures 7-3 and 7-4.

The Robertson (2009) method on site 1 and 4 grossly over-predicted liquefaction of the entire profile. The fine-grained soil has a very low factor of safety and this is reflected in the LPI and LSN analysis for sites 1 and 4. The LPI was reasonably consistent between the other for all methods at sites 2-1 and 2-2. Idriss and Boulanger (2012) predicted more severe liquefaction potential and hazards than the Boulanger and Idriss (2014) method. Idriss and Boulanger (2012) was especially over conservative for site 4 lateral spreading. All methods seemed to over-predict liquefaction at site 2-2, which was the natural sandy deposit. The most reasonable and accurate CPT analysis method throughout seemed to be the Youd et al. (2001) method.

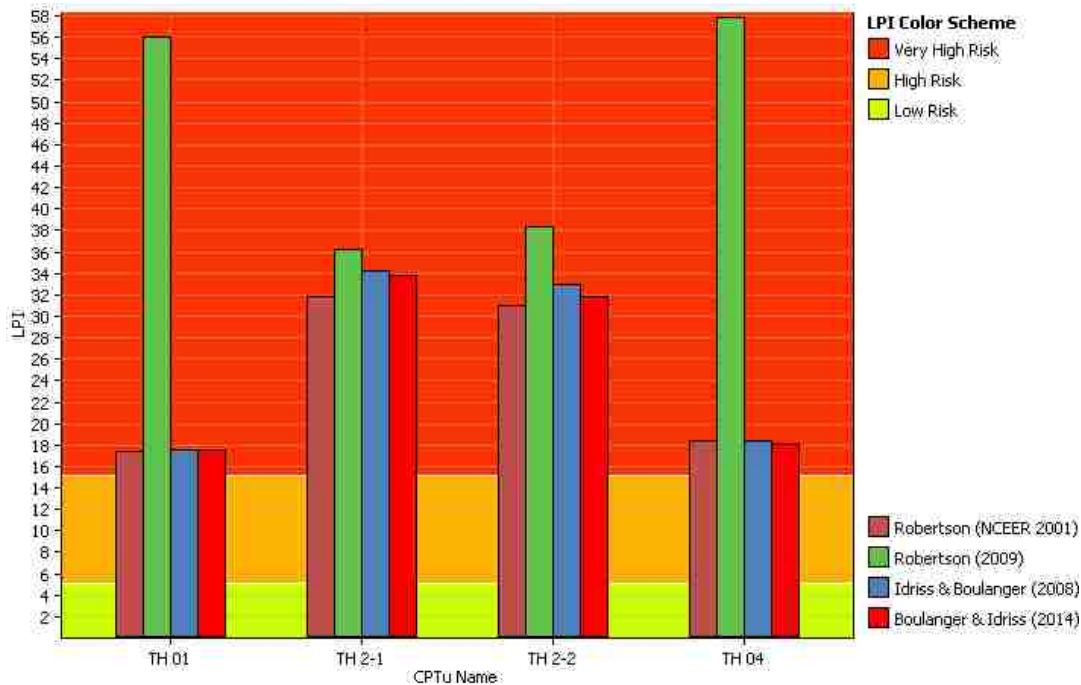


Figure 7-1: LPI for all sites with different methods

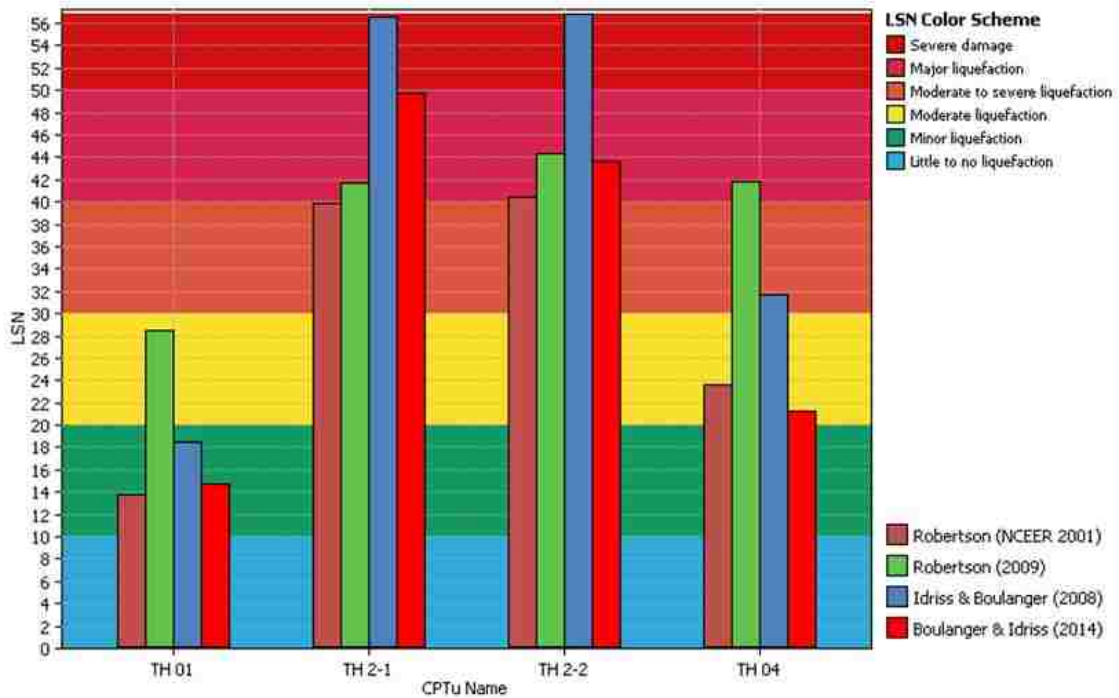


Figure 7-2: LSN for all sites with different methods

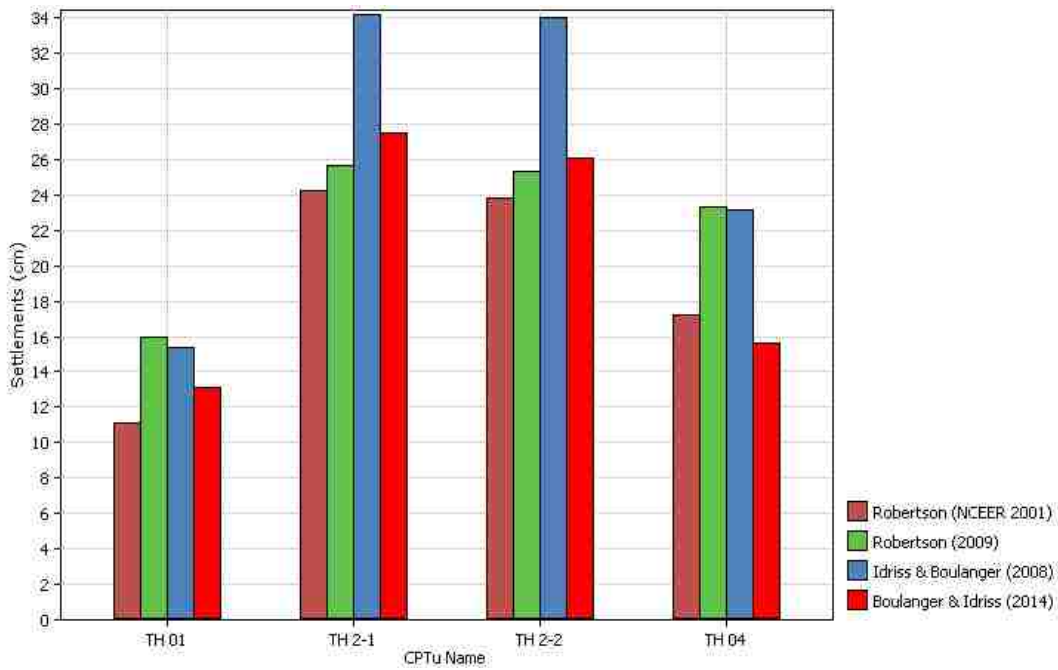


Figure 7-3: Predicted settlement for all sites with different methods

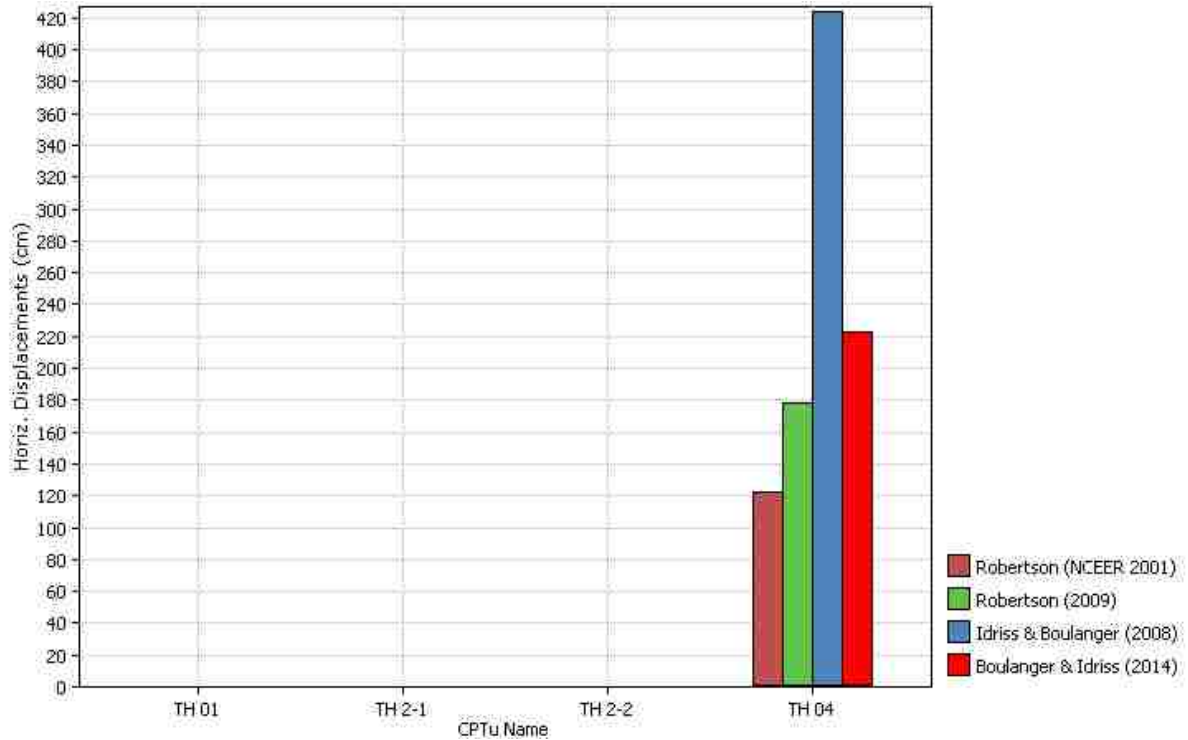


Figure 7-4: Predicted lateral spread for all sites with different methods

7.3 Soil Crushability and Soil Plasticity

Naturally deposited sand with low blow counts are typical throughout the Kumamoto Plain and a list of example boring log ID's is given in Appendix B. These example boring logs were found through KuniJiban, the Japanese public boring log database. The example boring logs all report soil profiles with thick sand layers and low blow counts, like those recorded at Site 2-2. None of the example locations experienced liquefaction. The GEER team (Kayen et al., 2017) may have seen these sandy materials in many of the boring logs and reasonably assumed the

sand would be susceptible to liquefaction. These low blow counts may be the result of soil crushability.

Geological maps roughly indicate around ten meters of sand and silt which encompasses the surface of the plain (Mukunoki et al., 2016). The sandy soils we encountered throughout our test holes usually had high fines content and plasticity. If our test holes are somewhat representative of other soil deposits in the Kumamoto Plain, that would explain the lack of significant liquefaction in these sandy deposits. The high fines content would have been the product of rapid weathering volcanic glasses.

7.4 Regional Geology

A map of liquefied sites overlain with geomorphology is shown in Figure 7-5. Circled areas represent areas with former river channels that are man-filled. Most serious liquefaction in the Kumamoto Plain occurred over man-filled former river channels with natural levees and floodplains having only sporadic pockets of minor liquefaction. This is consistent with Oya's (1995) observations regarding liquefaction susceptibility of geomorphological features.

The northern half of the Kumamoto Plain had almost no liquefaction, whereas the southern half of the plain had many instances of minor liquefaction. Since the northern half is composed of volcanic sediments which rapidly weather and generate fines, this observation is consistent with material covered in chapter 3 and 4. The southern half of the plain experienced more minor liquefaction which makes sense given the presence of metamorphic rocks, sandstone, and mudstone as well as volcanic soils.

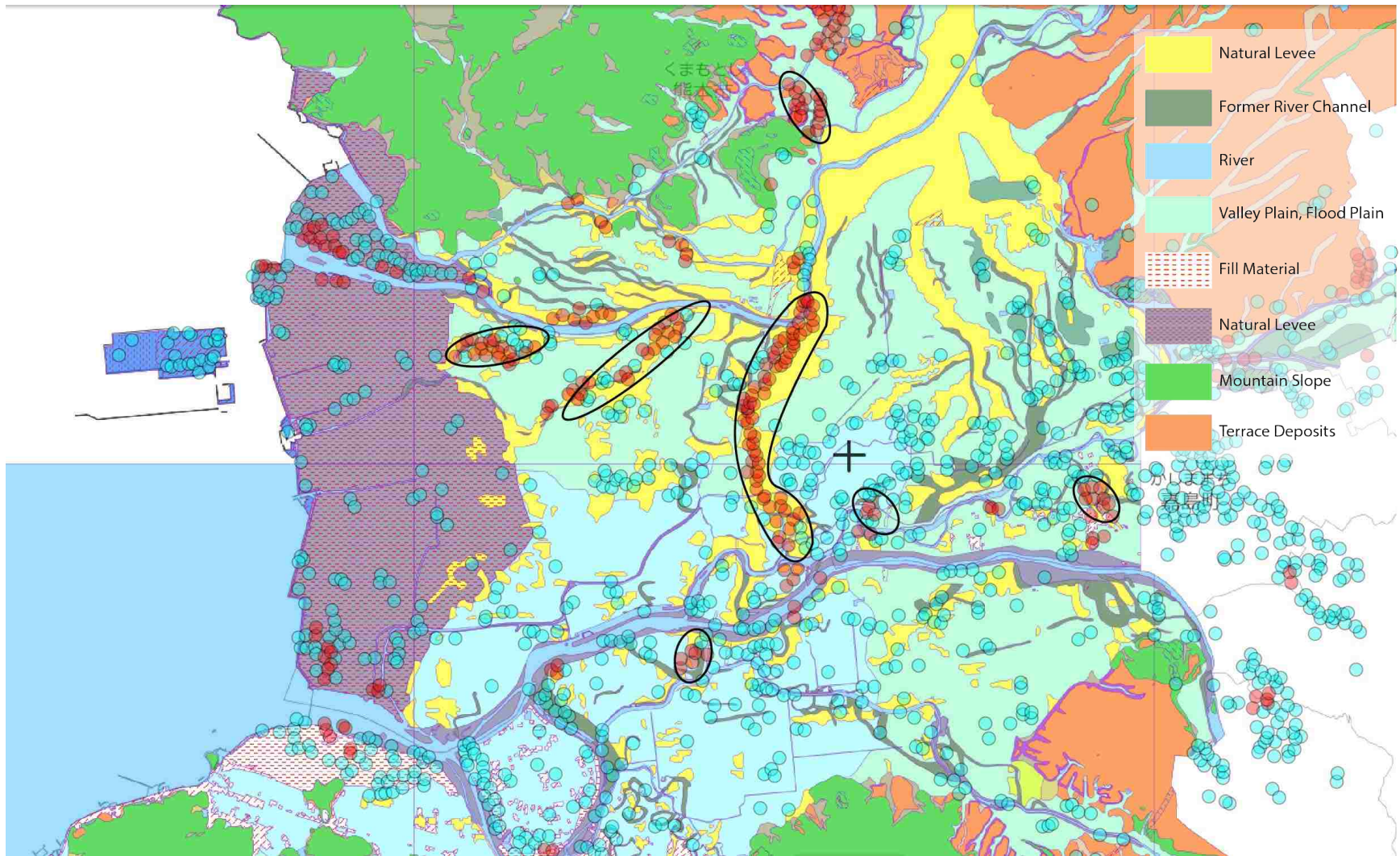


Figure 7-5: Kumamoto Plain geomorphological map with liquefaction sites. Circled sites are locations of former river channels (altered from Mukunoki et al., 2016)

7.5 Misreading of Japanese Logs

A simple reason why liquefaction was over predicted was confusion over Japanese public boring logs. Publicly available boring logs typically did not show laboratory testing data of the bore hole. The logs that did show laboratory data showed the soil's high degree of fine-grained materials and plasticity, even for sand. The un-updated boring logs cloaked the high fines content of the sandy soils. Tokyo Soils and Research also returned boring logs with field observations only, while laboratory testing showed different soil classifications.

In primarily coarse-grained soils, fines content seems to be less emphasized in Japan than in the Unified Soil Classification System (USCS). The differences in Japanese system and the USCS for laboratory test samples of the Kumamoto Plain test holes are listed in Table 7-1. See Appendix A-6 for an example of one Japanese soil classification system as provided by the University of Yokohama.

The classification "Fine sand" was widely written on boring logs but is not defined under either the Japanese classification system or the USCS. Fine sand seems to correlate to clayey sand and medium sand to silty sand, at least based on our boring logs. Japanese publicly available boring logs should be used with caution for liquefaction analysis unless the full testing data is available. The GEER (Kayen et al., 2017) team were likely misled by the incomplete and vague boring logs for the Kumamoto Plain.

Table 7-1: Sample Japanese classification and US classification

Japanese		American (Unified System)	
Abr.	Name*	Abr.	Name
FS-G	Gravelly Sandy Clay		-
CH-S	Sandy Clay (High LL)	CH	Fat Clay
CH-S	Sandy Clay (High LL)	CH	Fat Clay
CH	Clay (High LL)	CH	Fat Clay
SF-G	Gravelly Fine Sand	SC	Clayey Sand
S	Sand	SP	Poorly Graded Sand
SF	Fine Sand	SC	Clayey Sand
SF	Fine Sand	SC	Clayey Sand
SF	Fine Sand	SC	Clayey Sand
ML-S	Sandy Silt Fine Sand (Low LL)	ML	Silt
FS	Sand with Fines		-
SF	Fine Sand	SC	Clayey Sand
S-FG	Gravelly Fine Sand	SW- SM	Well graded sand with silt
SF	Fine Sand	SC	Clayey Sand
MH-S	Sandy Silt Fine Sand (High LL)	CH	Fat Clay
MHSG	Gravelly Sand with Silt (High LL)	CH	Sandy Fat Clay with Gravel
OH-SG	Gravelly Organic Clay (High LL)	OH	Organic Clay with Sand
MLS	Sandy Silt (Low LL)	ML	Silt with Sand

8 CONCLUSION

The Kumamoto earthquake of 2016 was predicted to cause extensive and severe liquefaction throughout the Kumamoto Plain (GEER, 2017). Immediately following the earthquakes, a GEER team led by Professor Rob Kayen of UC Berkley was dispatched to the area. The Japanese and U.S. engineers in the GEER team however, observed mostly minor and sporadic liquefaction. I investigated the paucity and limited scale of liquefaction in the Kumamoto Plain, in direct response to the GEER team's preliminary findings. The findings from this research are listed below.

- 1) SPT and CPT testing predicted liquefaction reasonably well at site 2-1, a former river channel that was filled with sand. Other man filled river channels experienced similar liquefaction but naturally filled river channels showed no signs of liquefaction.
- 2) Liquefaction was over-predicted for sandy deposits that were naturally placed. Volcanic soils, especially prevalent in the northern half of the Kumamoto Plain, were likely resistant to liquefaction due to their high fines content, plasticity, and organic content. Likewise, their crushable nature may have led to artificially low resistance readings for the SPT and CPT. The less volcanic soils of the southern half of the Kumamoto Plain experienced much more sporadic minor liquefaction. Volcanically derived sands in general also showed a higher resistance to liquefaction based on our

cyclic triaxial results and tests by Enomoto & Kubo (2016), though our results would need to be validated with higher quality samples.

- 3) Multiple CPT methods were compared and gave significant differences, especially for clay deposits at sites 1 and 4. Robertson (2009) vastly over-predicted liquefaction at these sites. In general, Boulanger and Idriss (2014) and Youd et al. (2001) gave similar results and Idriss and Boulanger (2012) gave the most conservative results for the test sites. Youd et al. (2001) was the most consistent between all sites.
- 4) The cracking at site 4 was determined to be a lateral spread and seismic slope instability. The combination of seismic loading, organic soils, and a pyroclastic flow layer at a depth of ten meters, which acted as a slip plane, resulted in a low factor of safety for the embankment. This reflects the general state of levee damage in the southern half of the Kumamoto Plain, where minor liquefaction sometimes accompanied predominant seismically induced cracking (MLIT, 2017).
- 5) Japanese boring logs do not always have consistent accuracy and do not consistently identify soil types for the same material. Field tests should be performed and then supplemented with boring logs with laboratory data that is available.

Due to constraints on time, scope, and budget, there were several topics not extensively researched that are worthy of additional research. Some suggestions for future research are on understanding the weathered and eroded daughter products of volcanic soils and deep liquefaction of the Kumamoto Plain pyroclastic pumice layers.

REFERENCES

- Agency, N. E. (2018). Climate of Japan. N. E. Agency.
- Akiyoshi, T., & Fuchida, K. (1998). Kumamoto Earthquake in 1889. *Historical Studies in Civil Engineering*, 18, 245-252.
- Alan, E. K. (2006). "Geology for engineers and environmental scientists." Prentice Hall 46: 257.
- Andrus, R. D. and K. H. Stokoe II (2000). "Liquefaction resistance of soils from shear-wave velocity." *Journal of geotechnical and geoenvironmental engineering* 126(11): 1015-1025.
- Aomine, S., & Wada, K. (1962). Differential weathering of volcanic ash and pumice, resulting in formation of hydrated halloysite. *American Mineralogist: Journal of Earth and Planetary Materials*, 47(9-10), 1024-1048.
- Been, K. and M. G. Jefferies (1985). "A state parameter for sands." *Géotechnique* 35(2): 99-112.
- Bhattacharya, S., et al.. (2018). "Geotechnical and infrastructural damage due to the 2016 Kumamoto earthquake sequence." *Soil Dynamics and Earthquake Engineering* 104: 390-394.
- Birrell, K. S. and M. Fieldes (1952). "Allophane in volcanic ash soils." *European Journal of Soil Science* 3(2): 156-166.
- Boulanger, R. W. and I. Idriss (2006). "Liquefaction susceptibility criteria for silts and clays." *Journal of geotechnical and geoenvironmental engineering* 132(11): 1413-1426.
- Boulanger, R. W., & Idriss, I. M. (2007). Evaluation of cyclic softening in silts and clays. *Journal of Geotechnical and Geoenvironmental Engineering*, 133(6), 641-652.

- Boulanger, Ross W., and I. M. Idriss. (2014). CPT-based liquefaction triggering procedure. *Journal of Geotechnical and Geoenvironmental Engineering* 142, no. 2: 04015065
- Bowen, H., et al.. (2012). Lateral spreading in the Canterbury earthquakes—Observations and empirical prediction methods. Proceedings, 15th World Conference on Earthquake Engineering.
- Bray, J. D., Stewart, J. P., Baturay, M. B., Durgunoglu, T., Onalp, A., Sancio, R. B., ... & Barka, A. (2000). Damage patterns and foundation performance in Adapazari. *Earthquake Spectra*, 16(S1), 163-189.
- Bray, J. D. and R. B. Sancio (2006). "Assessment of the liquefaction susceptibility of fine-grained soils." *Journal of geotechnical and geoenvironmental engineering* 132(9): 1165-1177.
- Bray, J. D., et al.. (2004). Liquefaction susceptibility of fine-grained soils. *Proc., 11th Int. Conf. on Soil Dynamics and Earthquake Engineering and 3rd Int. Conf. on Earthquake Geotechnical Engineering*, Stallion Press, Singapore.
- Casagrande, A. (1936). "Characteristics of cohesionless soils affecting the stability of slopes and earth fills," *Journal of the Boston Society of Civil Engineers*, reprinted in *Contributions to Soil Mechanics*, Boston Society of Civil Engineers, 1940, pp.257-276.
- Castro, G. (1969). "Liquefaction of sands." ph. D. Thesis, *Harvard Soil Mech.*
- Cubrinovski, M. and K. Robinson (2016). "Lateral spreading: Evidence and interpretation from the 2010–2011 Christchurch earthquakes." *Soil Dynamics and Earthquake Engineering* 91: 187-201.
- Egashira, K. and M. Ohtsubo (1982). "Smectite in marine quick-clays of Japan." *CLAYS CLAY MINER.* Clays Clay Miner. 30(4): 275.
- El-Sekelly, W., Dobry, R., Abdoun, T., & Steidl, J. H. (2017). Two case histories demonstrating the effect of past earthquakes on liquefaction resistance of silty sand. *Journal of Geotechnical and Geoenvironmental Engineering*, 143(6), 04017009.
- El-Sekelly, W., Abdoun, T., & Dobry, R. (2015). Liquefaction resistance of a silty sand deposit subjected to preshaking followed by extensive liquefaction. *Journal of Geotechnical and Geoenvironmental Engineering*, 142(4), 04015101.

- Enomoto Tadao, & Kubo Kazuyuki (2016). Liquefaction damage survey in the southern district of Kumamoto City due to the Kumamoto earthquake in 2016. *Geotechnical Engineering Journal*, 11 (4), 399-409.
- Epstein, W., et al.. (2016). The Kumamoto Earthquake investigation: a preliminary report.
- Evans, M. D., & Zhou, S. (1995). Liquefaction behavior of sand-gravel composites. *Journal of Geotechnical Engineering*, 121(3), 287-298.
- Figuroa, J. L., et al.. (1994). "Evaluation of soil liquefaction by energy principles." *Journal of Geotechnical Engineering* 120(9): 1554-1569.
- Fukuoka University Repository. (2016). "Kumamoto Japan Earthquake: Liquefaction map." Retrieved from <http://www.tec.fukuoka-u.ac.jp/tc/labo/drr/gis/H28KumamotoEQ/KumamotoLique.html>. Accessed on July, 2018.
- Geological Society of Japan (GSJ). (2018). *Active Volcanoes of Japan*. Retrieved from https://gbank.gsj.jp/volcano/Act_Vol/aso/text/eng/exp04-1e.html.
- Geological Society of Japan (GSJ). (2018). *Seamless Geological Map*. Retrieved from <https://gbank.gsj.jp/seamless/seamless2015/2d/index.html?lang=en>.
- Geospatial Information Authority of Japan (GSI). (2018). *Seamless Geographical Map of Japan*. Retrieved from <https://maps.gsi.go.jp/#5/36.104611/140.084556/&base=std&ls=std&disp=1&vs=c1j0h0k0l0u0t0z0r0s0f1>.
- Giesecking, J. E. (2012). *Soil Components: Vol. 2: Inorganic Components*, Springer Science & Business Media.
- Goda, K., et al.. (2016). "The 2016 Kumamoto earthquakes: cascading geological hazards and compounding risks." *Frontiers in built environment* 2: 19.
- Goda, Katsuichiro & Campbell, Grace & Hulme, Laura & Ismael, Bashar & Ke, Lin & Marsh, Rebekah & Sammonds, Peter & So, Emily. (2017). The Kumamoto Japan Earthquakes of 14 and 16 April 2016: A Field Report by EEFIT. 10.13140/RG.2.2.10956.92806.
- Goodman, R. E. (1999). *Karl Terzaghi: The engineer as artist*, American Society of Civil Engineers.

- Government, K. P. (2009). Summary Report. Kumamoto Prefectural Government.
- Group, A. B. R. (1965). "Quaternary system of the Ariake and the Shiranui Bay areas, with special reference to the Ariake soft clay." Assoc, Geol. Collab. Japan, Monograph 11.
- Hamada, M. (1992). Large ground deformations and their effects on lifeline: 1964 Niigata Earthquake. Proceedings, Case Studies of Liquefaction and Lifeline Performance During Past Earthquakes, *Japanese Case Studies*, 1.
- Hashimoto, M. (1991). Geology of Japan, Springer Science & Business Media.
- Hatanaka, M., et al.. (1985). "Liquefaction resistance of two alluvial volcanic soils sampled by in situ freezing." *Soils and Foundations* 25(3): 49-63.
- He, P., Ohtsubo, M., Higashi, T., Kanayama, M. (2015). "Sensitivity of salt-leached clay sediments in the Ariake Bay area, Japan." *Marine Georesources & Geotechnology* 33(5): 429-436.
- Henmi, T. and K. Wada (1976). "Morphology and composition of allophane." *American Mineralogist* 61(5-6): 379-390.
- Hiroshi Kohara, Yoshinobu Putian, Kazunori Kamiyama, Toshiaki Maekima, Yuji Maenjima, Masayoshi Wakabayashi, and Takashi Kanda. (2016). Comprehensive soil classification 1 / 200,000 Japanese soil map based on the first draft. Agricultural environmental technology research Report = *Bulletin of National Institute for Agro-Environmental Sciences*, (37), 133-148.
- Hudson, P. F. (2005). Natural levees, Taylor and Francis. DOI. 10.
- Hynes-Griffin, M. E., & Franklin, A. G. (1984). Rationalizing the seismic coefficient method (No. WES/MP/GL-84-13). Army Engineer Waterways Experiment Station Vicksburg Ms Geotechnical Lab.
- Hyodo, M., et al.. (2002). Effect of fines and crushability on liquefaction of volcanic soil 'Shirasu'. *The Twelfth International Offshore and Polar Engineering Conference*, International Society of Offshore and Polar Engineers.
- Ideue, M., & Watanabe, S. (2012). A Study on the River Bed Gravel of Midori River in Kumamoto as Materials for Teaching Science –A Link between Elementary Science

- Teaching Materials with a Welded Tuff as a Key –. University of Kumamoto Repository, Natural Science Department. (61), 47-56.
- Idriss, I. M., & Boulanger, R. W. (2012). Examination of SPT-based liquefaction triggering correlations. *Earthquake Spectra*, 28(3), 989-1018.
- Idriss, I. M., and R. W. Boulanger. (2014). CPT and SPT based liquefaction triggering procedures. *Centre for Geotechnical Modelling*.
- Ishihara, K. (1985). Stability of natural deposits during earthquakes. Proc. of 11th ICSMFE, 1985, 1, 321-376.
- Ishihara, K. (1999). Geotechnical aspects of the 1995 Kobe earthquake. In *Fourteenth International Conference on Soil Mechanics and Foundation Engineering*. Proceedings International Society for Soil Mechanics and Foundation Engineering (Vol. 4).
- Ishizaka, S., et al.. (1995). "Subsidence rate and sediments of the last interglacial epoch in the Kumamoto Plain, Japan." *The Quaternary Research (Daiyonki-Kenkyu)* 34(5): 335-344.
- Iwasaki, T. (1978). A practical method for assessing soil liquefaction potential based on case studies at various sites in Japan. In Proc. Second Int. Conf. Microzonation Safer Construction Research Application, 1978 (Vol. 2, pp. 885-896).
- Japan Meteorological Agency (2013) National catalogue of the active volcanoes in Japan, 4th edn.
https://www.data.jma.go.jp/svd/vois/data/tokyo/STOCK/souran_eng/volcanoes/084_asosan.pdf
- Japan Meteorological Agency (2019). "Table explaining the JMA Seismic Intensity Scale."
<https://www.jma.go.jp/jma/en/Activities/inttable.html>. Accessed on 19 Feb 2019.
- Japan Seismic Hazard Information Station (J-SHIS) (2009). "Site Amplification Factor (Vs=400m/s – surface)." <http://www.j-shis.bosai.go.jp/map/?lang=en>. Accessed on Sept 2018.
- Kabay, N., et al.. (2015). "Properties of concrete with pumice powder and fly ash as cement replacement materials." *Construction and Building Materials* 85: 1-8.

- Kamata, H. and K. Kodama (1994). "Tectonics of an arc-arc junction: an example from Kyushu Island at the junction of the Southwest Japan Arc and the Ryukyu Arc." *Tectonophysics* 233(1-2): 69-81.
- Kanno, I., et al.. (1965). "Characteristics and classification of an unirrigated anthropogenic-alluvial soil found in the Kumamoto Plain." *Soil Science and Plant Nutrition* 11(1): 14-23.
- Kayen, R. E., et al.. (2017). Geotechnical aspects of the 2016 MW 6.2, MW 6.0, and MW 7.0 Kumamoto earthquakes, Geotechnical Extreme Events Reconnaissance Association.
- Kayen, R. E., et al.. (1992). Evaluation of SPT-, CPT-, and shear wave-based methods for liquefaction potential assessment using Loma Prieta data. *Proceedings of the 4th Japan-US workshop on earthquake resistant design of lifeline facilities and countermeasures for soil liquefaction*, Honolulu, Hawaii.
- Kazama, M., et al.. (2006). "Liquefaction mechanism of unsaturated volcanic sandy soils." *Journal of Geotechnical Engineering*, Japan Society of Civil Engineers 62(2): 546-561.
- Kitaura, M., & Miyajima, M. (1996). Damage to water supply pipelines. *Soils and Foundations*, 36(Special), 325-333.
- Kiyota, T., et al.. (2017). "Geotechnical Damage Caused by the 2016 Kumamoto Earthquake, Japan." *ISSMGE International Journal of Geoengineering Case Histories* 4(2): 78-95.
- Knighton, A. (1980). "Longitudinal changes in size and sorting of stream-bed material in four English rivers." *Geological Society of America Bulletin* 91(1): 55-62.
- Kokusho, T., et al.. (2004). "Undrained shear strength of granular soils with different particle gradations." *Journal of geotechnical and geoenvironmental engineering* 130(6): 621-629.
- Kokusho, T., et al.. (2015). Energy-Based Liquefaction Potential Evaluation and its Application to a Case History. *Proc. 6th International Conference on Earthquake Geotechnical Engineering*, Christchurch, NZ, Paper.
- Konagai, K., Shiga, M., Kiyota, T., & Ikeda, T. (2017). Ground deformation built up along seismic fault activated in the 2016 Kumamoto earthquake. 土木学会論文集 A1 (構造・地震工学), 73(4), I_208-I_215.

- Kotoda, K., et al.. (1988). Mapping liquefaction potential based on geomorphological land classification. *Proceedings of Ninth World Conference on Earthquake Engineering*.
- Kotoda, K., et al.. (1988). "Seismic microzoning on soil liquefaction potential based on geomorphological land classification." *Soils and Foundations* 28(2): 127-143.
- Kumamoto City (2014). Liquefaction Hazard Map of Kumamoto City. (in Japanese), http://www.city.kumamoto.jp/common/UploadFileDsp.aspx?c_id=5&id=2121&sub_id=2&flid=39134. Accessed on May, 2018.
- Kumamoto City (2015). A World-class Pure Groundwater City Kumamoto, Japan. http://www.city.kumamoto.jp/kankyo/hpkiji/pub/Detail.aspx?c_id=5&id=20548. Accessed on 20 Feb 2019.
- Kyushu Regional Development Bureau (2012). Midorikawa water system river maintenance management plan. Kumamoto National River Highway Office. (in Japanese), http://www.qsr.mlit.go.jp/kumamoto/site_files/file/river/kanri/h24_midorikawa_ijikanri.pdf. Accessed on 24 Feb 2019.
- Kyushu Regional Development Bureau (2017). On the inspection of the Midorikawa water system river maintenance. Kumamoto National River Highway Office. (in Japanese), http://www.qsr.mlit.go.jp/kumamoto/site_files/file/river/sonotanokaigi/siryou1-6kai.pdf. Accessed on 24 Feb 2019.
- Larsson, R., & Mulabdic, M. (1991). Piezocone tests in clay. SGI REPORT, (42).
- Leamy, M., et al.. (1984). "The morphological characteristics of Andisols."
- Licata, V., et al.. (2015). "A laboratory investigation on the cyclic liquefaction resistance of pyroclastic soils." *Volcanic Rocks and Soils*: 141.
- Low, H. E., Lunne, T., Andersen, K. H., Sjursen, M. A., Li, X., & Randolph, M. F. (2010). Estimation of intact and remoulded undrained shear strengths from penetration tests in soft clays. *Géotechnique*, 60(11), 843.
- Machida, H. (2002). "Volcanoes and tephra in the Japan area." Global environmental research English edition- 6(2): 19-28.

- Matsumoto, Hidetoshi. (2016). "The Kumamoto earthquake and liquefaction." *Kumamoto University Repository System*. <http://hdl.handle.net/2298/35341>. Accessed Sep 2018.
- Maurer, B. W., Green, R. A., Cubrinovski, M., & Bradley, B. A. (2014). Evaluation of the liquefaction potential index for assessing liquefaction hazard in Christchurch, New Zealand. *Journal of Geotechnical and Geoenvironmental Engineering*, 140(7), 04014032.
- Ministry of Land, Infrastructure, Transport and Tourism (MLIT) Kyushu Division (2017). "Midorikawa and Shirakawa Levee Management Committee Report." Accessed from http://www.qsr.mlit.go.jp/kumamoto/site_files/file/river/midorikawasirakawateiboutyousaiinkai/houkokusyo.pdf on July, 2018.
- Miura, S., et al.. (2003). "Deformation-strength evaluation of crushable volcanic soils by laboratory and in-situ testing." *Soils and Foundations* 43(4): 47-57.
- Mukunoki, T., et al.. (2016). "Reconnaissance report on geotechnical damage caused by an earthquake with JMA seismic intensity 7 twice in 28 h, Kumamoto, Japan." *Soils and Foundations* 56(6): 947-964.
- Naito, Kazuki. (2014). "GeoMap Navi." Geological Survey of Japan, AIST. 3(3): 83-86. <https://gbank.gsj.jp/geonavi/geonavi.php#12,32.75836,130.77161>. Accessed on Sept 2017.
- Nagasawa, K. (1978). Kaolin minerals. *Developments in sedimentology*, Elsevier. 26: 189-219.
- Nagasawa, K. (1978). Weathering of volcanic ash and other pyroclastic materials. *Developments in Sedimentology*, Elsevier. 26: 105-125.
- Nanjo, K. Z., et al.. (2016). "Seismicity prior to the 2016 Kumamoto earthquakes." *Earth, Planets and Space* 68(1): 187.
- Nanzyo, M., et al.. (1993). Physical characteristics of volcanic ash soils. *Developments in Soil Science*, Elsevier. 21: 189-207.
- Nippon.com. (2014) An Agricultural Wonder: Japan's Vanishing Terraced Rice Fields (Photos). Images. <https://www.nippon.com/en/images/i00027/an-agricultural-wonder-japan%E2%80%99s-vanishing-terraced-rice-fields-photos.html>. Accessed on 19 Feb 2019.

- Ogo, K & Hazarika, H & Kokusho, Takaji & Matsumoto, D & Ishibashi, S & Sumartini, Wa. (2018). Analysis of liquefaction of volcanic soil during the 2016 Kumamoto Earthquake based on boring data. *Lowland Technology International*. 19. 245-250.
- Ohtsubo, M., et al.. (1995). "Depositional and post-depositional geochemistry, and its correlation with the geotechnical properties of marine clays in Ariake Bay, Japan." *Géotechnique* 45(3): 509-523.
- Ohtsubo, M., et al.. (1982). "Marine quick clays from Ariake Bay area, Japan." *Soils and Foundations* 22(4): 71-80.
- Okumura, K. (2016). "Earthquake geology of the April 14 and 16, 2016 Kumamoto earthquakes." Kumamoto earthquake investigation: a preliminary report. [http://janet-dr.com/11_saigaiji/The% 20Kumamoto% 20Earthquake% 20Investigation_ % 20A% 20Preliminary% 20Report. pdf](http://janet-dr.com/11_saigaiji/The%20Kumamoto%20Earthquake%20Investigation_%20A%20Preliminary%20Report.pdf). Accessed 11.
- Orense, R. P., Pender, M. J., & O'Sullivan, A. S. (2012). Liquefaction characteristics of pumice sands. *Earthquake Commission*.
- Orense, R. P., & Pender, M. J. (2013, September). Liquefaction characteristics of crushable pumice sand. In *Proceeding of the 18th International Conference on Soil Mechanics and Geotechnical Engineering* (pp. 2-6).
- Orense, R. P., Pender, M. J., & Tai, A. (2014). Undrained cyclic shear strength of crushable sands. *International Journal of Geotechnical Engineering*, 8(4), 426-430.
- Ota, Y., et al.. (1982). "Notes on the Holocene sea-level study in Japan." *The Quaternary Research* (Daiyonki-Kenkyu) 21(3): 133-143.
- Oya, M. (1995). Geomorphological Maps of Alluvial Plains and their Utilization for Mitigation of Natural Hazards. *Geographical review of Japan, Series B.*, 68(2), 218-242.
- Rao, S. M. (1995). "Mechanistic approach to the shear strength behaviour of allophanic soils." *Engineering Geology* 40(3-4): 215-221.
- Rao, S. M. (1996). "Correlations between plasticity angle and engineering properties of volcanic ash soils." *Soils and Foundations* 36(2): 123-127.

- Riemer, M. F. and R. B. Seed (1997). "Factors affecting apparent position of steady-state line." *Journal of geotechnical and geoenvironmental engineering* 123(3): 281-288.
- Robertson, P. K., & Wride, C. E. (1998). Evaluating cyclic liquefaction potential using the cone penetration test. *Canadian Geotechnical Journal*, 35(3), 442-459.
- Robertson, P. K. (2009). Performance based earthquake design using the CPT. *Proc. IS-Tokyo*, 3-20.
- Saigusa, M. and N. MATSUYAMA (1998). "Distribution of allophanic Andosols and non-allophanic Andosols in Japan." *Tohoku journal of agricultural research* 48(3/4): 75-83.
- Saito, R. (1968). "The Regularity of the Eruption of Volcanoes in Japan." *Kumamoto Journal of Science* 7(2): 105-123.
- Seed, H. B., & Idriss, I. M. (1971). Simplified procedure for evaluating soil liquefaction potential. *Journal of Soil Mechanics & Foundations Div.*
- Setiawan, H., et al.. (2017). "Structural damage to houses and buildings induced by liquefaction in the 2016 Kumamoto Earthquake, Japan." *Geoenvironmental Disasters* 4(1): 13.
- Shoji, S., et al.. (1993). Genesis of volcanic ash soils. *Developments in Soil Science*, Elsevier. 21: 37-71.
- Shoji, S., et al.. (1975). "Chemical and mineralogical studies on volcanic ashes I. Chemical composition of volcanic ashes and their classification." *Soil Science and Plant Nutrition* 21(4): 311-318.
- Skempton, A. W. (1986). Standard penetration test procedures and the effects in sands of overburden pressure, relative density, particle size, ageing and overconsolidation. *Geotechnique*, 36(3), 425-447.
- Sudo, T. and S. Shimoda (1978). *Clays and clay minerals of Japan*, Elsevier.
- Suzuki, M., & Yamamoto, T. (2004, August). Liquefaction characteristic of undisturbed volcanic soil in cyclic triaxial test. In Proceedings of 13th world conference on earthquake engineering, Vancouver, BC, Canada, Paper (No. 465).
- Takahashi, T. and S. Shoji (2002). "Distribution and classification of volcanic ash soils." *Global environmental research English edition*- 6(2): 83-98.

- Takai, F. (1963). *Geology of Japan*, Univ of California Press.
- Takashi Oyama, Masashi Aoyama (2017). Liquefaction Damage Distribution and Land Condition in the 2016 Kumamoto Earthquake from the Viewpoint of Geography. In Japanese Abstracts of the Geography Society of Japan 2017 *Spring Science Congress of the Geography Society of Japan* (p. 100273) Japan Geography Association.
- Tokimatsu, K., Suzuki, H., Katsumata, K., & Tamura, S. (2013). Geotechnical Problems in the 2011 Tohoku Pacific Earthquakes.
- Tokimatsu, K., et al.. (2018). "Liquefaction-induced settlement and tilting of buildings with shallow foundations based on field and laboratory observation." *Soil Dynamics and Earthquake Engineering*.
- Tokimatsu, K. and A. UCHIDA (1990). "Correlation between liquefaction resistance and shear wave velocity." *Soils and Foundations* 30(2): 33-42.
- Torrance, J. and M. Ohtsubo (1995). "Ariake Bay quick clays: a comparison with the general model." *Soils and Foundations* 35(1): 11-19.
- Toshio, S. (1954). "Clay mineralogical aspects of the alteration of volcanic glass in Japan." *Clay Minerals Bull* 2: 96-105.
- United States Geological Survey. "Why do USGS earthquake magnitudes differ from those published by other agencies?" Natural Hazards. https://www.usgs.gov/faqs/why-do-usgs-earthquake-magnitudes-differ-those-published-other-agencies?qt-news_science_products=0#qt-news_science_products. Accessed on 19 Feb, 2019.
- Vaid, Y. P., Chern, J. C., & Tumi, H. (1985). Confining pressure, grain angularity, and liquefaction. *Journal of Geotechnical Engineering*, 111(10), 1229-1235.
- Vaid, Y., et al.. (1990). "Stress path and steady state." *Canadian Geotechnical Journal* 27(1): 1-7.
- Vaid, Y., et al.. (1990). "Particle gradation and liquefaction." *Journal of Geotechnical Engineering* 116(4): 698-703.
- Van Ballegooy, S., Malan, P., Lacrosse, V., Jacka, M. E., Cubrinovski, M., Bray, J. D., ... & Cowan, H. (2014). Assessment of liquefaction-induced land damage for residential

- Christchurch. *Earthquake Spectra*, 30(1), 31-55.
- Wada, K. (1987). "Minerals formed and mineral formation from volcanic ash by weathering." *Chemical Geology* 60(1-4): 17-28.
- Wakamatsu, K. (2012). Recurrence of liquefaction at the same site induced by 2011 Great East Japan Earthquake compared with previous earthquakes. *15th World Conference on Earthquake Engineering*, Lisbon.
- Wakamatsu, K., et al.. (2001). "Geomorphological criteria for evaluating liquefaction potential considering the level-2 ground motion in Japan."
- Wakamatsu, K, et al.. (2016). "2006 Kumamoto earthquake liquefaction evaluation summary (Report 1)." http://committees.jsce.or.jp/eec205/system/files/liq_survey_2016kumamoto.pdf
- Wang, W. (1979). Some findings in soil liquefaction, Earthquake Engineering Department, Water Conservancy and Hydroelectric Power Scientific Research Institute.
- Watanabe, K. (1978). "Studies on the Aso pyroclastic flow deposits in the region to the west of Aso Caldera, southwest Japan." I: geology. *Mem. Fac. Educ. Kumamoto Univ.*, no. 27, Natural. Sci.: 97-120.
- Watanabe, K. (1979). "Studies on the Aso pyroclastic flow deposits in the region to the West of Aso Caldera, southwest Japan, II: Petrology of the Aso-4 pyroclastic flow deposits." *Mem. Fac. Educ. (Natural Science) Kumamoto Univ.* 28: 75-112.
- Watanabe, K., Ono, K., Sakaguchi, K., Takada, A., & Hoshizumi, H. (1999). Co-ignimbrite ash-fall deposits of the 1991 eruptions of fugen-dake, unzen volcano, japan
doi:[https://doi.org/10.1016/S0377-0273\(98\)00126-7](https://doi.org/10.1016/S0377-0273(98)00126-7)
- Wesley, L. (1973). "Some basic engineering properties of halloysite and allophane clays in Java, Indonesia." *Géotechnique* 23(4): 471-494.
- Wesley, L. D. (2001). "Determination of specific gravity and void ratio of pumice materials." *Geotechnical testing journal* 24(4): 418-422.
- Yagi, K. (2003). "Mechanical behaviour and particle crushing of volcanic coarse-grained soils in Japan." *Characterisation and Engineering Properties of Natural Soils 2*: 1169.

- Youd, T. L., & Hoose, S. N. (1977). Liquefaction susceptibility and geologic setting. In *Proc., 6th World Conf. on Earthquake Engineering* (Vol. 6, pp. 37-42). Roorkee, India: Indian Society of Earthquake Technology.
- Youd, T. (1984). "Geologic effects-liquefaction and associated ground failure." Proceedings, Geologic and Hydrologic Hazards Training Program, Open File Report: 84-760.
- Youd, T. (1984). Recurrence of liquefaction at the same site. *Proc. 8th World Conf. Earthq. Engng*, Prentice-Hall Inc.
- Youd, T. L., Idriss, I. M., Andrus, R. D., Ignacio, A., Gonzalo, C., Christian, J. T., . . . Stokoe, K. H. (2001). Liquefaction resistance of soils: Summary report from the 1996 NCEER and 1998 NCEER/NSF workshops on evaluation of liquefaction resistance of soils. *Journal of Geotechnical and Geoenvironmental Engineering*, 127(10), 817-833.
doi:10.1061/(ASCE)1090-0241(2001)127:10(817)
- Youd, T. L., DeDen, D. W., Bray, J. D., Sancio, R., Cetin, K. O., & Gerber, T. M. (2009). Zero-displacement lateral spreads, 1999 Kocaeli, Turkey, earthquake. *Journal of Geotechnical and Geoenvironmental engineering*, 135(1), 46-61.
- Youd, T. L., Hansen, C. M., & Bartlett, S. F. (2002). Revised multilinear regression equations for prediction of lateral spread displacement. *Journal of Geotechnical and Geoenvironmental Engineering*, 128(12), 1007-1017.
- Zhang, G. (2007). Soil nanoparticles and their influence on engineering properties of soils. *Advances in Measurement and Modeling of Soil Behavior*: 1-13.

APPENDIX A: SUPPLEMENTARY EARTHQUAKE AND KUMAMOTO PLAIN DATA

This appendix contains Figures and Tables which I considered useful, though not important enough to post in the main text of this paper. There is earthquake response spectrum data for various sites in the area along with general site amplification, shear wave, and bedrock depth maps. Lastly, there are additional maps that record the extent of observed liquefaction damage.

● Human perception and reaction, indoor situation, outdoor situation

Seismic intensity	Human perception and reaction	Indoor situation	Outdoor situation
0	Imperceptible to people, but recorded by seismometers.	–	–
1	Felt slightly by some people keeping quiet in buildings.	–	–
2	Felt by many people keeping quiet in buildings. Some people may be awoken.	Hanging objects such as lamps swing slightly.	–
3	Felt by most people in buildings. Felt by some people walking. Many people are awoken.	Dishes in cupboards may rattle.	Electric wires swing slightly.
4	Most people are startled. Felt by most people walking. Most people are awoken.	Hanging objects such as lamps swing significantly, and dishes in cupboards rattle. Unstable ornaments may fall.	Electric wires swing significantly. Those driving vehicles may notice the tremor.
5 Lower	Many people are frightened and feel the need to hold onto something stable.	Hanging objects such as lamps swing violently. Dishes in cupboards and items on bookshelves may fall. Many unstable ornaments fall. Unsecured furniture may move, and unstable furniture may topple over.	In some cases, windows may break and fall. People notice electricity poles moving. Roads may sustain damage.
5 Upper	Many people find it hard to move; walking is difficult without holding onto something stable.	Dishes in cupboards and items on bookshelves are more likely to fall. TVs may fall from their stands, and unsecured furniture may topple over.	Windows may break and fall, unreinforced concrete-block walls may collapse, poorly installed vending machines may topple over, automobiles may stop due to the difficulty of continued movement.
6 Lower	It is difficult to remain standing.	Many unsecured furniture moves and may topple over. Doors may become wedged shut.	Wall tiles and windows may sustain damage and fall.
6 Upper	It is impossible to remain standing or move without crawling. People may be thrown through the air.	Most unsecured furniture moves, and is more likely to topple over.	Wall tiles and windows are more likely to break and fall. Most unreinforced concrete-block walls collapse.
7		Most unsecured furniture moves and topples over, or may even be thrown through the air.	Wall tiles and windows are even more likely to break and fall. Reinforced concrete-block walls may collapse.

Figure A-1. Table explained the JMA Seismic Intensity Scale (JMA, 2019)



Figure A-2. Kumamoto City (KMM006) and Uto City (KMM008)

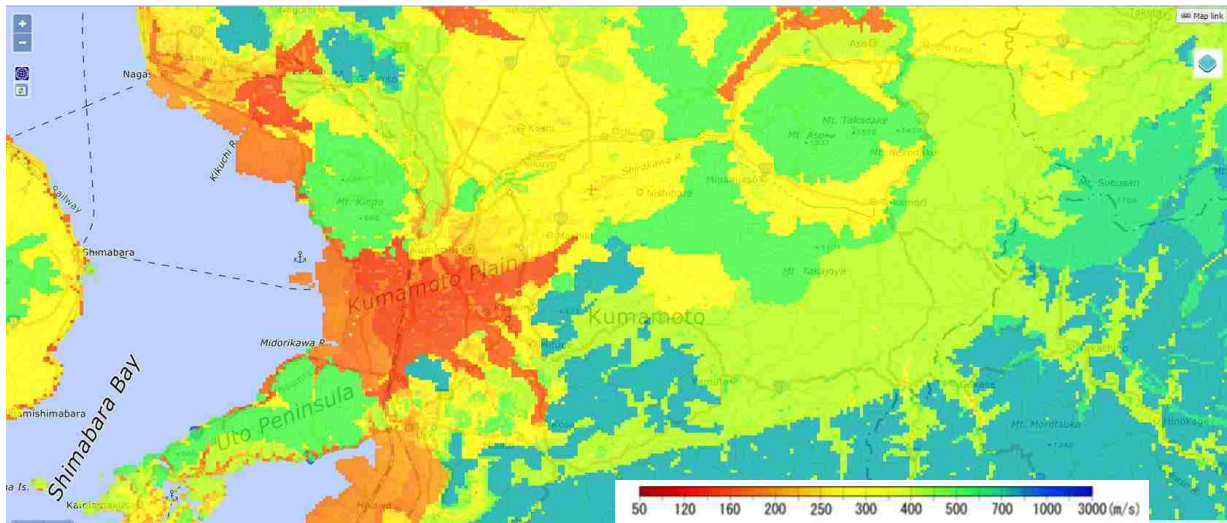


Figure A-3. Upper 30 m average shear wave velocity from J-shis map

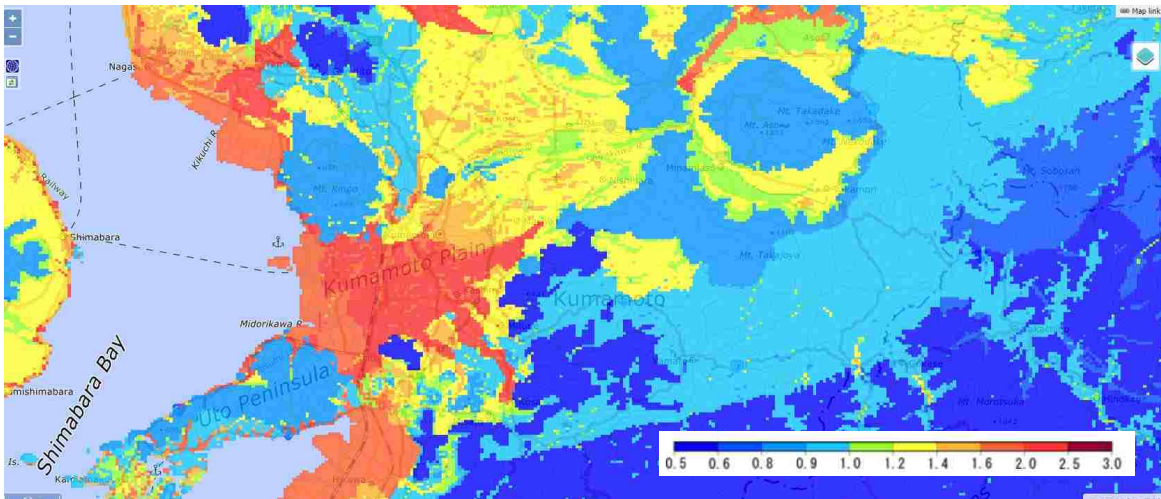


Figure A-4. Site Amplification Factor from J-shis map

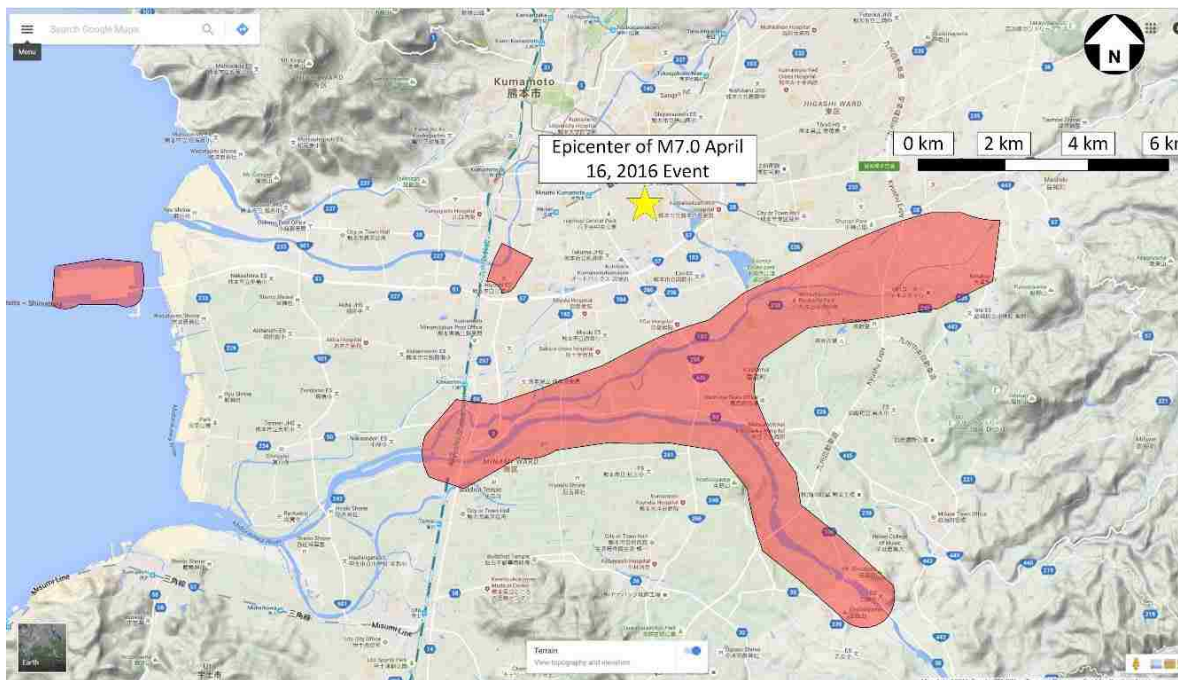


Figure A-5. Observed soil liquefaction from GEER team (Kayen et al., 2017)

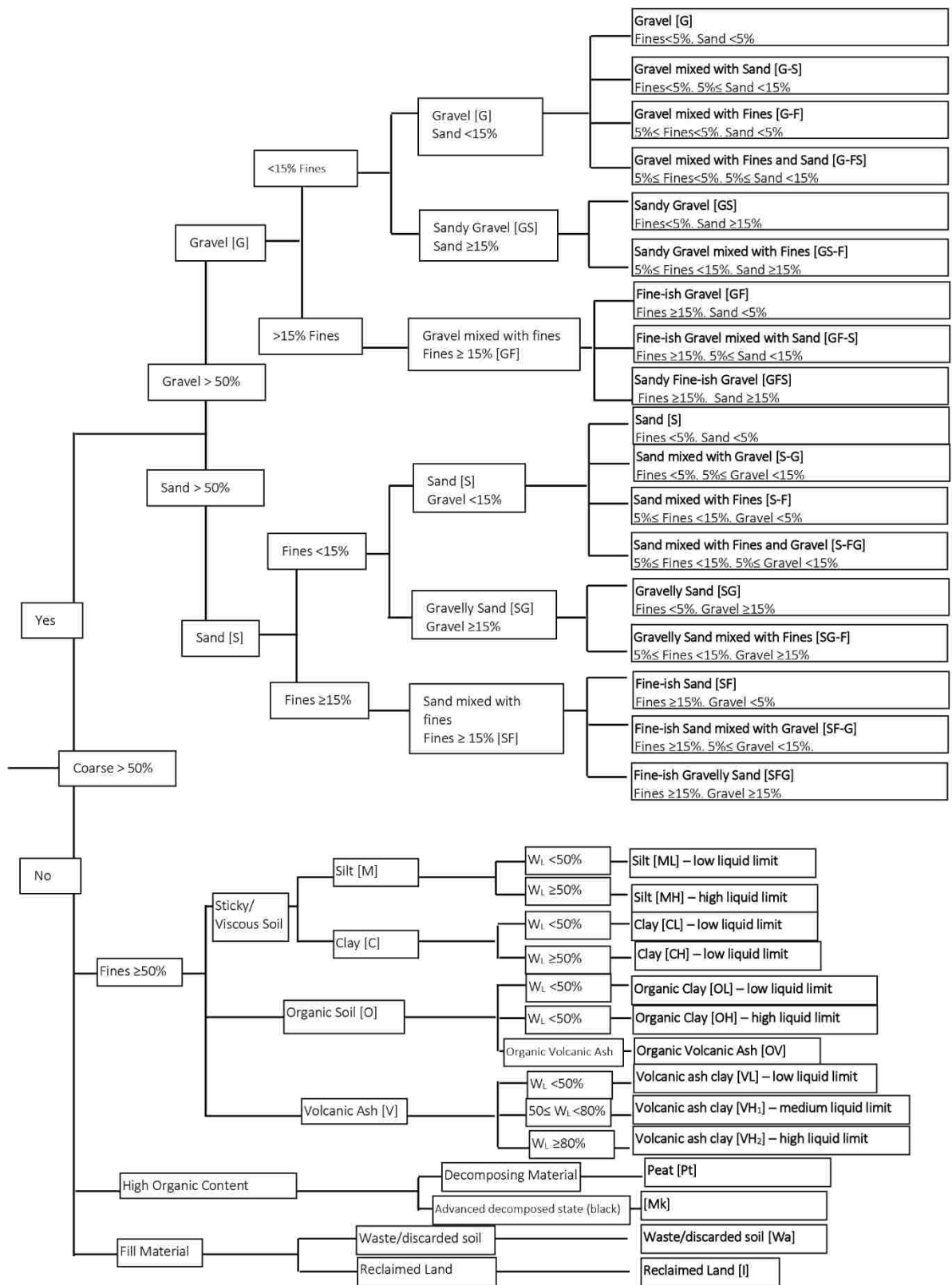


Figure A-6: Japanese soil classification chart (translated to English)



Figure A-7: Observed soil liquefaction in Kumamoto City (Bhattacharya et al., 2018)

APPENDIX B: LABORATORY AND SITE EXPLORATION DATA

The following section contains the disaggregated data collected through soil boring, SPT, and CPT testing. There is also laboratory data on soil plasticity, gradation, and classification.

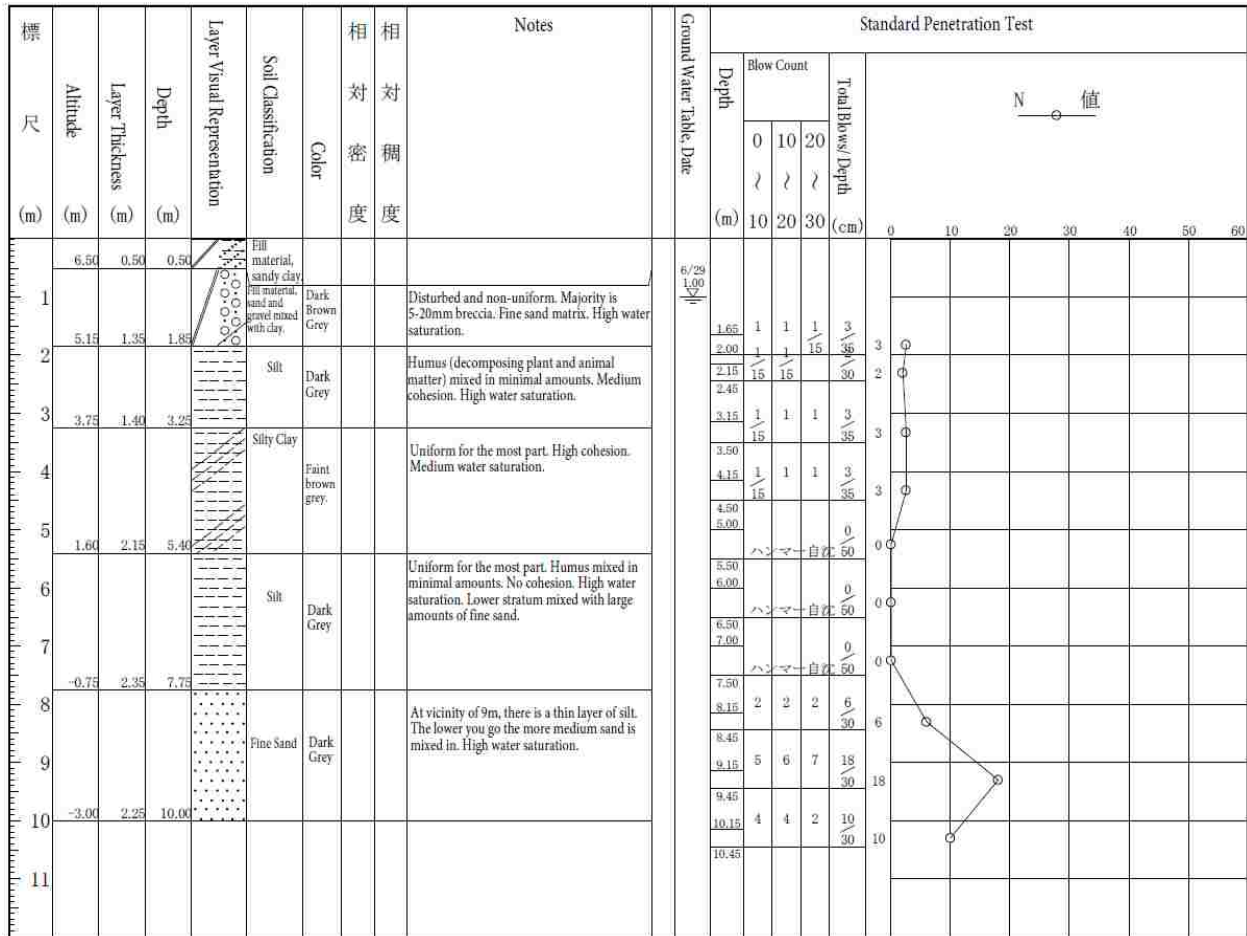


Figure B-1. Boring log for site 1

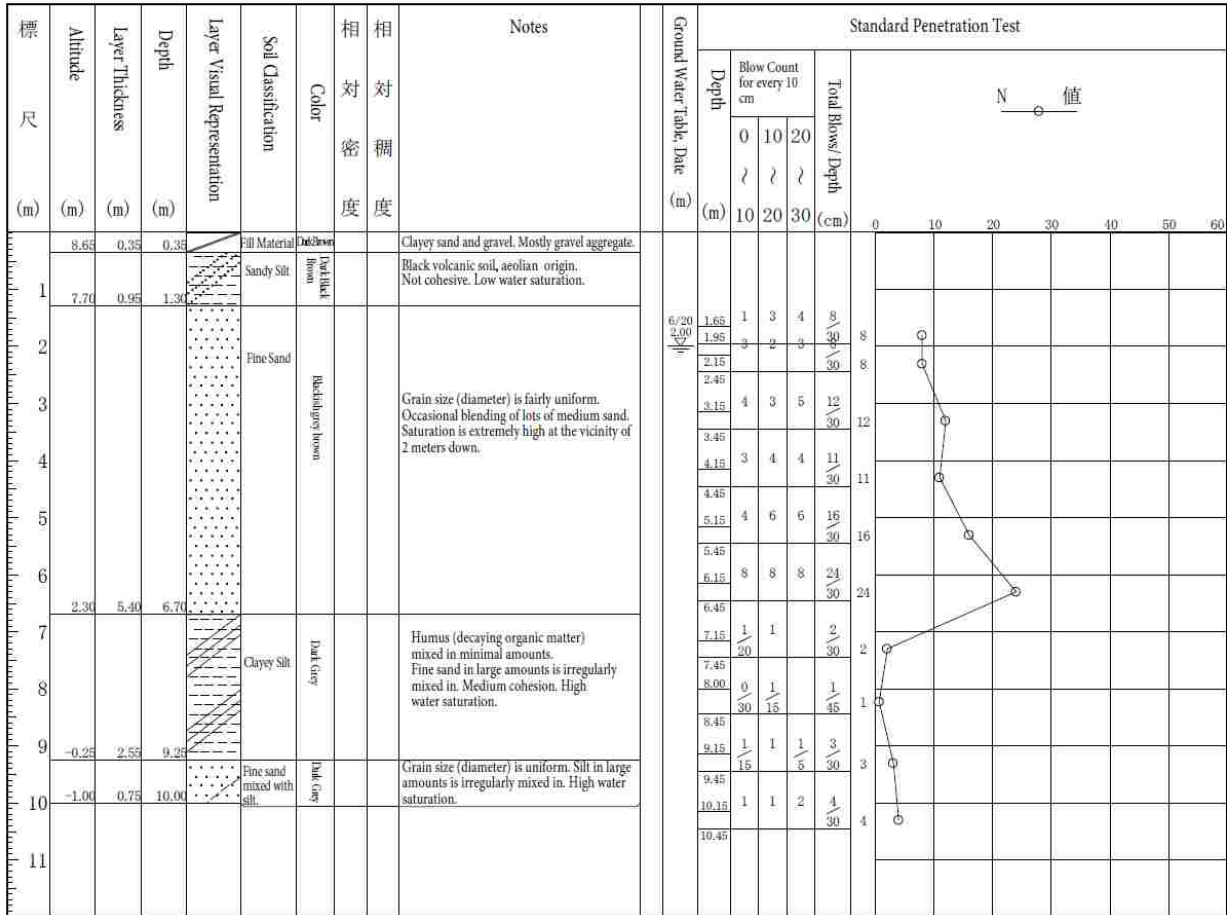


Figure B-2. Boring log for site 2-1

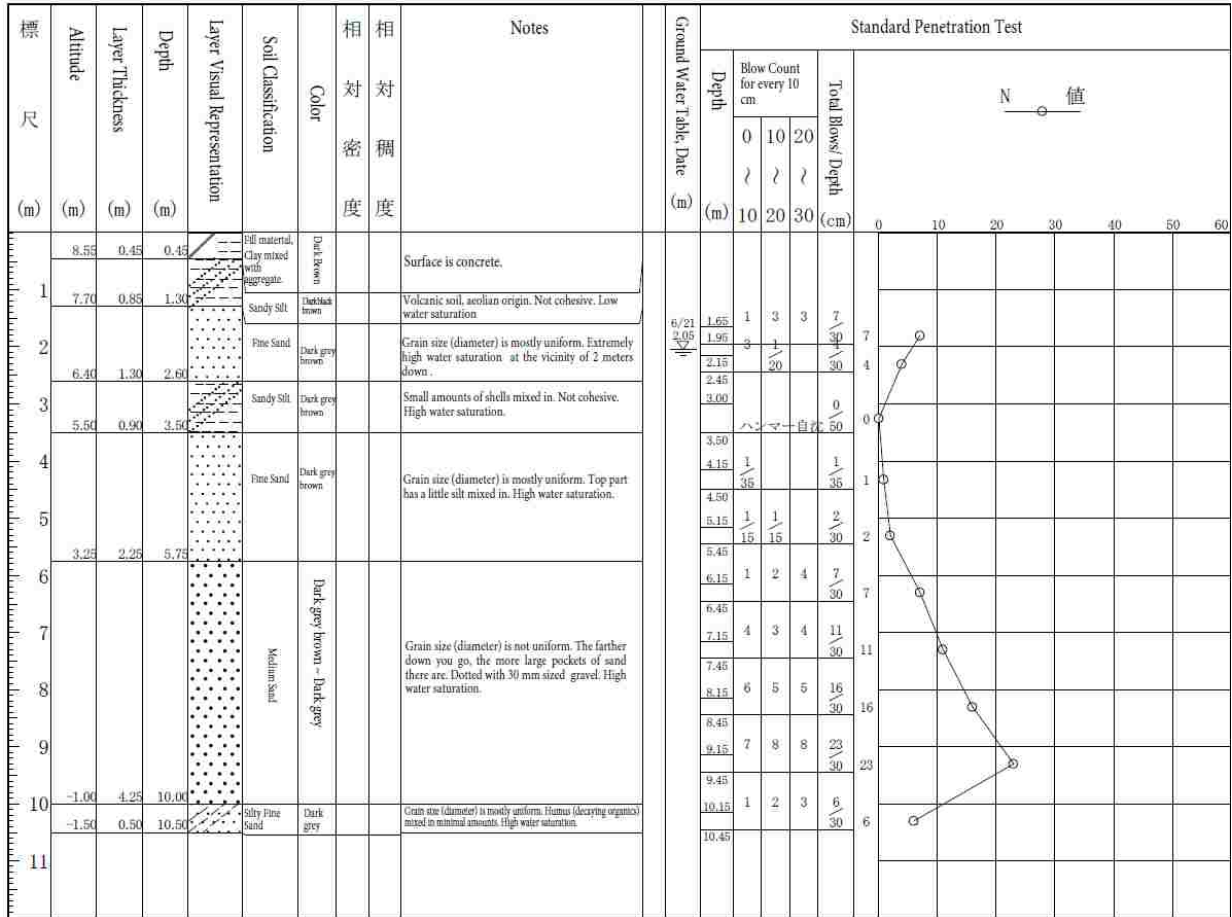


Figure B-3. Boring log for site 2-2

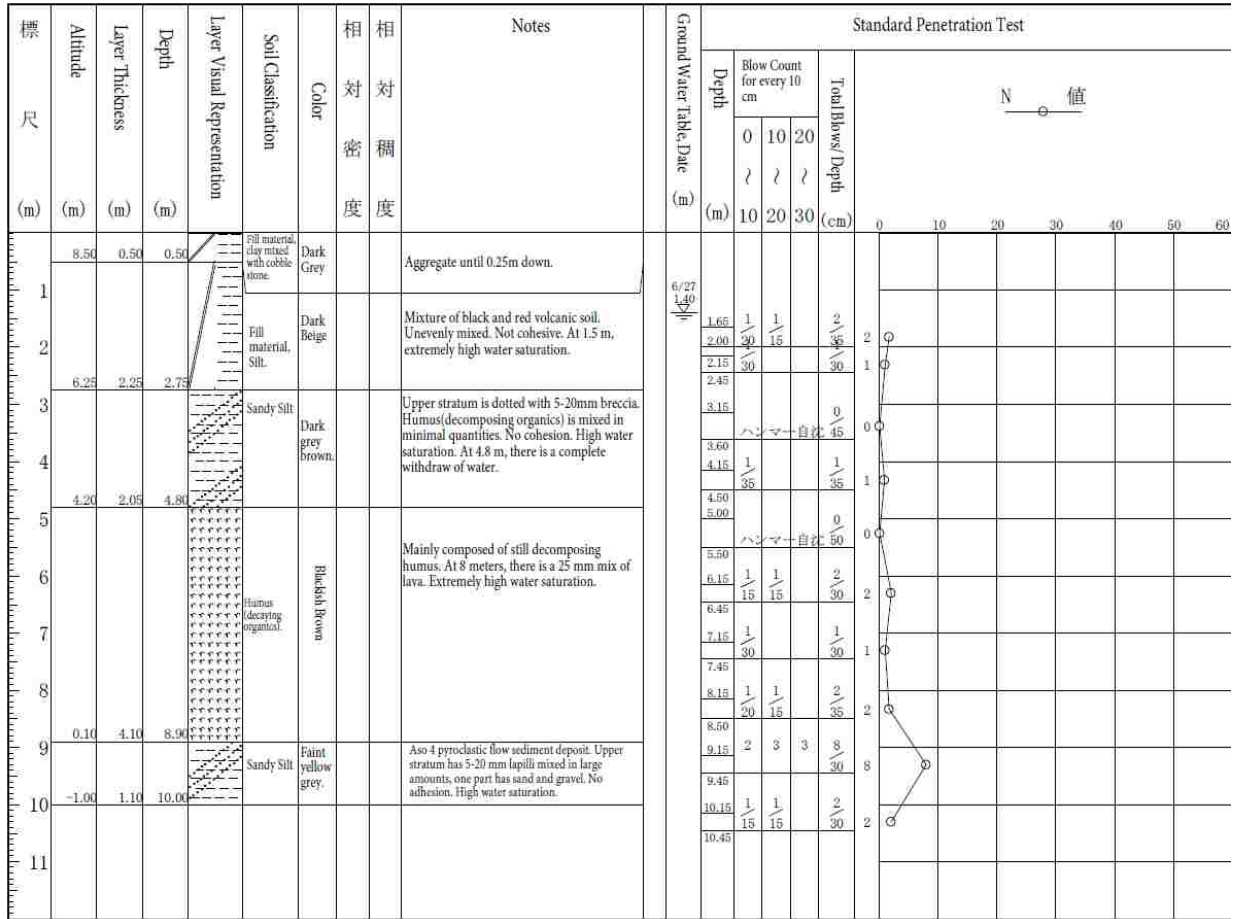


Figure B-4. Boring log for site 4

SOIL TESTING RESULTS (BEDROCK)						
Project				investigate the 2016 Kumamoto earthquake		
Date				28/8/2017		
Name						
Sample No. (Depth)		No.2-1-1 (3.45~4.15m)	No.2-1-2 (7.45~8.00m)	No.2-1-3 (10.15~10.45m)		
Natural	Bulk Density ρ_t	g/cm ³				
	Dry Density ρ_d	g/cm ³				
	Density of Soil Particle ρ_s	g/cm ³	2.858	2.696	2.770	
	Natural Moisture Content w_n	%	22.3	61.2	32.9	
	Natural Void Ratio e					
Grain-Size Analysis	Degree of Saturation S_r	%				
	Rock-Size Fraction ($7.5\text{mm} <$)	%				
	Gravel-Size Fraction ¹⁾ ($2 \sim 7.5\text{mm}$)	%	0.0	0.0	1.2	
	Sand-Size Fraction ¹⁾ ($0.075 \sim 2\text{mm}$)	%	96.5	55.1	77.1	
	Silt-Size Fraction ¹⁾ ($0.005 \sim 0.075\text{mm}$)	%	3.5	17.8	9.3	
	Clay-Size Fraction ¹⁾ ($0.005\text{mm} >$)	%		27.1	12.4	
	Max. Grain Size	mm	0.850	2	4.75	
	Uniformity Coefficient U_c		1.96	-	-	
Consistency	Liquid Limit w_L	%	NP	65.6	31.6	
	Plastic Limit w_P	%	NP	24.9	19.6	
	Plasticity Index I_P		—	40.7	12.0	
Classification	Classification Name of Soil		sand	fine sand	fine sand	
	Classification Mark		(S)	(SF)	(SF)	
Consolidation	Testing Method					
	Compression Index C_c					
Unconfined Compression	Consolidation Yield Stress ρ_c	kN/m ²				
	Unconfined Compression Strength q_u	kN/m ²				
Shear	Testing Method					
	Total Stress	c kN/m ² ϕ °				
	Effective Stress	c' kN/m ² ϕ' °				

Note

1) A percentage of the soil that removed Stone-Size Fraction

Figure B-6. Soil testing data for site 2-1

SOIL TESTING RESULTS (BEDROCK)										
Project			investigate the 2016 Kumamoto earthquake		Date		28/8/2017			
Name										
Sample No.		No.4-1		No.4-2		No.4-3		No.4-4		
(Depth)		(2.15~2.45m)		(3.00~3.45m)		(6.15~6.45m)		(10.15~10.45m)		
Natural	Bulk Density ρ_s	g/cm ³								
	Dry Density ρ_d	g/cm ³								
	Density of Soil Particle ρ_s	g/cm ³		2.529	2.609	2.265	2.651			
	Natural Moisture Content w_n	%		91.5	34.9	214.6	58.8			
	Natural Void Ratio e									
	Degree of Saturation S_r	%								
Grain-Size Analysis	Rock-Size Fraction (7.5 mm <)	%								
	Coarse-Size Fraction (2~7.5 mm)	%		0.0	19.5	10.9	0.0			
	Sand-Size Fraction (0.075~2 mm)	%		6.7	28.2	8.3	21.5			
	Silt-Size Fraction (0.005~0.075 mm)	%		66.7	31.8	47.6	39.0			
	Clay-Size Fraction (0.005 mm >)	%		26.6	20.5	33.2	39.5			
	Max. Grain Size	mm		0.425	19	19	2			
	Uniformity Coefficient U_c			-	-	-	-			
	Consistency	Liquid Limit w_L	%		111.2	57.1	197.5	48.5		
		Plastic Limit w_p	%		44.7	31.1	73.3	28.6		
Plasticity Index I_p				66.5	26.0	124.2	19.9			
Classification of Soil	Classification Name	sandy silt fine sand (high liquid limit)		gravelly sand with silt (high liquid limit)	gravelly organic clay (high liquid limit)	sandy silt (low liquid limit)				
	Classification Mark	(MH-S)		(MHSG)	(OH-SG)	(MLS)				
Consolidation	Testing Method									
	Compression Index C_c									
	Consolidation Yield Stress p_c	kN/m ²								
Unconfined Compression	Unconfined Compression Strength q_u	kN/m ²								
Shear	Testing Method									
	Total Stress	c	kN/m ²							
		φ	°							
	Effective Stress	c'	kN/m ²							
φ'		°								

Note

1) A percentage of the soil that removed Stone-Size Fraction

Figure B-8. Soil testing data for site 4

Table B-1. Kunijiban sandy low blow count profiles throughout the Kumamoto Plain

B4KJ201801008-9583	B4KJ201801010-5234
B4KJ201801009-1161	B4KJ201801010-5244
B4KJ201801008-9584	B4KJ201801010-5241
B4KJ201801009-1195	B4KJ201801010-5247
B4KJ201801008-9589	B4KJ201801010-5251
QS2004895060020030003	B4KJ201801010-5274
B4KJ201801008-9585	B4KJ201801009-9073
B4KJ201801010-5215	B4KJ201801009-1168
B4KJ201801010-4917	B4KJ201801010-5184
B4KJ201801010-4924	B4KJ201801009-8954